EXPERIMENTAL AND SIMULATION STUDIES ON THIXO-FORMING OF AA 2017 ALLOY

A Dissertation
Submitted In partial fulfilment of the requirement for
the award of Degree of

DOCTOR OF PHILOSOPHY

In

MECHANICAL ENGINEERING

Submitted by

CHAKUNTA SHASHIKANTH
(R.NO: 701107)

Under the Guidance of

Dr. M.J DAVIDSON

DEPARTMENT OF MECHANICAL ENGINEERING

NATIONAL INSTITUTE OF TECHNOLOGY

WARANGAL, T.S, INDIA - 506004

AUGUST – 2016

DEPARTMENT OF MECHANICAL ENGINEERING
NATIONAL INSTITUTE OF TECHNOLOGY
WARANGAL, T.S, INDIA-506004

CERTIFICATE

This is to certify that the dissertation work entitled "**EXPERIMENTAL AND SIMULATION STUDIES ON THIXO-FORMING OF AA 2017 ALLOY**", which is being submitted by **Mr. CH.Shashikanth** (Roll No.701107), is a bonafide work submitted to the Department of Mechanical Engineering, National Institute of Technology, Warangal in partial fulfilment of the requirement for the award of the degree of **Doctor of Philosophy in Mechanical Engineering.**

To the best of our knowledge, the work incorporated in this thesis has not been submitted elsewhere for the award of any degree.

Dr.M.J. DAVIDSON
Supervisor
Department of Mechanical Engineering
National Institute of Technology
Warangal-506004

Prof. C. S. P. Rao
Head
Department of Mechanical Engineering
National Institute of Technology
Warangal-506004

APPROVAL SHEET

This Thesis entitled "**EXPERIMENTAL AND SIMULATION STUDIES ON THIXO-FORMING OF AA 2017 ALLOY"** by **CH.Shashikanth** is approved for the degree of Doctor Philosophy

Examiners

Supervisor

Dr. M.J. Davidson

Assistant Professor, MED, NIT WARANGAL

Chairman

Prof. C. S. P. Rao

Professor, MED, NIT WARANGAL

DECLARATION

This is to certify that the work presented in the thesis entitled. **"EXPERIMENTAL AND SIMULATION STUDIES ON THIXO-FORMING OF AA 2017 ALLOY"** is a bonafide work done by me under the supervision of Dr.M.J. Davidson and was not submitted elsewhere for the award of any degree. I declare that this written submission represents my ideas in my own words and where others' ideas or words have been included, I have adequately cited and referenced the original sources. I also declare that I have adhered to all principles of academic honesty and integrity and have not misrepresented or fabricated or falsified any idea / data / fact / source in my submission. I understand that any violation of the above will be a cause for disciplinary action by the Institute and can also evoke penal action from the sources which have thus not been properly cited or from whom proper permission has not been taken when needed.

(CH.Shashikanth)

(701107)

Date: _____

ACKNOWLEDGEMENT

It gives me an immense pleasure to express my deep sense of gratitude to my supervisor Dr.M.J.Davidson for his constant inspiration, encouragement, motivation, and invaluable guidance and above all for their ever co-operating attitude that enabled me in shaping the thesis in the present form.

I am grateful to Prof. T. Srinivasa Rao, Director-NIT Warangal who has been constant source of inspiration for me. My heartfelt thanks to Prof. Ch. Surya Prakash Rao, Head of the Department of Mechanical Engineering for his help and continuous encouragement to complete this work. I would like to express my sincere thanks to Prof. Dr. A.R.C. Reddy (Professor, Physics Department) and Dr.N. Selvaraj (Professor, Mechanical Engineering Department), learned members of my Doctoral Scrutiny Committee for being helpful and generous during the entire course of this work. I am also thankful to the teaching and non teaching faculty members of the Mechanical Engineering Department of NIT, Warangal.

I would like to express my sincere thanks to M. Ramesh reddy, Secretary and correspondent of Sree Chaitanya College of Engineering, Karimnagar and Prof. R.V.R.K. Chalam, Principal Sree Chaitanya College of Engineering, Prof.G.Venkateswarlu,Head of the Department of Mechanical Engineering, Sree Chaitanya College of Engineering,Karimnagar.

I thank my family members, Vanitha chakunta and Shubham chakunta for their unforgettable support and their patience during this work.

Finally, I am extremely thankful to my friends and well wishers whose list cannot be quoted, for extending their co-operation in successful completion of this work.

CH. Shashikanth
Research Scholar
Department of Mechanical Engineering
National Institute of Technology
Warangal-506004, India

CONTENTS

ABSTRACT

Thixo-forming is one of the near net shaped manufacturing processes in which the final product is made between the liquidus and solidus temperatures. Forming the product at this temperature range provides large benefits compared to conventional forming methods. In the present work, deformation mechanism of AA2017 alloy in the semi-solid state has been studied. As the mechanical behaviour and deformation mechanism of semi-solid metal is completely different from that of the solid state forming, it is necessary to investigate its nature at the semi solid range. To analyze the metal flow, the stress behaviour and the corresponding strain induced, extensive finite element analysis (FEA) based simulation studies have been performed. The commercial software, DEFORM 2D was used for the simulation. The flow behaviour was modelled by formulating an Arrhenius type constitutive relation.

The alloy has been heated between 570^0C to 610^0C and it was extruded in a die having die cone angles of 30, 45 and 60 degrees. Simulation studies have been performed by using the constitutive relation that was developed by performing disc compression tests at different temperatures and strain rates. A good agreement was found between the experimental and the simulation results.

High strength materials can be processed easily by using this method. In this work, the experiments were conducted in the semi-solid state to know the effect of thixo extrusion process parameters on the microstructure of AA 2017 alloy. The results show that fine and globular microstructures could be achieved in this process. It is observed from the microstructures that, the front end of the rod is evidence for semi-solid extrusion. However, the rear end failed to extrude in the semi-solid state due to loss of heat.

In semi-solid extrusion, producing the complex parts with better mechanical properties is the main aim of the present researchers. To achieve this, knowledge of the influence of every parameter on the mechanical properties of final specimen is the key in production of high quality complex parts. The aim of the present work is to optimize process parameters namely, temperature of billet, strain rate, approach angle and percentage reduction in area during

semi-solid extrusion of AA2017 alloy. In this research work, experiments were designed according to Taguchi experimental design and L9 orthogonal array was used to conduct the experiments. Analysis of variance (ANOVA) method was used to find the significance of every process parameter on the thixo-extrusion process responses. The results indicate that percentage reduction area is the most important factor influencing the mechanical properties of thixo-extrusion specimen followed by temperature and strain rate.

AA2017 aluminium alloy billets were compressed till the appearance of crack on semi-solid compression tests conducted at 570^0C, 590^0C and 610^0C under strain rates of $0.16s^{-1}$,$0.18s^{-1}$,$0.2s^{-1}$ to establish the fracture criterion during semi-solid forming process. The tests conditions were simulated in a finite element based simulation package DEFORM 2D. The critical damage factor based on Cockcroft and Latham algorithm was obtained by analyzing the results of the corresponding finite element calculation. The results show that the critical damage factor at different temperatures and strain rates is not constant but varying between 0.471 to 0.264. The Zener-Hollomon parameter which combines the effect of temperature and strain rate has been introduced in to the fracture criterion.

LIST OF TABLES

LIST OF FIGURES

CHAPTER 1

INTRODUCTION

1. Introduction

Thixo-forming or semi-solid forming is a near net shaped manufacturing process in which the final product is made between the liquidus and solidus temperatures. Forming the product at this temperature range provides large benefits compared to conventional forming methods. Flemings and co-workers studied the flow behaviour of metals in a semi-solid state in the early 1970s. At the end of the 1980s, companies like Pechiney (France), Ormet (USA) and SAG (Austria) started an intensive development programme on thixo forming with the help of electromagnetic stirring methods. These companies utilized advanced heating technologies and online-controlled pressure casting machines to develop the process. This resulted in the production of large amount of thixo formed automotive components such as the production of automotive chassis by Porsche, DaimlerChrysler, Alfa Romeo etc and car body components by Audi, Fiat and DaimlerChrysler.

However, one of the major challenges for the manufacturers of thixo components was the availability of only a narrow process window for billet production, reheating and forming, which have to be maintained to achieve highly repeatable production. This requires a fundamental and detailed understanding of the physical basics of each process step, taking into account details of the material behaviour and microstructure development.

1.1 Advantage of thixo-forming over Conventional Processes

As thixo-forming is a hybrid process of the conventional casting and forging, the advantages and disadvantages of both the processes might be inevitable. However, the specific difference between thixo forming and the conventional casting and forging may be stated as below.

1.1.1 Thixo forming and conventional casting

The process behaves differently at different solid fractions. However, a solid fraction closer to about 40% during die filling in semi-solid forming avoids volume loss during complete solidification, leading to products with reduced shrinkage porosity. Further, thixo forming reduces air intake problem faced in conventional casting, and thus leading to the delivery of products with nice microstructures suitable for subsequent welding and heat treatment. Moreover, the tool life also increases due to reduced process temperature that the conventional casting.

However, the high viscosity of the semi-solid metal creates macroscopic turbulence during die filling which may result in air entrapment issues and subsequently problems like porosity and cracks.

1.1.2 Thixo forming and conventional forging

Thixoforming offers significantly reduced forming loads than the conventional forging as the forming is done on a semi solid working medium and thus even very complex shaped components can be made with lesser load requirement than the conventional forging. Also, as thixo forming is a near net shaped manufacturing process, the additional production costs and times required for secondary finishing manufacturing processes can be avoided.

However, on the negative side, thixoforming may not yield the superior mechanical properties offered by conventional forging because of small amount of porosity and leakage problems. Also, thixo forming takes a longer production time as the component has to be heated before forming. The melting and solidification cycle takes a longer production time and thus affecting the productivity.

1.2 Major Challenges to overcome

1. High thermal loading of tools and dies
2. Difficulties in achieving a homogeneous temperature distribution in the billet.
3. Tendency for oxidation and scale formation
4. Complex microstructure evolution during heating of samples.

1.3 Early Work on Semi-Solid Forming

Flemings and his co workers in the early 1970s studied the behaviour of solidifying metallic melts which had suspended globular primary solid particles in a liquid metallic melt (Fig.1.1b). This was achieved by stirring the slurry while cooling it to the desired temperature. They reported that viscous metals in the semi-solid state depend on the solid fraction, shear rate and time history. It was considered a fairly new discovery for metallic systems, as under normal conditions the metals would have shown dendritic microstructure (Fig. 1.1a)

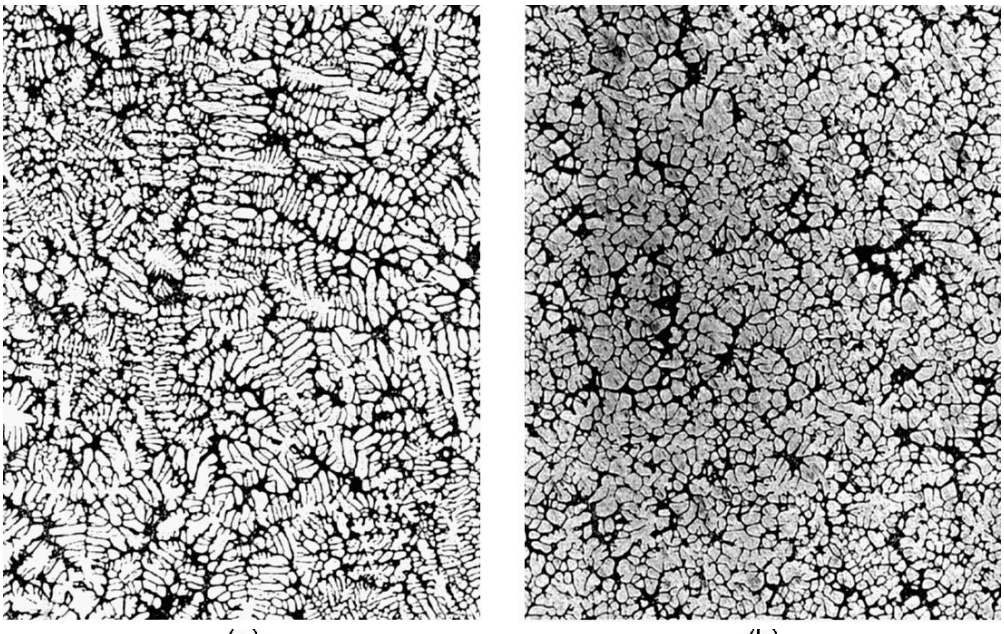

Fig. 1.1 (a) Dendritic and (b) globular microstructure. Flemings M.C [1970**]**

Many studies have been performed by different investigators since then to investigate this behaviour in more detail for different alloys, to explain the governing mechanisms and to derive models to describe the material response. One mechanism, which distinguishes semi-solid metal

slurries from other suspensions, is that the particle shape and size vary irreversibly with time, as shown in Fig. 1.2.

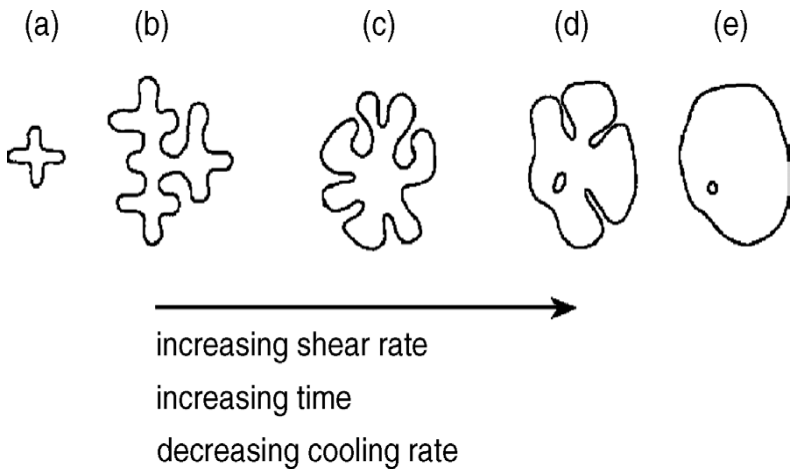

Fig.1.2 Evolution of structure during semi-solid solidification process. (a) initial dendritic fragment; (b) dendritic growth; (c) rosette; (d) ripened rosette; (e) spheroid Flemings M.C [1991]. Since the first work by Fleming, the process has undergone several improvements (Kenney, M.P et al. [1988], Fan, Z [2002], de Figueredo, A. [2001] and Midson, S.P [1996]). Some of the developed processes are being used in industries and some are still in the laboratory stage. New methods of preparing the samples for semi solid forming have been proposed by different researchers. The first method proposed was slurry preparation adopted in the initial discovery stage of the process. Nowadays, slurries are prepared either by a reheating stage or a homogenization and/or consolidation stage or directly from liquid stage Shun-sheng Wang [1994]

1.4 Motivation/Gap Analysis

Though there are quite good number of literatures on the experimental investigations on the thixo forming of various alloys, study on the modelling of thixo forming process is limited as far as the knowledge of the researchers goes. Moreover, little or no work has been reported on the semi solid forming of AA2017 alloy. As a good modelling methodology will enhance the process design capability of the users, and as it is felt that only limited work have been reported

in the literature, the present researcher was motivated to work on the semi solid forming of AA2017 alloy and their modelling aspects.

1.5 Objective of the work

After the extensive literature study performed on the evolution of the various thixo forming processes, the existing gap in the process development has been identified and it is planned to perform the following studies as part of the PhD work.

I) Develop constitutive relation for thixo forming of AA2017 alloy in the thixo range.

II) To determine the hot and thixo forming material parameters involved in the constitutive relation for modelling the process.

III) To develop the modelling strategy and to analyze the model to predict the material flow path, its stresses and strains.

IV) To perform the micro structural analysis and to develop the process map from the desired microstructures.

V) To evaluate the mechanical properties and to predict the fracture of the alloy after forming.

1.6 Summary of the work

The work that has been done can be summarized as follows.

Chapter 1 gives a brief introduction about thixo-forming and thixo-extrusion processes. The objectives of the present work have been discussed as well.

Chapter 2 presents the summary of the previous investigations that have been carried out by various researchers on related topics such as thixo-forming, thixo-extrusion, micro structural analysis, mechanical properties of thixo-extruded products etc.

Chapter 3 explains the detailed scheme of investigation for the present research work.

Chapter 4 presents the deformation mechanism of AA2017 in the semi- solid state. As the mechanical behaviour and deformation mechanism of semi-solid metal is completely different from that of the solid state forming, it is necessary to investigate its nature at the semi solid range. The flow behaviour was modelled by formulating an Arrhenius type constitutive relation.

Chapter 5 explains the finite element based simulation model adopted in the present study. An Arrhenius type constitutive relation involving the solid fractions and the strain rate has been developed. The developed relation has been used to simulate the thixo-forming process in DEFORM 2D. The different modelling aspects followed and the post processed results have been given in this chapter

.

Chapter 6 explains the fracture criterion for AA2017 alloy in the semi-solid state, capable of predicting the initiation of crack during the forming process and to optimize the processing parameters in such a way that the initiation of crack is delayed or avoided. The Zener-Hollomon parameter which combines the effect of temperature and strain rate has been introduced in to the fracture criterion.

Chapter 7 presents the micro structural study performed on the thixo- extruded samples at different temperatures and strain rates.

Chapter 8 presents the Taguchi experimental design based optimisation technique followed in the present thesis work. The process parameters namely, temperature of billet, strain rate, approach angle, percentage reduction in area on the semi-solid extrusion of AA2017. Experiments were optimised according to L9 orthogonal array.

Chapter 9 provides the conclusions drawn from the present work with suggestion for the future work.

1.7 Material and experimental method

The material used for thixo- extrusion was AA2017 aluminium alloy having chemical composition of 0.376% Si, 0.345% Fe, 3.33% Cu, 0.66%Mn, 0.65% Mg, 0.180% Zn, 0.034% Cr, 0.076%Ti and 97.349 Al (Wt%). The AA2017 aluminium alloys are used in aircraft, automotive structural parts and other highly stressed applications.

An electric resistance furnace with two thermocouples to measure the temperature of furnace and billet was used to heat the billets. The operation of thixo extrusion was carried out on a hydraulic press. Cylindrical billets of size 15 mm diameter and 15 mm height were placed in an electric resistance furnace and heated from room temperature to the required extrusion temperature. To achieve homogenous temperature, the specimen was held at the forming temperature for 30 minutes and then the billets were extruded with a 50 ton hydraulic press. The experiments were performed at different temperatures namely 570^0C, 590^0C and 610^0C, different strain rates namely $0.16s^{-1}$, $0.18s^{-1}$ and $0.2s^{-1}$, different approach angles such as 30^0, 45^0 and 60^0 and various area reductions such as 35%, 55% and 75%. Samples for microstructure study were prepared by standard metallurgical technique. The prepared samples were examined after etching with Keller's solution (solution of HCL, HF and HNO_3). The microstructure of the samples was observed under metallographic microscope. The complete experimental setup and the die used for semi-solid extrusion are shown in the Fig .3.5

CHAPTER 2

LITERATURE REVIEW

Starting from the pioneer work done by Flemings and his co-workers in the early 1970s, several researchers have done commendable work in the various aspects of semi solid forming. Most of the work can be grouped into developmental studies, microstructural studies, mechanical property evaluation studies, etc. The present chapter summarizes the work performed by several researchers on the various aspects of semi solid process technology.

2.1 Literature Review on semi-solid forming

As was stated earlier in the introduction part, the semi solid forming process was developed by Fleming and his co workers in the early 1970s. Flemings in his classical paper (M. C. Flemings, R. G. Riek and K. P. Young, 1976) termed the process as "Thixocasting" and "Thixoforming". The idea that metals can be formed at semi solid state arised from the rheological studies performed by D. B. Spencer [1972], P. A. Joly [(1974] and D. B. Spencer [1971] on different alloys. These rheological studies brought in a new concept that non dendrite structures if formed will produce a homogenous deformation. Most of the work performed during the initial period of evolution of the process was concentrated on

characterizing the material behaviour through experiments. Kiuchi [1979] has conducted numerous experimental studies measuring the flow stress as a function of solid fraction for various semi-solid alloys. The studies revealed the existence of the relationship between the flow stress and the solid fraction.

Kang et al. [1998] used FEA technique to investigate the mushy state forming process. The authors investigated the role of stress state and the morphology of the phase in the forming process. Kiuchi et al. [2001] proposed mathematical models for yield criterion and developed equations for mushy/semi-solid alloys. Ko et al. [1996] used finite element method to know the material flow and to simulate the process while forming A356 aluminium alloy in the mushy state condition. Nguyen et al. [1994] investigated the isothermal flow behaviour of aluminium alloys in the mushy state. Gunasekera [1992] formed the constitutive equation of mushy state materials using geometrical shape of the solid particle and liquid. Numerical analysis of the upsetting process was performed by Toyoshima [1994]. Compression behaviour of Sn-15% Pb alloy in the semi-solid state and the effect of strain rate were studied by Suery et al. [1982] and Toyoshima et al. [1994]. Kenny et al. [1988] suggested that 60-70% of solid fraction is required to obtain the best quality product. Microstructure and liquid flow state of Al-Cu alloy in the semi-solid state was given by Yoshida et al. [1992].

Martin et al. [1995] investigated the shear deformation behaviour of a Sn–Pb alloy under various conditions namely a coarse dendritic shape, a globular shape resulting from reheating fine dendritic shapes, and a globular shape obtained from mechanical stirring. Lower shear rate dependence was observed at high solid fractions at a steady state.The stress–strain curve showed strong dependence on shear rates for samples with globular structures obtained by vigorous stirring. The author interpreted the results in terms of agglomeration/disagglomeration model [1993-1994].At low solid fractions, material modelling has been approached from a fluid-based framework. Laxmanan and Flemings in 1980, investigated deformation behaviour of non dendritic Sn–Pb alloys having solid fractions between 0.15 and 0.60.

There were also attempts to characterize the structural evolution of the semi-solid material. Kumar et al., in 1993, developed an internal variable model that characterized the degree of agglomeration within the slurry for materials at solid fractions of 0.1–0.6 [1994].

Mada and Ajersch in 1996, proposed a structural parameter, to describe the evolution of the semi-solid structure of A356 alloys reinforced with SiC particles. The model described the kinetics of the structural degradation of primary solid phase particles as a function of the shear rate, duration of shear, and the solid fraction. The experiments done by Salvo et al. [1995**]** also support the microstructural evolution approach to describe the behaviour of semi-solid slurry.

Numerical methods have been developed to validate and/or to predict actual forming processes. However, only limited literatures are available on the simulation studies of semi solid forming process. Koç et al. [1996] evaluated the flow stress of A356 semi-solid alloy using a two-dimensional 2D finite element analysis (FEA). The authors compared the simulation results with the experimental findings in terms of forming loads and specimen inspection. Though the authors found discrepancies in the load prediction, separation and rewelding of the material during semi solid forming was predicted accurately. Yoon et al. [1999 & 2001] developed a finite element code for semi-solid forming using the mixture theory and Darcy's law. The solid phase of the material was modelled using the Von Mises yield condition. Ko and Min [2000] used a similar approach for developing their finite element code and modelled the solid phase with viscoplastic material and Darcy's law for the liquid flow. Kang et al. [2001] performed simulations with DEFORM in which the authors used the experimentally determined stress–strain–strain rate curves as constitutive curves. The authors studied die filling patterns by varying the forming temperatures and the forces.M. S. Salleh et al.[2012] have discussed the rheological behaviour of aluminium alloy which is a very important element in semi solid processing.

2.2 Literature Review on Thixo-extrusion

Kiuchi et al. [1979] was the first to investigate on semisolid extrusion. The authors performed semi solid extrusion on a horizontal device, and studied the influence of extrusion force and tool temperature for Pb and Al alloys with a billet of 40 mm diameter and different heights ranging from 25 to 40 mm under different test conditions. The extrusion was done for varied channel diameters ranging between 2 and 10 mm, and the extrusion channel length, ranging from 4 to 100 mm. A preliminary level investigation revealed that the initial press force increases with decreasing liquid fraction. The extrusion ratio was varied between 16 and 400.

The authors used different press velocities ranging between 37 and 47 mm s^{-1}. A simultaneous heating process was adopted by the authors. The author of this thesis has also adopted a similar technique. The authors found the optimum liquid fraction to be 5–10% and the press force one-quarter to one-fifth of the force used in conventional extrusion process.

Kiuchi et al. much later in the year 1994 performed thixo extrusion studies on aluminium and their alloys on dies with diameter of 2 to 10 mm in steps of 2 mm and a liquid fraction of about 20–30%.

Moller, T. [2004] extruded billets of aluminium alloy A356 + 20 vol. % SiC with 100 mm height and 76 mm diameter. The extrusion was done up to a height of 600 mm using an extrusion channel with a 10 x 10 mm rectangular cross-section. The authors detected shell formation in the extruded samples. The authors could not solve the shell formation issue by increasing the tool temperature or by increasing the pressure in the extrusion channel.

Miwa. K. and Kawamura, S. [2000] performed experiments which were similar to semi-solid impact extrusion. Billets of diameter 30 mm and height 20 mm made of stainless-steel alloy UNS: S30400 (AISI 304) was made in a ceramic container. These experiments helped the authors to investigate the effect of press velocity on the segregation problem. The authors observed phase separation of the solid and liquid fractions at 100 –1800 mm s^{-1} press velocities. At a low press velocity of 10 mm s^{-1}, the authors observed a homogeneous phase distribution. The forming load was found to increase rapidly at this experimental condition. It was later found that the rapid solidification of the semi-solid slurry found in the cold extrusion dies to be the reason for the increase in forming load.

Rouff, C. et al. [2002] investigated the role of different shear rates on the impact extrudability of steel grade C80 (AISI 1080). The authors extruded billets of diameter of 30 mm and a height of 45 mm. The authors performed the study at 1430^0C, which is equal to 40% of liquid fraction. The authors used two different shear rates and found the segregation to vary.

Abdelfatah, S. et al. [2000] used similar experiments to analyze the influence of process parameters on thixo extrusion. They reported an increase in the required extrusion pressure when extrusion ratio was increased. The authors used steel grade C80 and performed the experiments

between 20 to 30% liquid fraction. The authors used different extrusion ratios and found the load to increase with increase in extrusion ratio. The values of yield strength and ultimate tensile strength of the extruded bars were comparable to conventional forged parts. However, the percentage reduction of area after fracture was found to be lower than conventional forged parts due to the presence of microporosity problem in the thixoforged parts.

Randhir Kumar and N. K. Singh[2012] analyzed the influence of the process parameters on tensile properties in the Semi-Solid Forging of A356 aluminum-alloy using Taguchi method. In Taguchi method, a three level orthogonal array has been used to determine the S/N ratio. Analysis of variance and the forging test values were used to determine the most significant process parameters affecting the tensile strength of A356 Al alloy. The results indicate that Forging temperature and deformation percent are the influential parameters to create appreciable improvement in the mechanical properties of the Semi-Solid Forged components. Simge Gencalp Irizalp and Nursen Saklakoglu [2014] investigated the effect of α-Fe and β-Fe intermetallics concentration and morphology as well as α-Al morphology on the microstructure and mechanical properties of thixoformed and gravity cast A380 alloy. The α- Al15Si2(Fe,Mn)3 intermetallic particle was observed to have polyhedral morphology in thixoforming while a Chinese script morphology was observed in conventional gravity casting. The β-Al5FeSi particle was solidified in the form of small plate in thixoforming while it was solidified in the form of needle-like in gravity casting at the grain boundaries of α-Al. The mechanical properties of the alloys have been enhanced by thixoforming compared with the conventional cast condition.

2.3 Constitutive Modelling Studies on Thixo Forming

The flow stress of the metals at elevated temperatures will be different than that at the cold state and it is different at different temperatures and strain rates. Knowledge of the relation between the hot deformation behaviour of the billet materials and its micro structural evolution helps to control the workability of the material. Workability refers to the ability to form when subjected to deforming forces.

Kumar, P et al. [1994] studied the flow response and structural evolution under shear deformation by using a new constitutive relation. The theoretical and experimental data of the

isothermal mechanical behaviour of alloys in the mushy state was compared by Nguyen, T.G et al. [1994]. Gunasekera, J.S [1992] formulated a constitutive equation for mushy state materials using the geometrical shape of the solid particle and the liquid. Numerical analysis of the upsetting process was performed by Toyoshima, S.[1994]. Compression behaviour of Sn-15%Pb alloy in the semi-solid state and the effect of strain rate were studied by Suery et al.[1982] and Toyoshima et al. [1994]. Kenny, et al. (1999) suggested that 60 - 70% of the solid fraction is required to obtain the best quality product. Microstructure and liquid flow state of Al-Cu alloy in the semi-solid forming was given by Yoshida et al. (1999)

2.4 Microstructural Studies on Thixo Forming

The microstructural evolution of Thixo-forming is different from conventional forming processes as the forming will be done in partly solid and partly liquid environment, and the microstructural features will not only be governed by the forming temperature but also by the forming process parameters. Rovira, M.M. et al. [1999] have performed the microstructural evolution of thixo extrusion done on Al-Cu alloys. The mechanical behaviour and microstructure during thixo-forging of semi-solid ZK60-Y magnesium alloys at high solid content was studied by Zhao, Z. et al. [2010]. Birol, Y. [2008] and Hong-min, G. et al. [2008] investigated the microstructure evolution of semi-solid 6082 and semi-solid 2024 Al alloys, respectively. Hossein Mohammadi and Mostafa Ketabchi [2013] studied the microstructure evolutions during partial remelting of AA7075 alloy, which has low extrudability, through backward thixo-extrusion process. The required feed stocks for thixo-forming was obtained by "stress induced and melts activation" (SIMA) route. The authors revealed that fine and globular microstructure can be obtained by the SIMA route. The authors performed back-extrusion of AA7075 alloy in the semi-solid state at 580°C for 10 min holding time. Microstructure and mechanical properties of thixo-formed components before and after the T6 heat treatment were examined at room temperature. It was observed by the authors that the low tensile and low hardness values in the as-thixoformed parts can be improved by subsequent heat treatment.

Y. Birol and L. J. Capan [2011] performed thixo extrusion studies on EN AW-2014 alloy in the semisolid state. The authors observed that forming during thixo-extrusion took place largely via rotation of the α-Al globules over one another, producing a microstructure having

predominantly uniform globular α-Al grains. The authors found the forming load to be less when compared to hot extrusion of the same alloy, thus emphasizing the need to extrude the hard to form 2XXX alloys in the semisolid state. It was found by the authors that at the end of the thixo extrusion step, due to the limited availability of liquid phase, the final part of the preheated slug, failed to extrude under favourable microstructural conditions. The large extrusion deformation and forming temperatures, which were well above the liquidus temperature, led to dynamic recrystallization of the slug resulting in equiaxed microstructure, instead of fibrous, structure in this region.

Ju-fu Jiang et al. [2013] used thermo-mechanically based route to extrude AZ61 Mg alloy in the semi solid range. The authors studied the effects of different process parameters on the tensile properties, the microstructural evolution and the die filling behaviour of the semisolid billets. Qiang Chen et al. [2014] examined the microstructure, thixo-formability and mechanical properties of wrought Mg–Zn–Y–Zr magnesium alloys which were reheated from the as-cast and extruded states. The authors tried to understand the relationship between microstructures and mechanical properties, for high performance wrought magnesium alloys, during semi-solid metal processing. The authors found the as-cast alloy to exhibit non-uniform microstructures with large amount of entrapped liquid, which are less spherical when compared to the extruded alloy in the semi-solid state. The grain coarsening rate was found to be relatively low in the extruded alloy than the as-cast alloy during reheating. The presence of fine and spherical solid grains which are weakly connected enables the slug to slide over each other without any plastic deformation in the extruded alloy. Thus, the as-cast alloy having heterogeneous and coarse solid grains can't be thixo-formed as easily as an alloy which is in the semi solid range with fine and spherical grains. Also, the tensile mechanical properties of thixo-formed from the extruded alloy were found to be better than the Mg–Zn–Y–Zr alloys thixo-formed from the as-cast alloy.

Lucas Bertolino Ragazzo et al.[2015] investigated the conditions needed to produce a partial or full martensitic structure instead of a conventional graphite-ferrite or graphite-ferrite/pearlite matrix in hypoeutectic gray cast iron severely deformed in the semisolid state in hot-compression tests. Three thixo formability parameters (liquid fraction, cooling rate, and holding time) were controlled to identify the conditions and parameters that can be adjusted to control the final microstructure of the thixoformed material. **Shujian Cheng et al.** [2016]

investigated the effect of process parameters on the microstructure of semi-solid ZL101 aluminum alloy produced by serpentine channel. The results show that, the morphology of primary α-Al grains transformed from rosette to spheroid with decreasing pouring temperature from 630°C to 670°C.

2.5 Constitutive Modelling of Thixo Extrusion

Constitutive equations describe the relationship between stress and strain at large plastic strain. It can be used to predict the state at which a material begins to deform and to calculate the deformation behaviour during metal-forming operations (Hartley, C.S and srinivasan, R. [1983]). For performing simulation studies, it is necessary to have a good constitutive equation which better matches the experimental results. Several empirical equations have been proposed by several researchers to describe experimental stress-strain curves and strain-hardening of metals. The Ludwik equation (1909) is believed to be the earliest known constitutive equation. Later, researchers such as Holloman, Voce, Swift, Ludwigson and Prager proposed different expressions to best fit the experimental results. Kiuchi, Sugiyama and Arai (1979) carried out compression tests in the mushy state which is considered the pioneer work in the constitutive modelling of mushy state processing. Suery and Flemings [1982] found the effect of strain rate on the deformation behaviour of semi-solid dendritic alloys. The authors found that for higher strain rates, the segregation of liquid and solid which was an issue in semi solid forming, does not occur to such a great extent and the deformation was found to be more homogeneous. Wakil [1984] developed a model to study analytically the yield criterion for alloys in their mushy state. Gunasekera [1992] developed a theoretical constitutive model for mushy materials. Nguyen et al. [1994] used a constitutive model for the semi-solid material based on the concept of mechanics of continuum media and the theory of mixtures. The authors considered the semi-solid material as a connected solid phase in a viscoplastic porous medium saturated with liquid.

2.6 Simulation studies on semi solid forming

Only limited studies have been performed on the simulation of the semi-solid forming process due to limited availability of mathematical and mechanical models. Koç et al. [1996] used a simple approximation of experimentally determined flow stresses of a semi-solid A356

alloy in the 2D FE analysis performed by them. Though deviations were found in the load prediction, separation and rewelding of the semi-solid alloy was predicted with reasonable accuracy during the forming process. Yoon et al. [1999 and 2001] developed an FE code for the semi-solid material using mixture theory and Darcy's law. Ko et al.[2000] used a similar approach for developing an FE code for semi solid processing. The authors assumed a viscoplastic model for the solid phase and used Darcy's law for the liquid flow. Kang et al. [2001] performed an FE simulation with DEFORM, by using the experimentally determined stress -strain rate relationship.

2.7 Fracture criterion during semi solid forming

The damage that a material undergoes during the forming processes can be simulated by incorporating damage models into finite element software. The occurrence of ductile damage fracture is the limiting factor in metal forming processes. Thus, the degree of damage, that is, the fracture tendency can be obtained by finding the ratio of damage value and ductile fracture criterion (DFC). Basically, DFC is based on the experimental work done on a deformation process that is related to actual industrial applications (Arabshahi [2009]). The fracture criterion based on Cockcroft-Latham algorithm has been used successfully in many metal-forming simulations for predicting ductile fracture (Zhang X.Q et.al.[2000]). Usually, DFC is a constant value of a particular material, like yield stress, ultimate strength etc. Most of the damage criteria are based on the accumulation of energy induced by deformation. There are many other algorithms in practice to predict ductile fracture apart from Cockcroft-Latham. They mainly differ in the way major stress components are used to calculate the accumulated energy. Freudenthal A.M [1950] used an effective stress and Cockcroft and Latham [1968] employed maximum principal stress, respectively. Brozzo et al. [1972] used a ratio between the maximum principal stress and maximum principal stress minus mean normal stress and Oyane [1972] used a ratio between mean normal and effective stress. Many investigators, Clift SE et.al [1990], Wifi AS [1998] , and Kim HS et.al.[1999] have applied these algorithms to various manufacturing processes.

CHAPTER 3

EXPERIMENTAL DETAILS

3.1 Introduction

To study the deformation behaviour of AA2017 at elevated temperatures, extensive experiments were conducted and to analyze the material flow, its strain path, damage position, shear zone etc, extensive simulations were performed using DEFORM 2D after incorporating the flow curve that was developed from the hot disk compression tests. The detailed experimental plan is shown in the following flow chart.

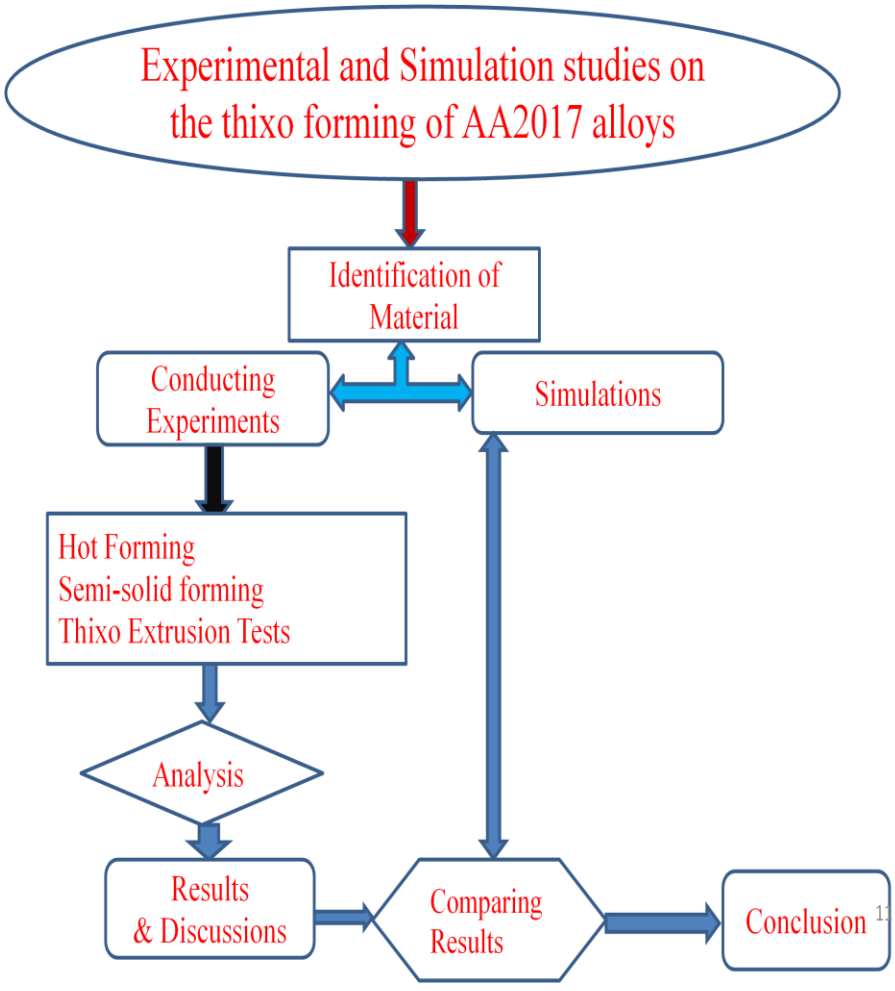

Fig.3.1Flow chart of work plan

3.2 Experimental procedures

3.2.1 Material for investigation

The material used for thixo extrusion is AA 2017 aluminium alloy having chemical composition of 0.376% Si, 0.345% Fe, 3.33% Cu, 0.66%Mn, 0.65% Mg, 0.180% Zn, 0.034% Cr, 0.076%Ti and 97.349 Al (Wt%). The AA 2017 aluminium alloys are used in aircraft, automotive structural parts and other highly stressed applications. The microstructure of the material is shown in Fig.3.2.

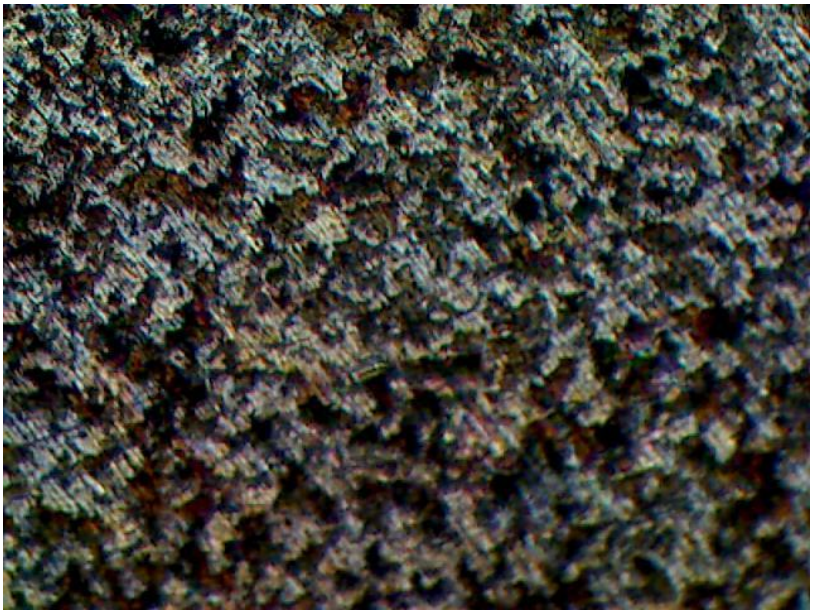

Fig. 3.2 Initial Microstructure of AA2017 aluminium sample

3.3 Differential scanning calorimetric analysis

To conduct any semi-solid forming process, it is necessary to know the temperature range of solidus and liquidus temperatures of the alloy. To know these values, differential scanning calorimetric analysis (DSC) of aluminium AA2017 alloy billet was performed on a NETZSCHSTA 449F integrated thermal analyzer.DSC curve of semi-solid AA2017 alloy is shown in Fig.3.3.The variation of the solidus and liquidus fraction with the temperatures is shown in Fig.3.4.The solidus and liquidus temperatures thus calculated are 545^0C and 646^0C

respectively. The difference between the liquidus and solidus temperatures is 100^0C. The percentage of solid fraction and liquid fraction within the solidification interval of the present alloy was found at any given temperature by using Scheil Eq. (3.1). The working temperature range for the thixo extrusion test has been selected from 570^0C to 610^0C so that a minimum to maximum solid fraction range can be achieved. The solid fraction of AA 2017 alloy at the temperatures 570^0C, 590^0C and 610^0C were found to be 0.81, 0.63 and 0.41 respectively from Eq. (3.1).

$$\mathbf{f_s = 1-(T_s-T/T_s-T_l)^{(1/1-k)}} \qquad (3.1)$$

Where k = Partition coefficient = 0.17

Ts = solidus temperature = 545.5^0C, T_l = liquidus temperature = 646.3^0C

Ts - T_l = 545.5^0C -646.3^0C = -100.8^0C

1-k = 1-0.17 = 0.83

(1/1-k) = 1/0.83 = 1.20

From Eq.3.1, the solid fraction at 570^0C is found as below

Ts – T = 545.5^0C - 570^0C = -23.5^0C

(Ts – T) / (Ts - T_l) = -23.5^0C / -100.8^0C = 0.233

$((Ts – T) / (Ts - T_l))^{(1/1-k)} = (0.233)^{1.20} = 0.174$

$f_s = 1-(T_s-T/T_s-T_l)^{(1/1-k)} = 1- 0.174 = 0.826 = 82\%$

From Eq.3.1, the solid fraction at 590^0C is found as below

Ts – T = 545.5^0C - 590^0C = -44.5^0C

(Ts – T) / (Ts - T_l) = -44.5^0C / -100.8^0C = 0.441

$((Ts – T) / (Ts - T_l))^{(1/1-k)} = (0.441)^{1.20} = 0.374$

$f_s = 1-(T_s-T/T_s-T_l)^{(1/1-k)} = 1- 0.374 = 0.626 = 62.6\ \%$

From Eq.3.1, the solid fraction at 610^0C is found as below

Ts – T = 545.5^0C - 610^0C = -64.5^0C

$(Ts - T) / (Ts - T_l) = -64.5^0C / -100.8^0C = 0.639$

$((Ts - T) / (Ts - T_l))^{(1/1-k)} = (0.639)^{1.20} = 0.586$

$f_s = 1-(T_s-T/T_s-T_l)^{(1/1-k)} = 1- 0.586 = 0.414 = 41.4\ \%$

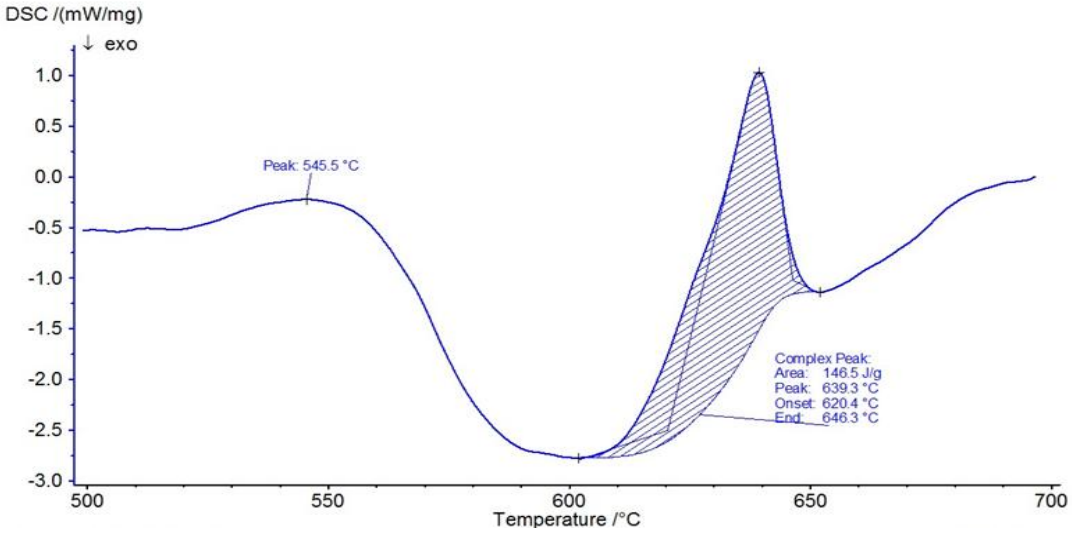

Fig.3.3 DSC curve for the semi-solid alloy AA2017

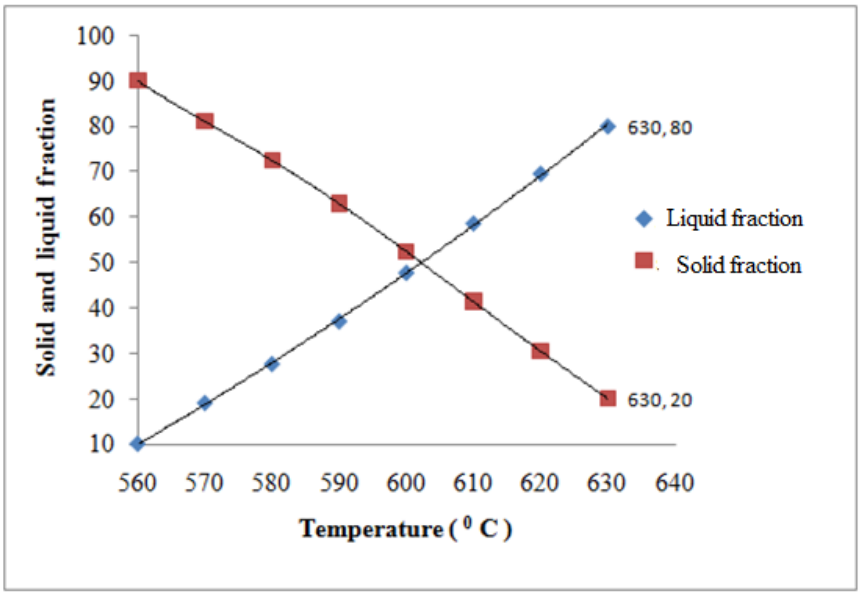

Fig.3.4 Relationship between the temperature and percentage of solid fraction

3.4 Thixo extrusion tests

An electric resistance furnace with two thermocouples to measure the temperature of furnace and billet was used to heat the billets. The operation of thixo extrusion was carried out on a hydraulic press. Cylindrical billets of size 15 mm diameter and 15 mm height were placed in an electric resistance furnace and heated from room temperature to the required extrusion temperature. To achieve homogenous temperature, the specimen was held at the forming temperature for 30 minutes and then the billets were extruded with a 50 ton hydraulic press. The experiments were performed at different temperatures namely 570^0C, 590^0C and 610^0C, different strain rates namely 0.16 s^{-1},0.18 s^{-1} and 0.2 s^{-1}, different approach angles such as 30^0, 45^0 and 60^0 and various area reductions such as 35%, 55% and 75%. Samples for microstructure study were prepared by standard metallurgical technique. The prepared samples were examined after etching with Keller's solution (solution of HCL, HF and HNO_3).The microstructure of the samples was observed under metallographic microscope. The complete experimental setup and the dies used for semi-solid extrusion are shown in the Fig .3.5

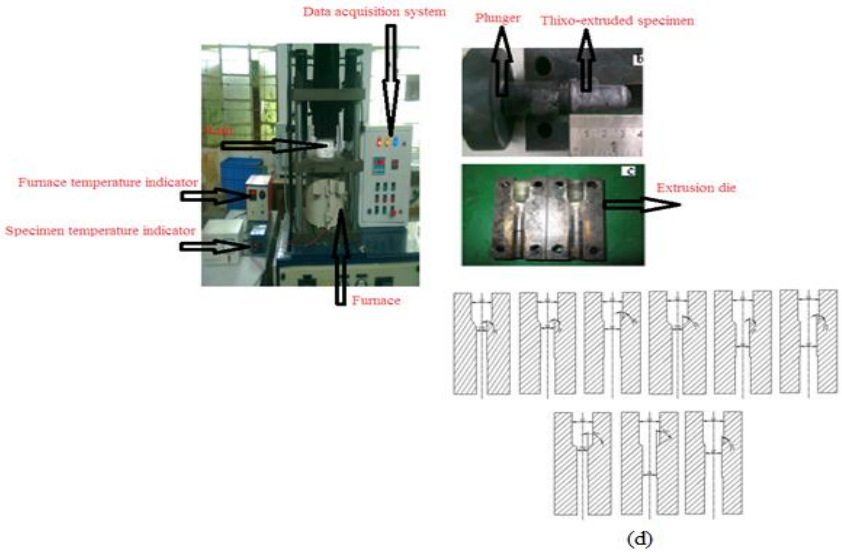

Fig. 3.5 Hydraulic press with furnace attachment (a) Hydraulic press with furnace attachment (b) Thixo-extruded specimen (c) Extrusion Die (d) Schematic diagram of dies

Note: All dimensions are in mm.

3.5 Microstructural investigation

The optical and scanning electron microscopy (SEM) techniques were used to study the microstructures of thixoextruded samples of AA 2017 alloy. Samples for microstructure study were prepared by standard metallurgical technique. The samples were cleaned by methanol in an ultrasonic cleaner to get clear and bright sample surface after polishing. The prepared samples were examined after etching with Keller's solution (solution of HCL, HF and HNO_3).

Fig.3.6 Optical microscope

3.6 Tensile testing

The tensile test is one of the most important and widely used material test as it provides data of basic mechanical properties regarding the strength of materials. The results from this test present the elastic and plastic behaviour of materials over complex loading histories. The tensile test was performed on PC 2000 Tensometer as shown in Fig.3.7.to obtain the standard material properties such as proof stress, ultimate strength and percentage reduction in area. The thixo-extruded specimen sample of AA 2017 alloy which is subjected to tensile test is shown in Fig.3.7

Fig.3.7 PC 2000 Tensometer

3.7 Finite element modelling of thixo-compression

The simulations were performed on cylindrical discs of size 15 mm diameter and 15 mm height. The discs were compressed between two dies at different temperature namely 570^0C, 590^0C and 610^0C and at different strain rates such as 0.16 s^{-1},0.18 $s^{-1}$and 0.2 s^{-1}. Axisymmetric analysis was performed as the shape of the specimen is axisymmtric. The solid fraction of the alloy in the initial stage of the experiment was assumed to be homogeneous. The material used was elasto-plastic and an Arrhenius type constitutive rule has been incorporated in the simulation software to model the flow curve for the alloy at the semi solid range. The material constants such as n, α, β, m and 'A' in the above relation have been evaluated from the semi-solid compression tests. The commercial software DEFORM 2D has been used to model the problem..

3.8 Finite element modelling of thixo-extrusion

The finite element based simulation software DEFORM 2D, has been used for the simulation of thixo- extrusion process of AA2017 aluminium alloy billets. Specimens of diameter 15 mm and height 15 mm were used for the simulation study. The bottom die was fixed. Axisymmetric analysis was performed because the shape of the specimen is axisymmtric. A friction coefficient value of m=0.4 was assumed between the top die and workpiece interface. The initial solid fraction was assumed as homogeneous. The material constants such as n, α,β, m and 'A' of AA2017 aluminium alloy evaluated from the mushy state compression tests were used as input variables in the constitutive relation. The constitutive equation developed has been given as input for relating the stresses and strains at various temperatures and strain rates.

CHAPTER 4

Simulation Studies on The Deformation Behaviour of AA2017 Alloy in the Semi-Solid State Using FEA

4.1 Introduction

The purpose of the present work is to study the deformation mechanism of AA2017 aluminium alloy in the semi-solid state through experimental and simulation methods. AA2017 is a hard to form metal in the cold state and the alloy loses some of its favourable qualities at high temperature. However, semi solid metal forming is one such method in which favourable properties are obtained even at high temperatures. As the mechanical behaviour and deformation mechanism of semi-solid metal is completely different from that of the solid state forming, it is necessary to investigate its nature at the semi solid range. To analyze the metal flow, the stress behaviour and the corresponding strain induced, extensive finite element analysis (FEA) based simulation studies have been performed. The commercial software, DEFORM 2D was used for the simulation. The flow behaviour was modelled by formulating an Arrhenius type constitutive relation.

4.2 Finite element modelling

The simulations were performed on cylindrical discs of size 15 mm diameter and 15 mm height. The discs were compressed between two dies at different temperature namely 570^0C, 590^0C and 610^0C and at different strain rates such as $0.16s^{-1}$, $0.18s^{-1}$ and $0.2s^{-1}$as shown in Fig. 4.1. Axisymmetric analysis was performed as the shape of the specimen is axisymmtric. The solid fraction of the alloy in the initial stage of the experiment was assumed to be homogeneous. The material used was elasto-plastic and an Arrhenius type constitutive rule of the form $\dot{\varepsilon} = A[(\sinh\ (\alpha\sigma)]^n \exp[-(Q)/(RT)]$ has been incorporated in the simulation software to model the flow curve for the alloy at the semi solid range. The material constants such as n, α, β, m and 'A' in the above relation have been evaluated from the semi-solid compression tests. The commercial software DEFORM 2D has been used to model the problem. A model for the upsetting experiment developed through the software package is shown in Fig 4.1.

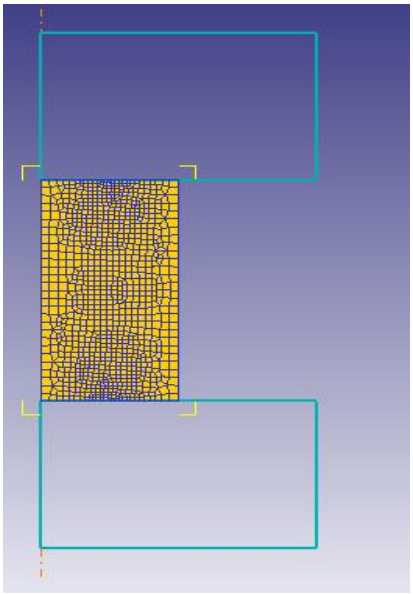

Fig.4.1 An upsetting model

DEFORM 2D uses constitutive equation of the type shown above to relate the strain rate, flow stress, and temperature. Depending on the type of stress that is developed, three types of flow rule (Mc Queen, H.J [2002] and N.D. Ryan [2002]) can be used to model the high temperature forming problems. The equation 4.1 shown below is used to model the flow stress

where the low stress state is experienced, equation 4. 2 is used where high stress state is experienced and equation 4.3 can be used for both the cases. In the present work, equation 4.3 has been used.

$$\dot{\varepsilon}\exp\left(\frac{Q}{RT}\right) = A'\sigma^{n'} \tag{4.1}$$

$$\dot{\varepsilon}\exp\left(\frac{Q}{RT}\right) = A''\exp(\beta\sigma) \tag{4.2}$$

$$\dot{\varepsilon}\exp\left(\frac{Q}{RT}\right) = A\,(\sinh\,(\alpha\sigma))^{n} \tag{4.3}$$

Where $\dot{\varepsilon}$ is the strain rate, A', A'', n', β, A (s^{-1}) and α (Mpa^{-1}) are constants, σ is the flow stress (MPa), 'n' is the stress exponent, 'R' is the universal gas constant (R = 8.314 J/mole K), 'T' is the absolute temperature and 'Q' is the activation energy. Activation energy indicates the deformation difficulty during plastic deformation. The value of 'Q' can be calculated by using the Eq. (4.4) shown below.

$$Q = R\left[\frac{\partial \ln(\dot{\varepsilon})}{\partial \ln\sinh(\alpha\sigma)}\right]_T \left[\frac{\partial \ln\sinh(\alpha\sigma)}{\partial\left(\frac{1}{T}\right)}\right]_{\dot{\varepsilon}} \tag{4.4}$$

The two terms on the right hand side of Eq.4.4 are the slopes of $\ln(\dot{\varepsilon})$-$\ln[\sinh(\alpha\sigma)]$ and $\ln[\sinh(\alpha\sigma)] - 1/T$ respectively.

4.3 Determination of material constants

The various constants used in the constitutive relations can be determined by performing different disc compression tests at various temperatures and strain rates. The deforming load and the subsequent reduction in height and increase in diameter of the test sample were noted after each stage of compression test. From the above measurements true stress and true strain of the deformed samples were calculated to draw the flow curve. The above compression tests were done for different temperatures and strain rates.

Figure 4.2 (a) shows the graph drawn between the ln (strain rate) and ln (true stress) and Fig.4.2 (b) shows the graph drawn between ln (strain rate) and true stress. The value of n' is the slope of the curve in Fig.4.2 (a) and measured at the minimum stress (corresponding to the temperatures of 590℃ and 610℃) and is found to be 0.87205. The value of 'β' is the

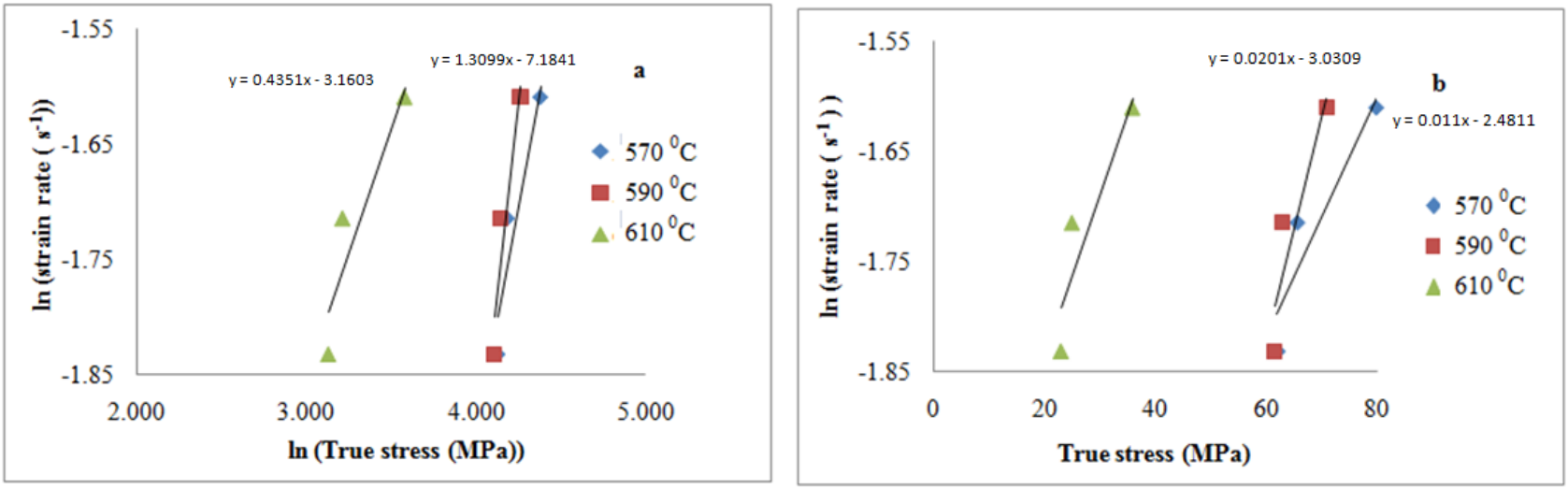

Fig.4.2 Effect of strain rate on true stresses: (a) ln (strain-rate) vs ln (True stress)
(b) ln (strain-rate) vs True stress

Table 4.1 Calculated values of (ασ) and sinh (ασ)

Strain rate(s^{-1})	**Stress in Mpa**			**ln(strainrate)**			**ln(stress)**			**(ασ)**			**Sinh (ασ)**		
	570^0C	590^0C	610^0C	570^0C	590^0C	610^0C	570^0C	590^0C	610^0C	570^0C	590^0C	610^0C	570^0C	590^0C	610^0C
0.16	62	61	23	-1.8326	-1.8326	-1.8326	4.12891	4.11087	3.13549	1.10742	1.08763	0.41009	1.348	1.315	0.422
0.18	66	63	25	-1.7148	-1.7148	-1.7148	4.18464	4.14313	3.21888	1.1709	1.12329	0.44575	1.457	1.375	0.461
0.2	80	71	36	-1.6094	-1.6094	-1.6094	4.38203	4.26268	3.58352	1.4264	1.26593	0.64188	1.962	1.632	0.687

slope of the curve in Fig.4.2 (b) measured at the maximum stress (corresponding to the temperatures of 570℃ and 590℃) and is found to be 0.0155. The value of the stress multiplier, α is 0.0178 and is calculated from the relation $\alpha = \beta / n'$.

Figure 4.3 has been drawn between ln (strain rate) and ln (sinh (ασ)). The value of n is the slope of the curve, and is found to be 0.614. Figure 4.4 has been drawn between ln (sinh (ασ)) and 1/T. It is found that the stresses increases with increase in the strain rate and it decreases with increase in temperature at any particular strain rate. Values of the first term on the right hand side of Eq.4.4 are determined from the slope of the graph drawn between ln(strain rate) and ln(sinh(ασ)) relation and the average slope value is equal to 0.614, whereas the second term corresponds to the value of the Q / R n. The value of Q / Rn is found from the curves in Fig. 4.4 which are drawn between $\ln[\sinh(\alpha\sigma)]$ and $1/T$ and the average value is found to be 20252. Thus, the deformation activation energy for the material is found to be 103.382 KJ.

4.4 Zener-Holloman parameter, Z

The relation between the constitutive equation and Zener-Hollomon parameter, Z is stated as

$$Z = \dot{\boldsymbol{\varepsilon}} \exp\left(\frac{Q}{RT}\right) = A[\sinh\ (\alpha\sigma)]^n \tag{4.5}$$

The Z-values are related to the stress, and thus the deformation of the material. It combines the deformation variable, strain rate and temperature through an Arrhenius type function with the activation energy, 'Q'. It is a temperature- compensated strain rate. In the present problem, the values of ln (Z) were calculated at different temperatures such as 570^0C, 590^0C and 610^0C and at different strain rates namely 0.16 s^{-1}, 0.18 s^{-1} and 0.2 s^{-1} using Eq.4.5. The values of ln (Z) thus calculated are given in Table 4.1. It is noticed that the value of ln (Z) decreases as the temperature increases at constant strain rate and it increases as the strain rate increases at constant temperature.

By using equation (4.5) the expression for the strain rate is obtained as

$$\dot{\varepsilon} = A[(\sinh\ (\alpha\sigma)]^n \exp[-(Q)/(RT)] \tag{4.6}$$

On substitution of the values for A, n, α, and Q the constitutive equation of strain rate for AA2017 alloy is expressed as

$$\dot{\boldsymbol{\varepsilon}} = 378333.2[(\sinh\ (0.017\sigma)]^{\mathbf{0.614}} \exp[-(103.38)/(RT)] \tag{4.7}$$

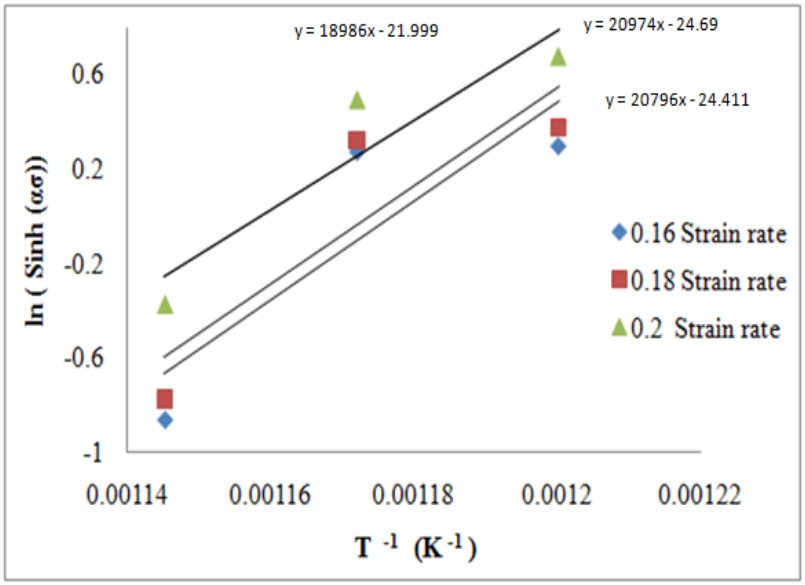

Fig.4.4 Variation of stress with deformation temperature ln (Sinh (ασ)) Vs 1/T

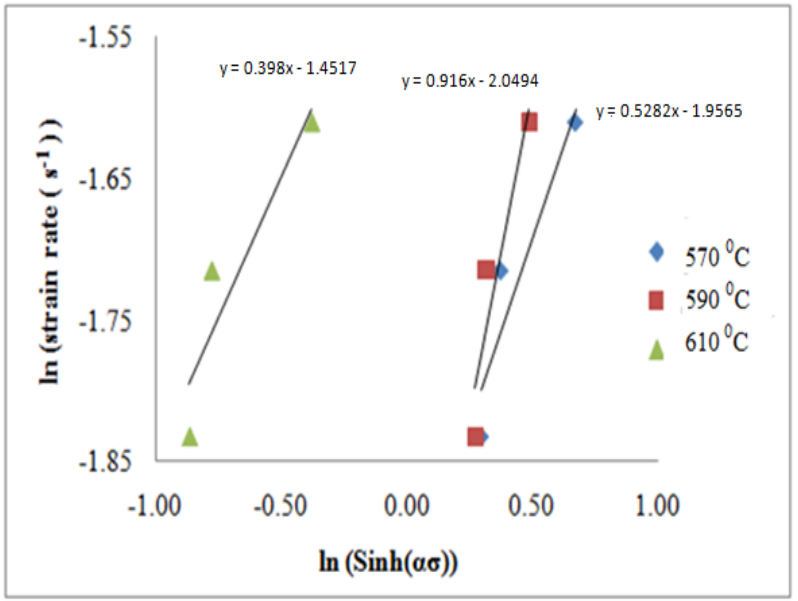

Fig.4.3 Relationship between ln (strain rate) and ln (sinh(ασ))

Table 4.2 Calculated values of (**Q**/RT**)** and exp(Q/RT)

ln (sinh (ασ))			**n ln (sinh(ασ))**			**Temperature**	**(Q/RT)*1000**	**exp(Q/RT)**
570^0C	590^0C	610^0C	570^0C	590^0C	610^0C			
0.29867	0.27392	-0.8635	0.18338	0.16819	-0.5302	570^0C	14.9249097	3032536
0.37665	0.31836	-0.7751	0.23126	0.19547	-0.4759	590^0C	14.5750319	2137253
0.67384	0.48993	-0.3756	0.41374	0.30082	-0.2306	610^0C	14.2411825	1530619

Table 4.3 Calculated values of A and Z

	Ln A=ln(Z)- n ln (sinh(ασ))			**A**				**strain rate(s^{-1})**	**Z**		
	0.16 s^{-1}	0.18 s^{-1}	0.2 s^{-1}						570^0C	590^0C	610^0C
570^0C	12.9089	12.5788	12.9417	403908.5553	289023.6	416146.7	369692.9533	0.16	485206	341960	244899
590^0C	12.9743	12.6648	12.6648	433153.4329	316399.1	316399.1	397660. 6961	0.18	545856	384706	275511
610^0C	12.9088	13.0023	12.8624	401006.9963	443429.5	385526.8	367645.9396	0.2	606507	427451	306124
				Average			378333.1964				

The hyperbolic sine equation is used to find the flow stress (K.P.Raoand and E.B. Hawbolt (1992), H. Mirzadeh and A. Najafizadeh (2010), Y.C. Lin et.al. (2008), S. Mandal et. al. (2009)). From equation 4.5, the flow stress of the material at a given strain can be obtained as follows

$$Z = A[\sinh(\alpha\sigma)]^n$$

$$Z/A = [\sinh(\alpha\sigma)]^n$$

$$(Z/A)^{1/n} = \sinh(\alpha\sigma)$$

$$\sigma = 1/\alpha\,[\sinh^{-1}(Z/A)]^{1/n}$$

After using sine hyperbolic function and by expanding the function the following expression can be obtained

$$\sigma = 1/\alpha \ln\{(Z/A)^{1/n} + [(Z/A)^{2/n}+1]^{1/2}\} \quad (4.8)$$

On substitution of the values for n and α, the constitutive equation of flow stress for AA2017 alloy is expressed as

$$\sigma = 56.179 \ln\{(Z/A)^{1.628} + [(Z/A)^{3.257}+1]^{1/2}\} \quad (4.9)$$

Eq. (4.5) can be modified to know the relation between the ln (Z) and $\ln[\sinh(\alpha\sigma)]$. Taking the natural logarithm on both sides of the Eq. (4.5) yields

$$\text{Ln } Z = \ln A + n\{\ln[\sinh(\alpha\sigma)]\} \quad (4.10)$$

From Eq. (4.10), it can be observed that a linear relationship exists between ln (Z) and $\ln[\sinh(\alpha\sigma)]$ and the plot is shown in Fig.4.5.

Table 4.4. Strain rate and values of ln (Z) at different temperatures

	ln(Z)		
Strain rate (s^{-1})	**570 ^{0}C**	**590 ^{0}C**	**610 ^{0}C**
0.16	13.08	12.74	12.40
0.18	13.20	12.85	12.52
0.2	13.31	12.96	12.63

The finite element studies performed in this present work were done by incorporating the constitutive relations derived as explained above and are given in equations 4.6- 4.10.

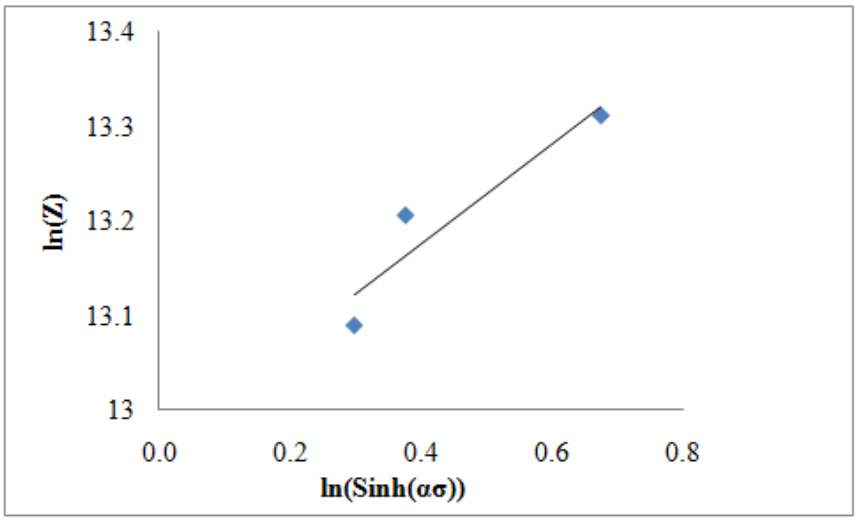

Fig.4.5 The relationship between ln (Z) and ln[sinh$(\alpha\sigma)$]

4.5 Relationships between stress and strain during semi-solid compression

The true stress - strain curves of thixotropic compression at different deformation temperatures (570^{0}C, 590^{0}C and 610^{0}C) and under various strain rates (0.16 s^{-1}, 0.18 s^{-1} and 0.2 s^{-1}) are shown in Fig. 4.7. It could be seen that the stress required for deforming the specimen increases rapidly initially and then it decreases in a smooth manner. The stress reached a maximum when the strain was approximately 0.2. The material in the mushy state acts more like a liquid or viscous material than a solid or an elastic material.

In compression forming of mushy state, at high temperatures, it was observed that the surface of the specimen breaks away during compression. This may be due to the flow of liquid towards the surface of the specimen. A sample cracked in the tip is shown in Fig 4.6.

Fig. 4.6 Mushy state compressed sample at 610^{0}C and at a strain rate of 0.2 s^{-1}

4.6 Effect of temperature on the deformation behaviour

The tests were conducted at different deformation temperatures. Fig.4.7 (a) shows the true stress-strain curve for the samples deformed at different temperatures. With increase in temperature, the liquid fraction of the samples increased, and the samples mostly flowed between patches of solid particles and partially slided under the deforming load. But, at low temperatures, the sample will be more of solid particles and a very scarce quantity of liquid pockets will be found randomly in the solid matrix. Hence, the deformation behaviour will be more of sliding between neighbouring solid particles and hence the load required to deform the samples will be more. This is obvious from the chart shown in Fig.4.7 (a). A microstructural evaluation conducted on the deformed samples revealed elongated grains for the samples with high solid fraction and spherical and evenly distributed grains for samples deformed with high liquid fraction. To validate the above claims, the effective strain plots on the simulated samples were analyzed. Figures 4.8 and 4.9 show the effective strain values for different height reductions.

The strain plot noted for 40 percent reduction showed a lengthy dead metal zone area for the samples with low solid fraction. This is due to the presence of high liquid content in the sample, due to which the samples without undergoing much deformation has flowed freely across the pressing die. The effective strain value for the sample with high solid fraction was high and the plot revealed the presence of high straining at the interface between the die and the sample. At higher reductions, the dead metal zone at the interface of the sample and the die disappeared for the simulation conducted with a solid fraction of 41 %. However, the effective strain was 0.8 for this case and the strain distribution was more or less even. However, for the sample with a solid fraction of 81 %, the effective strain value was 1.34 and the distribution of strain was heavy and was found throughout the sample. This explains the presence of elongated grains for samples deformed with higher solid fractions and the presence of round and evenly distributed grains for samples deformed with low solid fraction. Figure 4.10 shows the microstructures of samples compressed at different solid fractions.

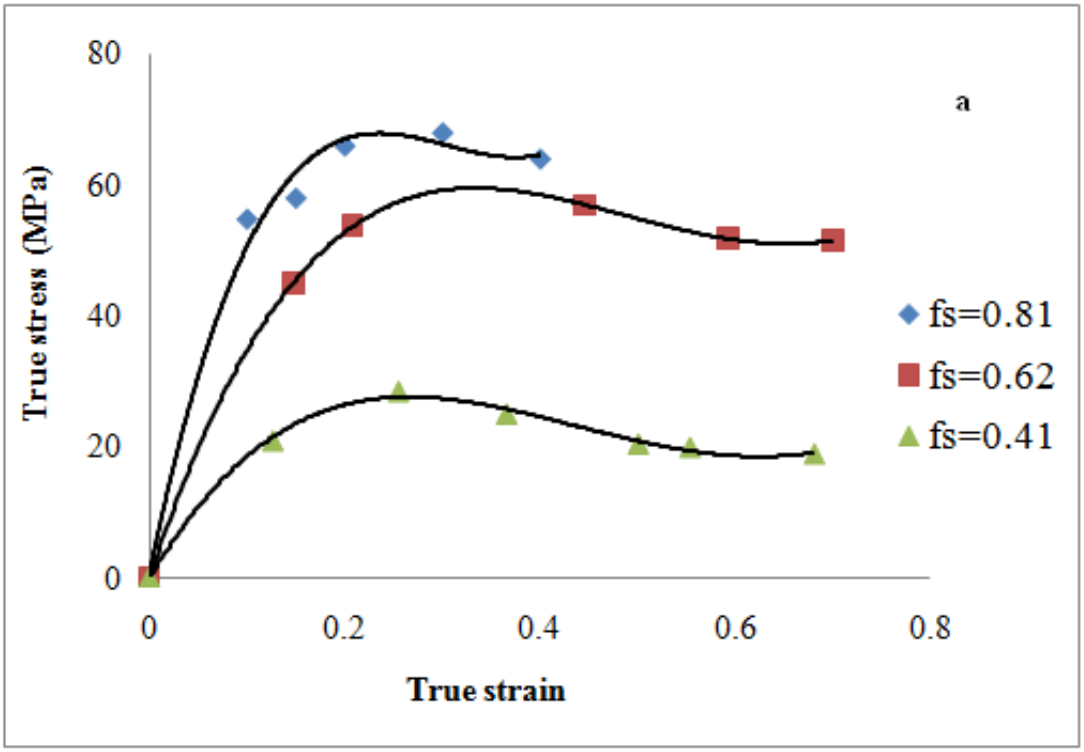

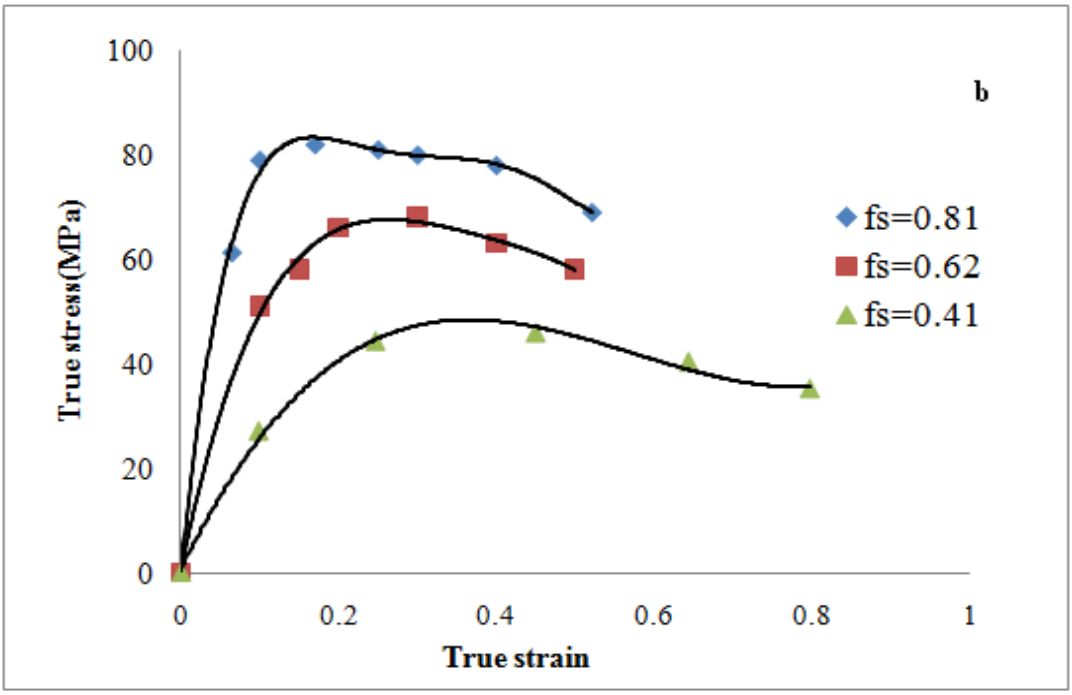

Fig.4.7 Relationship between true stress and true strain at (a) 0.16 s^{-1} strain rate and (b) 0.2 s^{-1} strain rate

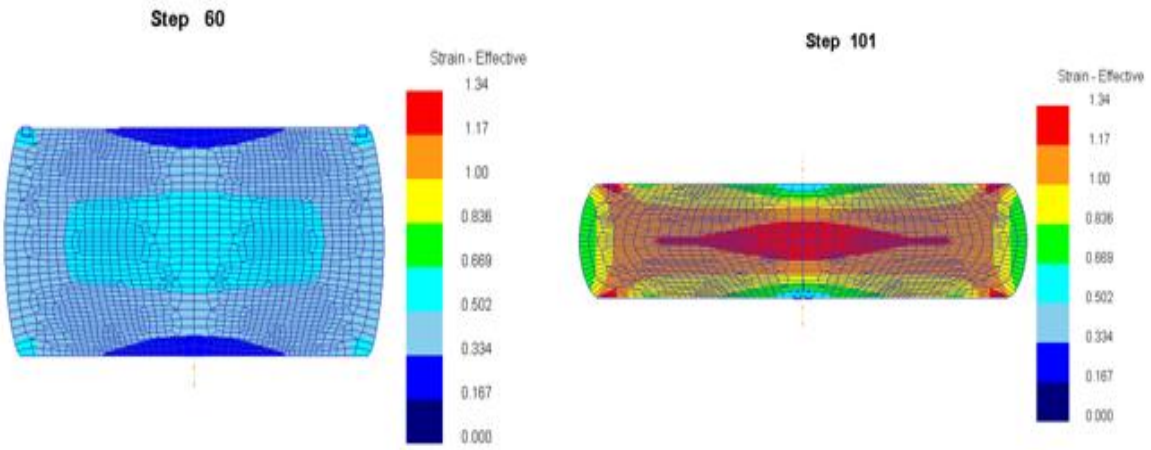

Fig.4.8 Effective strain at temperature 570^0C and 0.2 s^{-1} strain rate

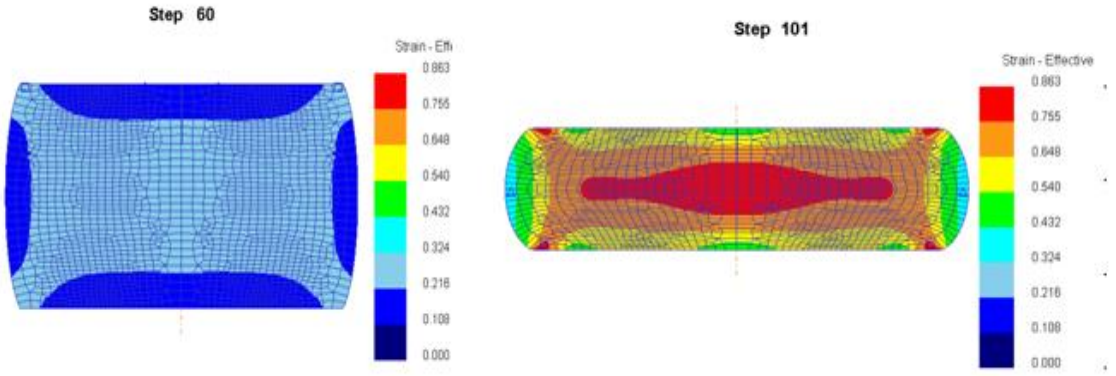

Fig.4.9 Effective strain at a temperature of 610^0C and at 0.2 s^{-1} strain rate

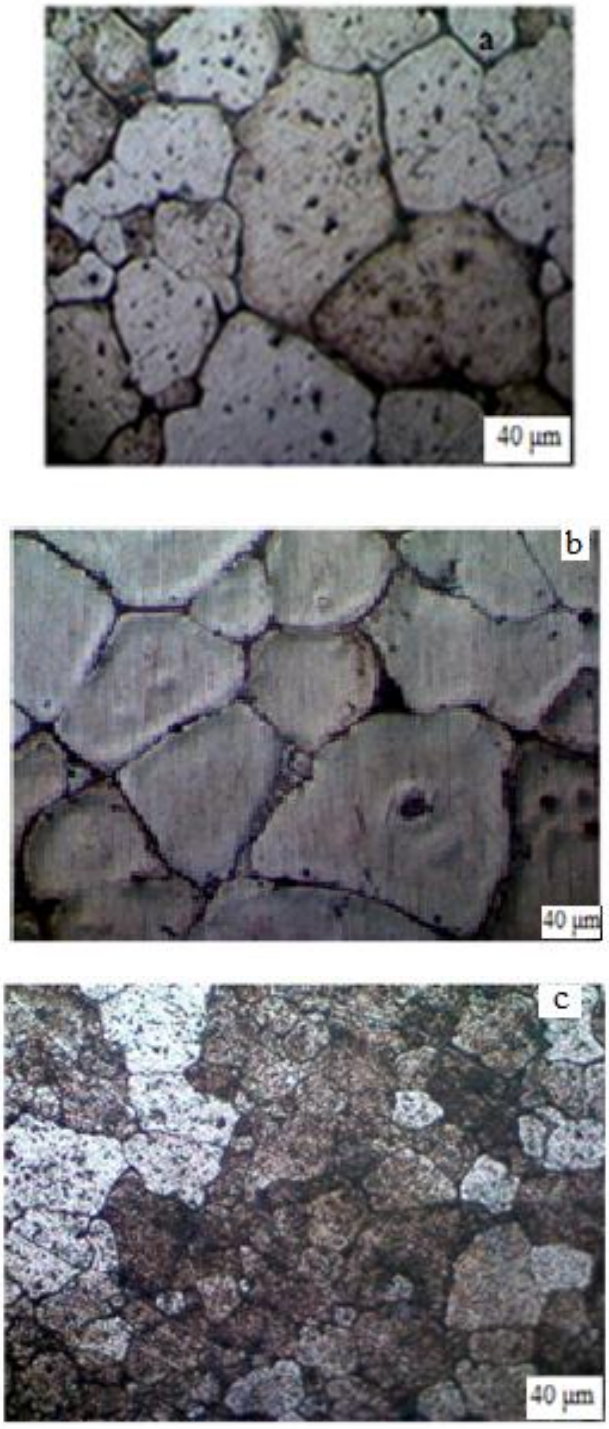

Fig.4.10 Microstructure of the samples compressed at different temperatures.
(a) 570^0C (b) 590^0C (c) 610^0C

4.7 Effect of strain rate on the deformation behaviour

In elevated temperature forming, strain rates play a major role in the deformation mechanism. Figure 4.11 shows the relationship between strain rate and true stress at two different temperatures namely 570^0C and 610^0C. Due to the presence of liquid surrounding the solid particles, the load required is less when compared to the samples deformed with large solid fraction. Also, the uniform elongation is wide and even for the sample deformed with large liquid fraction. However, the samples deformed with large strain rate showed dendrite structure. The samples deformed with a strain rate of 0.l8 s^{-1} showed round, spherical and evenly spaced grains. Figure 4.12 shows the microstructures of samples compressed at different strain rates.

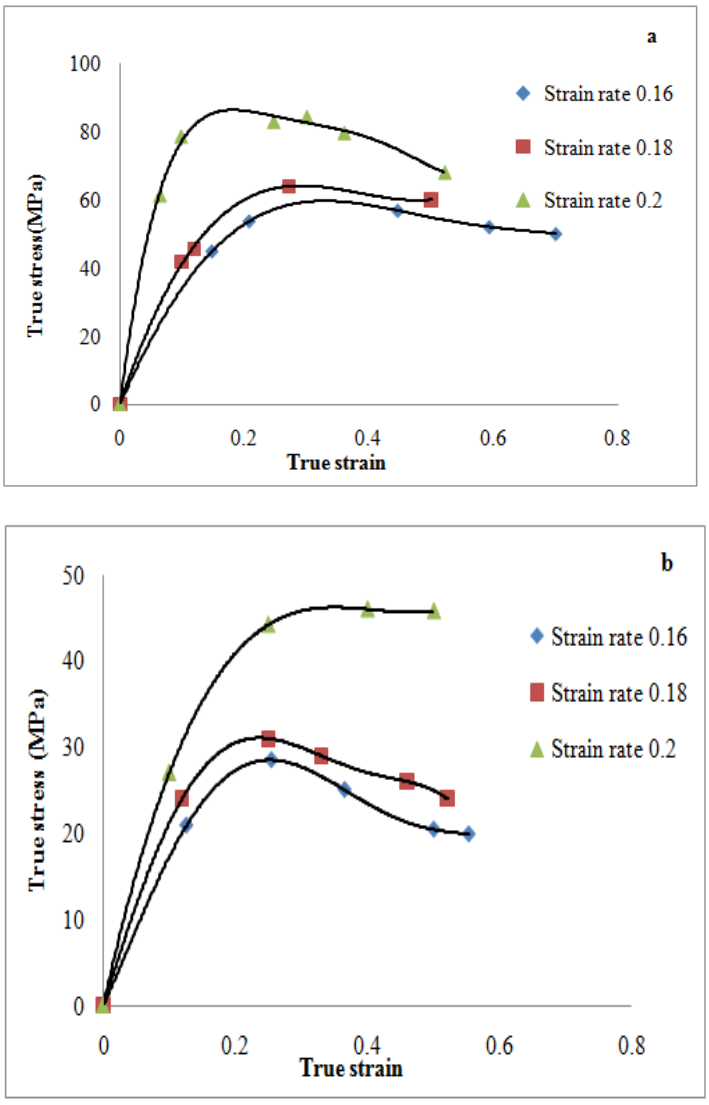

Fig.4.11 Relationship between true stress and true strain at (a) 570^0C and (b) 610^0C

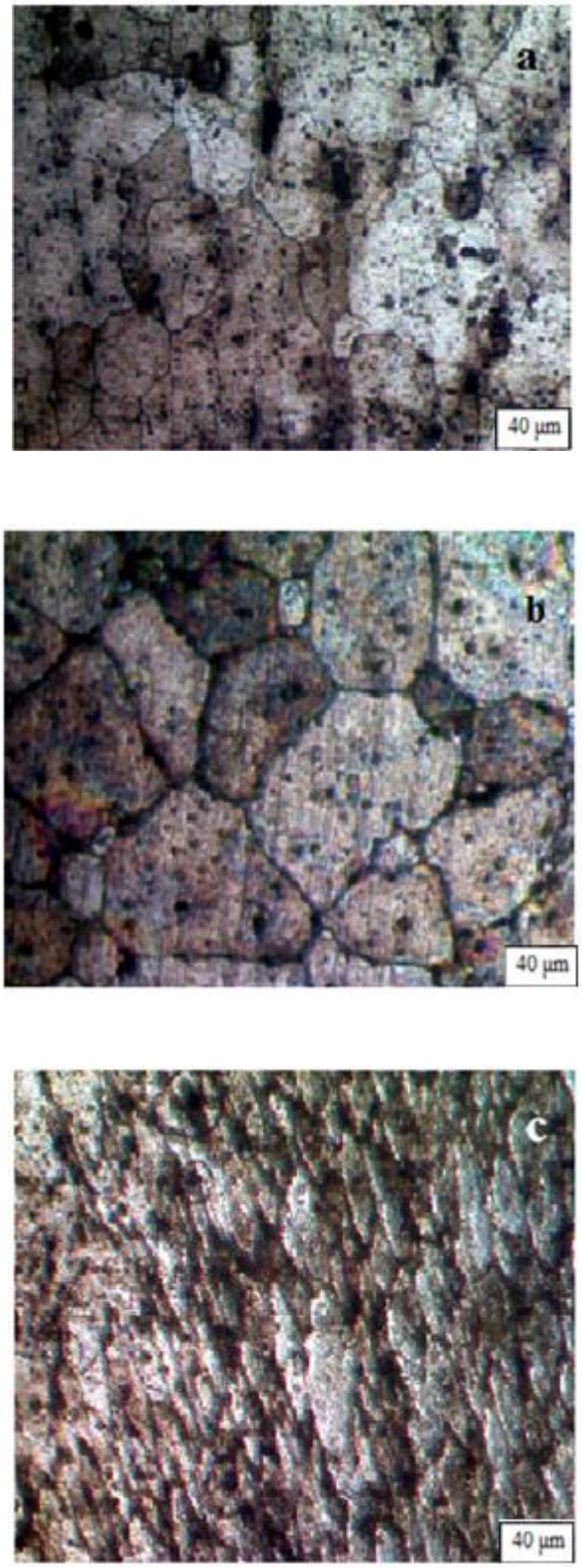

Fig.4.12 Microstructures of the samples compressed at different strain rates 0.16 s^{-1} (b) 0.18s^{-1} (c) 0.2s^{-1}C

4.8 Microstructures of semi-solid deformed samples

Figures 4.13-4.15 show the microstructures of the deformed AA2017 alloy samples after thixotropic compression at different temperatures and strain rates. At a low strain rate of 0.16 s^{-1}, the regular globular grains were flat and irregularly shaped, and are shown in Fig.4.13 (a) and Fig.4.14 (a). When the strain rate was increased, at lower deformation temperatures, due to the high solid fraction at these temperatures, the small liquid phase present in the semi-solid material at this temperature, were compressed and expelled out from the samples. Almost spherical grains were seen for the samples deformed at 590^0C and at strain rates of 0.18 s^{-1} and 0.2 s^{-1}. This is shown in Fig. 4.14 (b-c).

Figure 4.15 shows the microstructures of AA2017 alloy samples compressed at 610^0C. It is seen that the grains are more spherical than the samples which were compressed at lower temperatures and at a relatively low strain rate of 0.16 s^{-1}. With the increase in strain rate, more inhomogeneous distribution of solid-liquid phase was observed and the same can be seen from Fig.4.15 (b) and Fig.4.15 (c). The liquid volume fraction increased at this temperature, and at lower strain rates, the liquid phase had sufficient time to flow between the solid particles during the compression process. At higher strain rates, more liquid phase was entrapped in the specimens and the solid particles deformed accordingly.

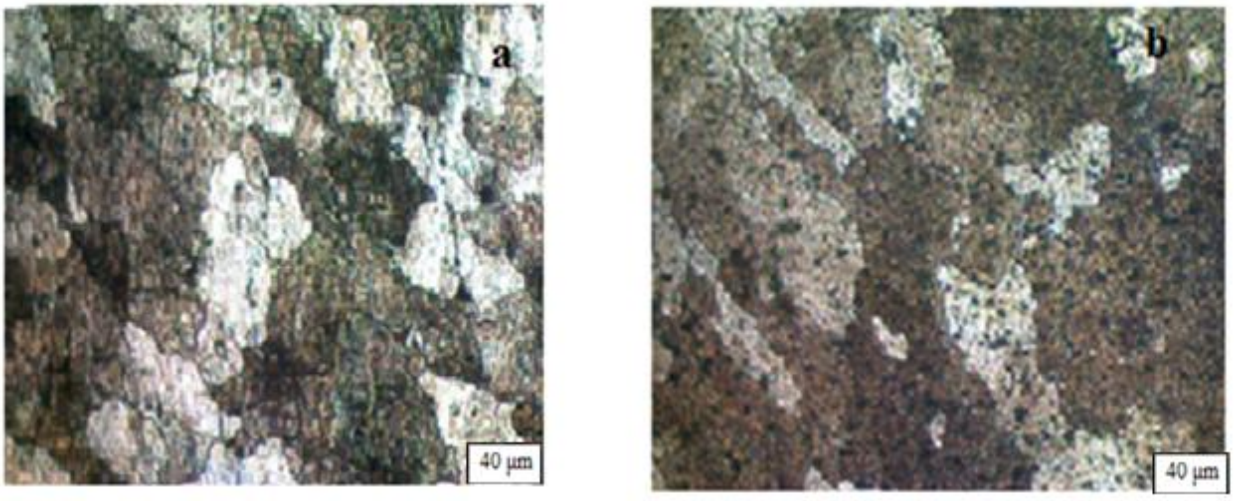

Fig.4.13. Microstructures of the samples compressed at 570^0C and at different strain rate of (a) 0.16 s^{-1} and (b) 0.2 s^{-1}

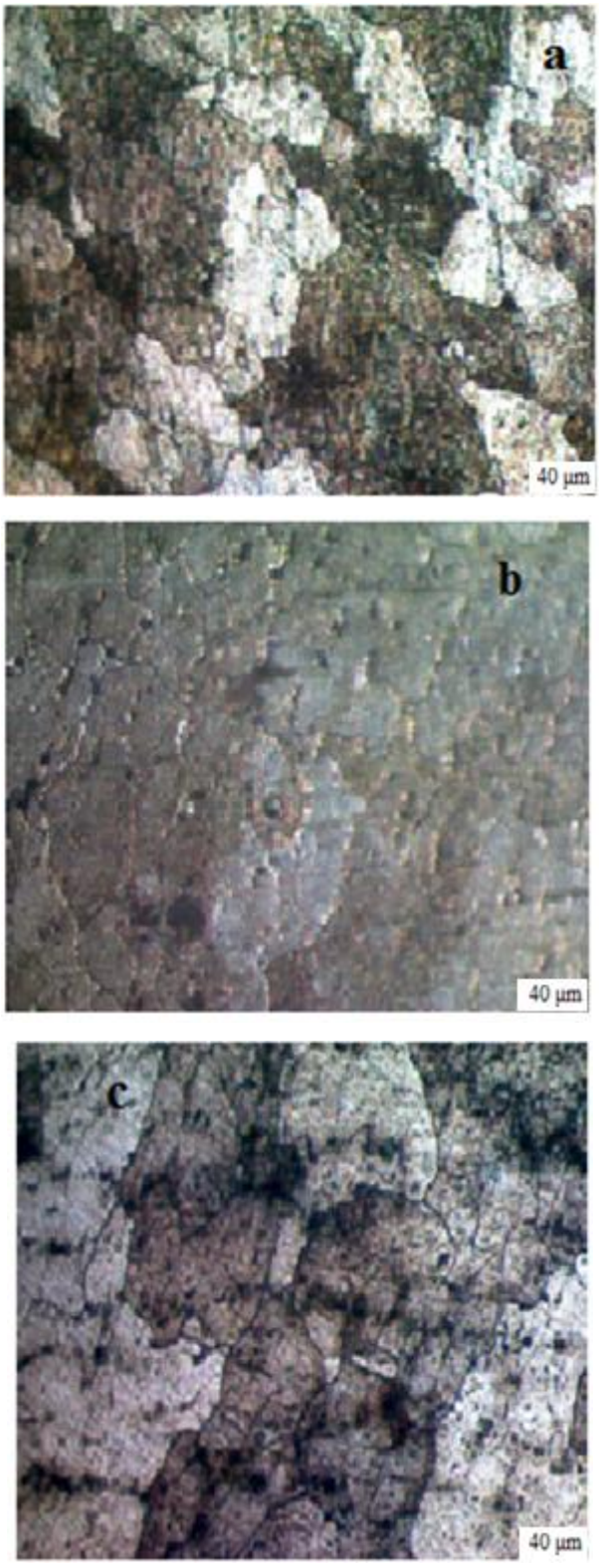

Fig.4.14 Microstructures of the samples compressed 590^0C and at different strain rate of (a) 0.16 s^{-1} (b) 0.18 s^{-1} and (c) 0.2 s^{-1}

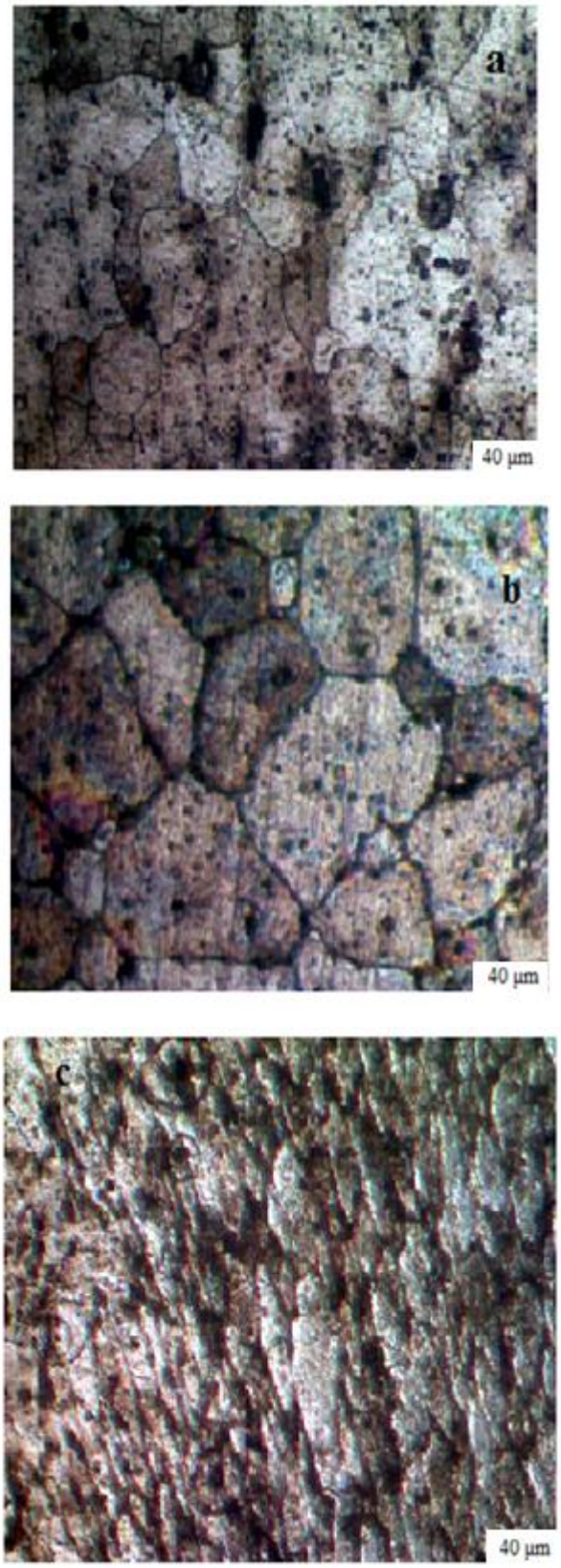

Fig.4.15. Microstructures of the samples compressed 610^0C and at different strain rate of (a) 0.16 s^{-1} (b) 0.18 s^{-1} and (c) 0.2 s^{-1}

4.9 Chapter Summary

The deformation characteristics of AA2017 alloy in the semi solid range has been investigated in the present chapter. Disc compression tests were performed between 570^0C and 610^0C and for different strain rates from 0.16 s^{-1} to 0.2 s^{-1}. The following conclusions have been drawn.

1. It was found that as the liquid fraction of the alloy increases, the samples mostly flowed between patches of solid particles and partially slided under the deforming load.
2. However, at lower liquid fractions, the samples mostly slided between neighbouring solid particles and hence the load required to deform the samples was more.
3. A microstructural evaluation conducted on the deformed samples revealed elongated grains for the samples with high solid fraction and spherical and evenly distributed grains for samples deformed with high liquid fraction.
4. The constitutive equation that was developed in the semi solid range simulated the semi-solid forming condition closer to the experimental and the relation thus formed is given by $\sigma = 56.179 \ln\{(Z/A)^{1.628} + [(Z/A)^{3.257}+1]^{1/2}\}$

CHAPTER 5

Experimental and Simulation Studies on the Thixo-Extrusion of AA 2017 Alloy

5.1 Introduction

The aim of the present study is to formulate a finite element based simulation model capable of simulating the thixo-extrusion process while extruding AA2017 alloy. An Arrhenius type constitutive relation involving the solid fractions and the strain rate has been used to simulate the thixo-forming process in DEFORM 2D, an FEA based simulation software. The experimental results were used to validate the claims made through the simulation study.

5.2 Constitutive relation for Thixo-forming

A series of mushy state compression tests have been conducted in the temperature ranging from 570^0C to 610^0C and at different strain rates namely 0.16 s^{-1}, 0.18 s^{-1} and 0.2 s^{-1}. An Arrhenius type relation of the form $\dot{\varepsilon} = A[(\sinh(\alpha\sigma)]^n \exp[-(Q)/(RT)]$ has been developed (C.Sellars [1966] and W.M.Tegart [1966]) and the detailed procedure followed in

developing the constitutive relation has been employed in chapter 4. The material constants such as A, α,β, and n, where 'α' is the stress multiplier, 'n' is the stress exponent, 'A' and 'β' the material constants, have been evaluated by performing disc compression tests at the above temperatures and strain rates. The deformation activation energy "Q" which indicates the degree of difficulty during plastic deformation is also calculated. The Zener-Hollomon parameter (Z value) which describes the effect of strain rate and temperature (T) on stress and microstructure during hot deformation of metallic materials has been calculated as well.

The equation that has been derived through the above mentioned procedure is given in Equation 5.1 below. This equation has been used in DEFORM 2D, as constitutive relation. Thus, the process has been simulated from the real time constitutive relation derived from the experiments.

$$\dot{\varepsilon} = 378333.2[(\sinh\ (0.017\sigma)]^{0.614} \exp[-(103.38)/(RT)] \qquad (5.1)$$

5.3 Results and discussion

To analyze the effect of each process parameter on the quality of extrusion product and on the extrusion load, nine different combinations of process parameters were chosen which are given in Table 5.1. Experimental and finite element simulation studies were performed for all the nine combinations and the results are tabulated in Table 5.2.

Table 5.1 Simulation combinations of thixo-extrusion process parameters

Simulation No	Temperature in (^{0}C)	Strain rate (s^{-1})	Approach angle in (^{0}.)	% Reduction in area(R.A)
1	570	0.16	30 ^{0}	35
2	570	0.18	45 ^{0}	55
3	570	0.20	60 ^{0}	75
4	590	0.16	45 ^{0}	75
5	590	0.18	60 ^{0}	35
6	590	0.20	30 ^{0}	55
7	610	0.16	60 ^{0}	55
8	610	0.18	30 ^{0}	75
9	610	0.20	45 ^{0}	35

5.3.1 Effect of solid fraction

Due to the presence of copper, the extrudability of AA2017 alloys is difficult and the alloys need high extrusion pressures. However, the alloy is extrudable at semi solid state due to the presence of globular grains at elevated temperatures. Thus, the solid fraction of the alloy is an important process condition for obtaining good products. However, the mechanical and metallurgical properties of the alloy depend on the amount of solid and liquid fractions of the alloy during the extrusion cycle. A mix of solid and liquid particles makes the solid particle to glide through the liquid matrix and makes it easy to form. However, too much liquid fraction at the end of the extrusion cycle results in cracking of the workpiece at the edge. It is preferable to have the workpiece with more liquid fraction in the initial stage of extrusion and more solid at the end of the extrusion cycle. To analyse the quality of product that can be achieved at different liquid and solid fractions, extensive finite element studies have been made with different solid and liquid fractions. The results have been verified with experimental verifications as well. Figure 5.1 shows the edge of the rod extruded at very high solid and liquid fractions. The microstructure of the alloy extruded at high liquid fraction shows globular grains as seen in Fig. 5.2.

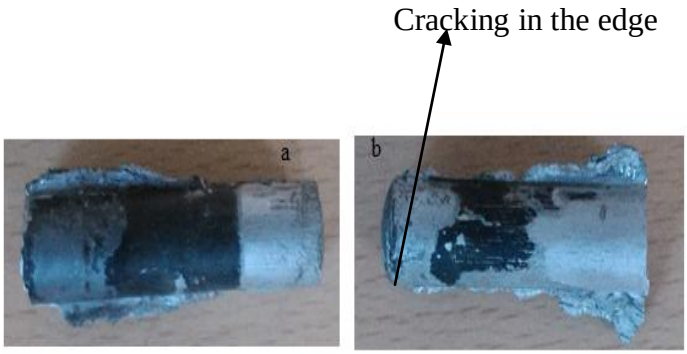

Thixo extruded specimens	Temperature in ^{0}C	Strain rate S^{-1}	Diameter in mm	Angle in degrees
	570	0.18	10	45
	590	0.16	7.5	45
	590	0.18	12.5	60
	590	0.2	10	30
	610	0.20	12.5	45

(C)

Fig.5.1 Thixo-extruded specimen at (a) 590^0 C (b) 610^0 C (C) Micrograph of extruded sample

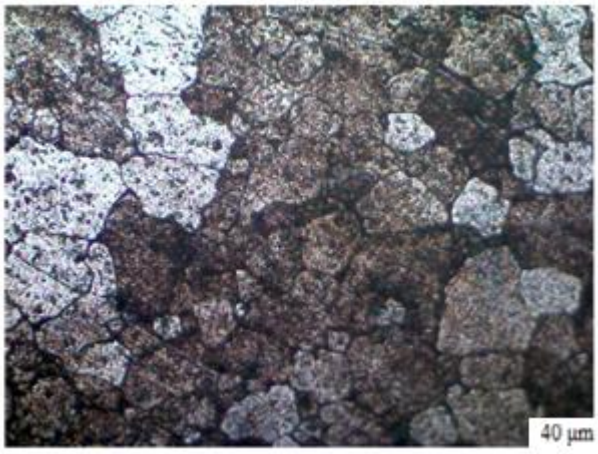

Fig.5.2 Microstructure of thixo-extruded sample extruded at 610^0 C shows globular grains.

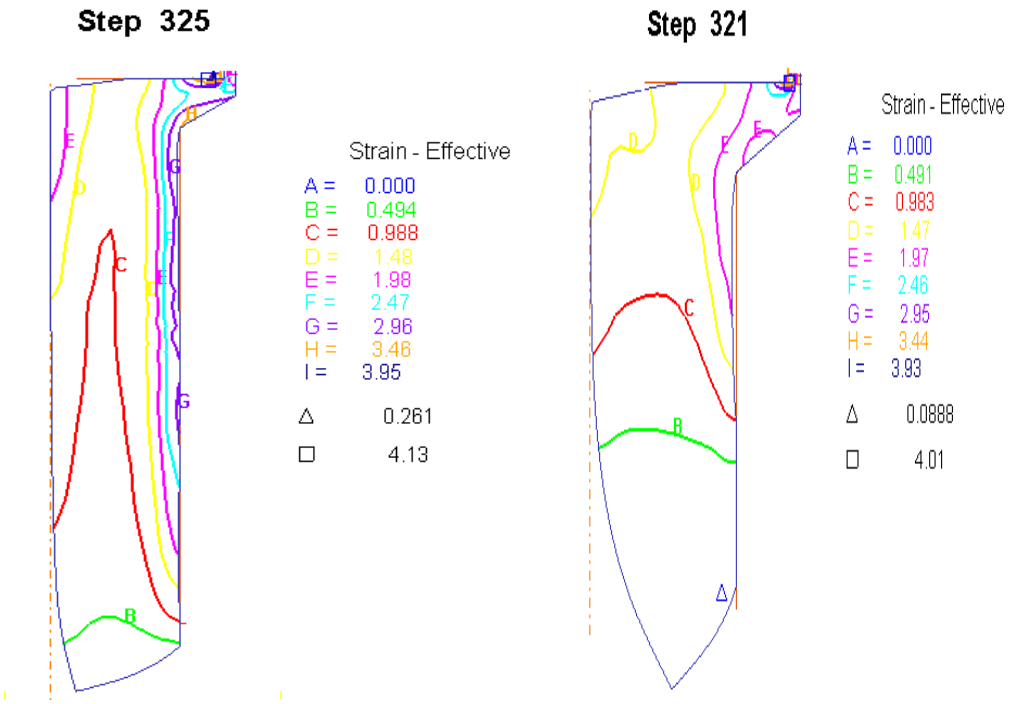

(a) (b)

Fig. 5.3 Distribution of effective strain at different solid fractions corresponding to the temperatures (a) 570^0C and (b) 610^0C for die angle of 60^0 and strain rate of 0.16 s^{-1}

The Fig.5.3 above shows the distribution of strain at 610^0 C and 570^0 C. The distribution of strain is found to be uniform at a temperature of 610^0 C due to the presence of more liquid fraction. The effective stress at 570^0 C (high solid fraction) was found to be 225 MPa and at low solid fraction (610^0 C) it was 152 MPa. This lower stress distribution is

attributed to the presence of more liquid particles embedded between the solid particles at high temperature, resulting in the solid particles gliding across the liquid medium, resulting in a flow containing liquid flow and solid particles gliding resulting in less stress.

5.3.2 Effect of strain rate

The strain rate with which the metal is extruded across the die is one of the most important factors that contribute to the success of the product. In the present study, the thixo extrusion study was performed with different strain rates namely, 0.16 s^{-1},0.18 $s^{-1}$and 0.20 s^{-1}. The Figure .5.4 below shows the effect of strain rate on the effective stress. The effective stress is found to increase with increase in the strain rate. The progression of the top die across the bottom die created primarily two zones of deformation namely dead zone and shear zone. The shear zone was found along the wall of the extrusion die. With increase in strain rate, the shear zone domain was found to increase and hence the effective strain increased as the strain rate was increased.

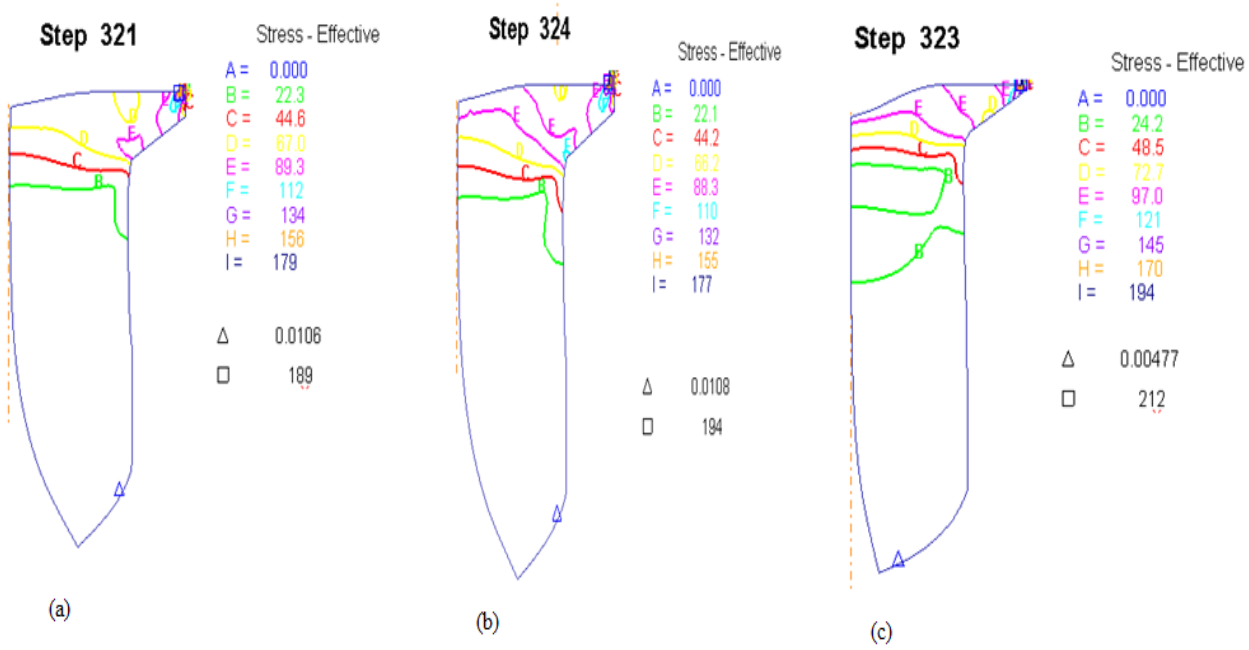

Fig. 5.4 Distribution of effective stress at 610^0 C, die angle of 60^0 and strain rate of (a) 0.16 s^{-1} (b) 0.18 s^{-1} and (c) 0.2 s^{-1}

Figure 5.5 (a-i) shows the microstructures of the alloy extruded at different strain rates ranging from $0.16s^{-1}$to$0.2\ s^{-1}$for different solid and liquid fractions. The microstructures revels that the inhomogeneity of the deformation increases with increase in strain rate at high solid fraction. At high liquid fraction at 610^0C the in homogeneity increases with low strain rate. Irrespective of the strain rate, the samples deformed at 590^0C were more homogeneous.

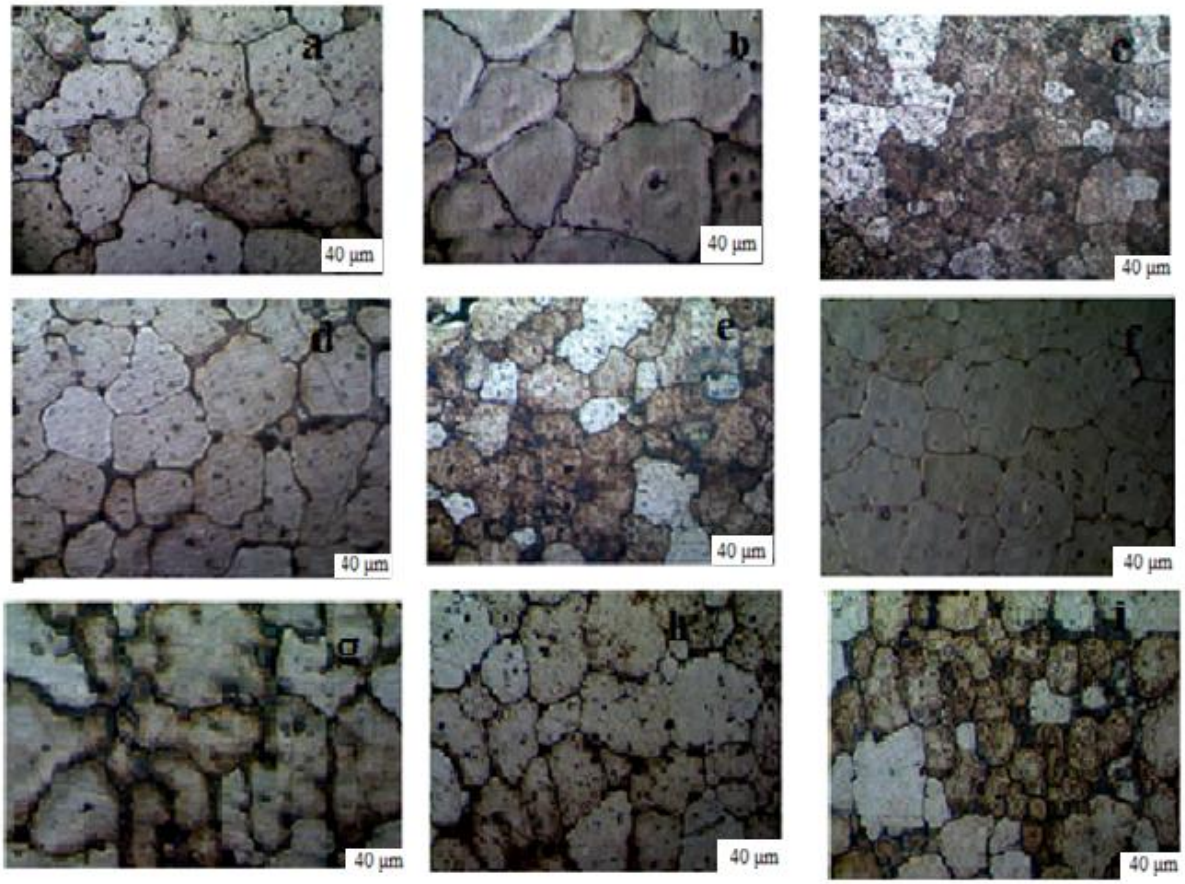

Fig.5.5 Microstructures of thixo-extruded samples at different temperatures and different strain rates

(a) 570^0C, 0.16 s^{-1} (b) $590\ ^0$ C, 0.16 s^{-1} (c) $610\ ^0$ C, 0.16 s^{-1} (d) 570^0C, 0.18 s^{-1} (e) 590^0C, 0.18 s^{-1} (f) 610^0C, 0.18 s^{-1} (g) 570^0C, 0.2 s^{-1} (h) 590^0C, 0.2 s^{-1} (i) 610^0C, $0.2s^{-1}$

5.3.3 Effect of approach angle

The approach angle of the die facilitates the heated metal to move along the die wall. The variation in the approach die angle creates different frictional conditions on the interface of the wall and the metal. The effective strain is found to be less for the metal extruded with a die with 30^0 approach angles and it is more for the die with 60^0 approach angles. A low effective strain implies that the metal being pressed is stronger than the alloy which has undergone higher strain. This implies that a narrower die is required to produce a stronger alloy. Thus, along with higher solid fraction a narrower die produces alloy with higher strength. The variation of effective strain with the die approach angle is shown in Fig.5.6 and 5.7.

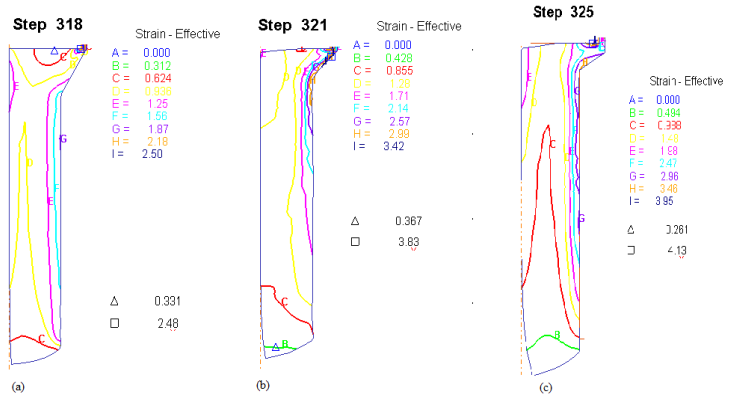

Fig.5.6 Distribution of effective strain at 570^0 C and strain rate of 0.16 s^{-1} for an approach angle of 30^0 (b) 45^0 and (c) 60^0

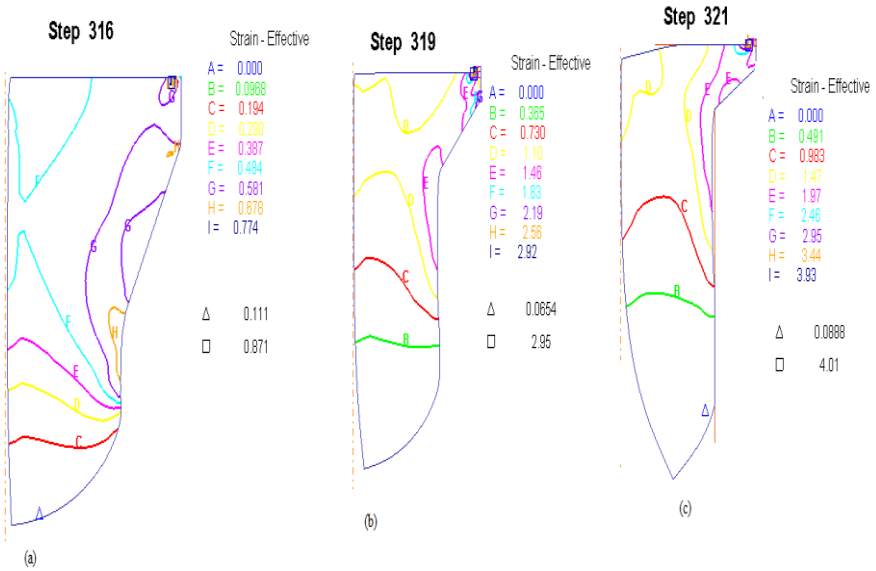

Fig.5.7 Distribution of effective strain at 610^0 C and strain rate of 0.16 s^{-1} for an approach angle of (a)30^0 (b) 45^0 and (c) 60^0

Comparing Fig.5.6 and Fig.5.7, It is observed that, the distribution of strain is uniform at higher liquid fraction and within the temperature ranges; the strain distribution is uniform on the samples extruded with higher approach angle.

Figure 5.8 shows the microstructures of the samples drawn at different temperatures and approach angles. It is evident from Fig.5.8 (a-d-g) that the in homogeneity increases as the approach angle is increased. As the temperature is increased to 610^0C, even for high approach angle a globular microstructure was found. However at this temperature more volume loss was experienced due to the fluidity of the sample. Irrespective of the approach angles, the sample deformed at 590^0C Fig.5.8 (b-e-h) resulted in a more homogeneous deformation.

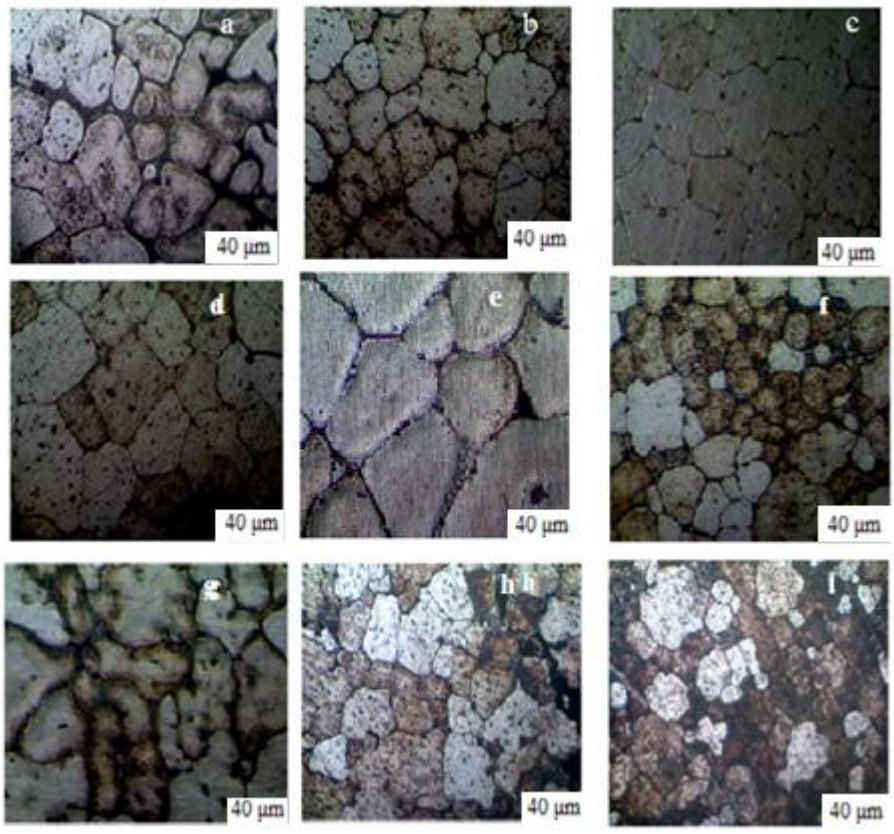

Fig. 5.8 Microstructures at different temperatures and different approach angles

(a) 570 ^{0} C, 30 ^{0} (b) 590 ^{0} C, 30 ^{0} (c) 610 ^{0} C, 30 ^{0}

(d) 570 ^{0} C, 45 ^{0} (e) 590 ^{0} C45 $^{0\,1}$ (f) 610 ^{0} C, 45 ^{0}

(g) 570 ^{0} C, 60 ^{0} (h) 590 ^{0} C, 60 ^{0} (i) 610 ^{0} C, 60 ^{0}

5.3.4 Effect of percentage reduction in area

The percentage reduction in area of the extrudate is proportional to the die diameter. The narrower the die, the stronger will be the alloy at the end of the extrusion stroke. The Fig.5.9 shows the plot of the effective stress for different percentage reductions. The effective stress is found to be more for the alloy produced in a die with narrow approach angle Fig.5.9 (a).

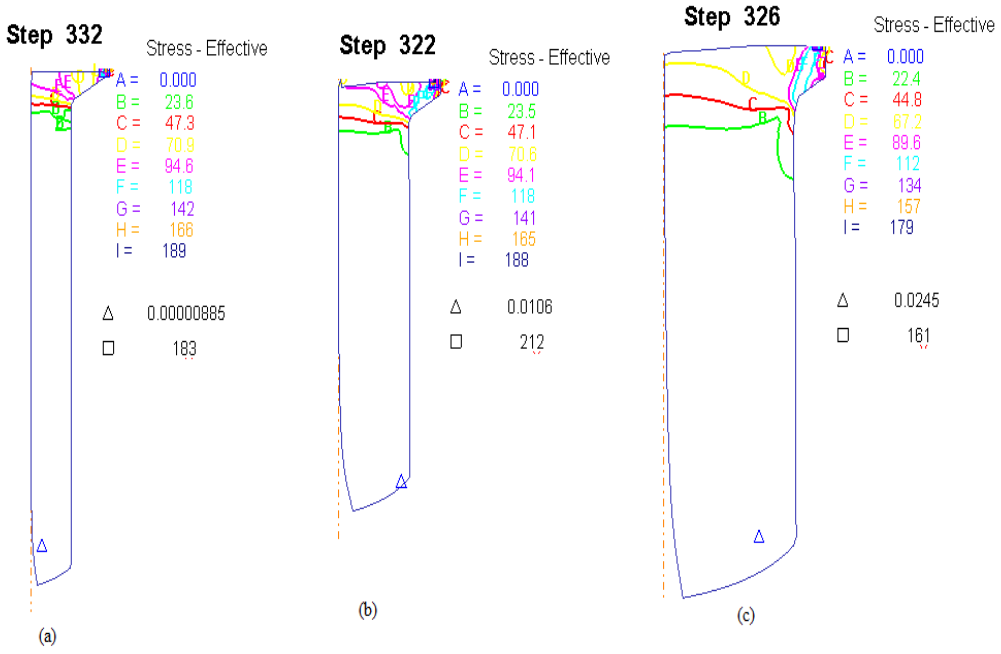

Fig. 5.9 Distribution of effective stress at 570^0 C, die angle of 60^0 and strain rate of 0.16 s^{-1}

(a) 75% (b) 55 % and (c) 35 %

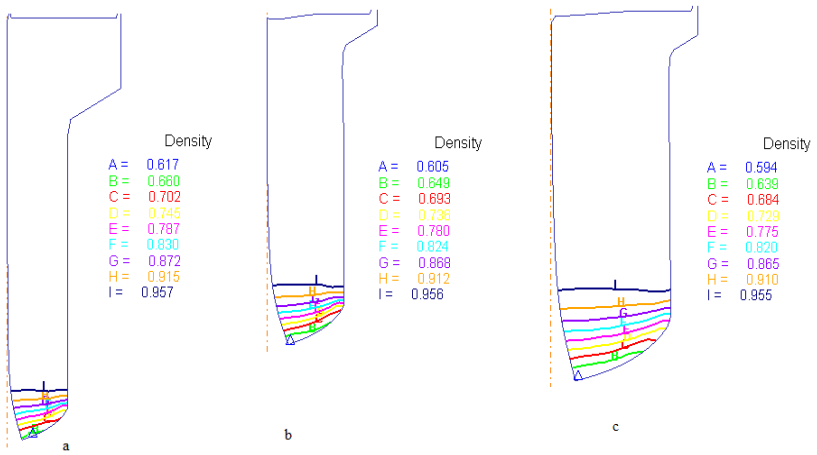

Fig.5.10 Density at 570^0 C die angle of 60^0 and strain rate of 0.16 s^{-1}(a) 75% (b) 55 % and (c)35%

It is observed from Fig. 5.10 that with increase in percentage reduction, the solid fraction increases. This shows that the amount of deformation is closely related to the densification of the solid phase. The densifications attained by the samples were measured by noting down their densities after the forming cycle. The large force with which the semi solid alloy is squeezed through the die has made the alloy to densify in the narrow exit portion of the extrusion die. This is the reason why the solid fraction increases with increase in percentage reduction. As it is evident from Fig.5.10, the solid fraction of the alloy increases as the semi solid slurry enters the converged portion of the die. Moreover, from Table 5.2, it is evident that the approach angle and the percentage reduction in area of the exit portion of the die plays a vital role in the deformation behaviour of the alloy. A narrow approach angle of die and increased percentage reduction in area increases the solid fraction and the deformation load. This shows that, at the exit portion of the die, due to the above factors, the solid fraction of the alloy increases and the alloy is extruded nicely. However, when the alloy is extruded out, due to liquid segregation and loss of pressure, small cracks were seen at the end of the workpiece. As the liquid phase flows heavily towards the free surface of die, liquid segregation happens and thus the alloy cracks. A rod that cracked due to fluid segregation is shown in Fig.5.11.

Fig.5.11 Thixo-extruded specimen cracked due to fluid segregation

Table 5.2 Simulated and experimental results

Simulation No.	Temperature in(^{0}C)	Strain rate(s-$^{-1}$)	Approach angle(^{0})	%Reduction area(R.A)	Simulation load in (kN)	Experimental load in (kN)	% loss of volume in experiments	% loss of volume in simulation
1	570	0.16	30 ^{0}	35	17	19	6	3
2	570	0.18	45 ^{0}	55	35	31	11	9
3	570	0.2	60 ^{0}	75	41	47	13	22
4	590	0.16	45 ^{0}	75	49	39	10	28
5	590	0.18	60 ^{0}	35	18	14	15	31
6	590	0.2	30 ^{0}	55	20	27	14	36
7	610	0.16	60 ^{0}	55	23	24	20	49
8	610	0.18	30 ^{0}	75	32	30	28	58
9	610	0.2	45 ^{0}	35	22	19	17	50

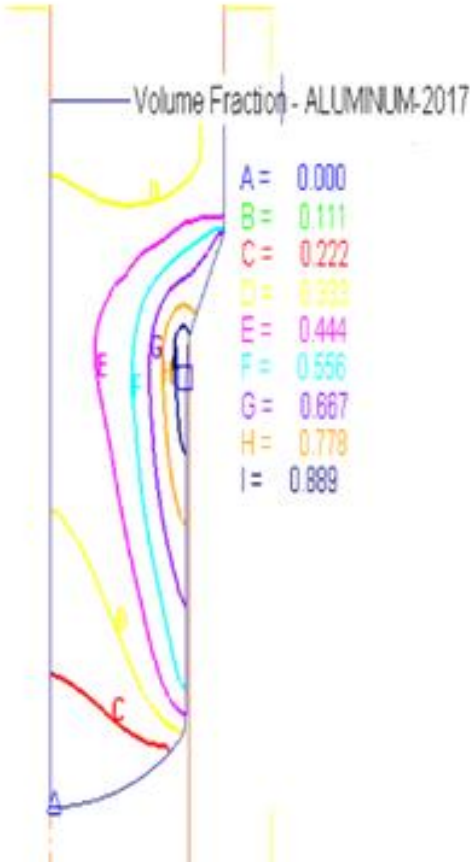

Fig.5.12 Distribution of volume fraction on a thixo-extruded sample

5.3.5 Effect of volume loss

Volume loss during thixo-forming is the loss in volume due to the excessive heating of the alloy. The semi solid slurry at the high temperature sticks to the dies, flows freely across the die to a smaller extend and loses its volume. From the simulation and the experiments, it is found that the volume loss is more at high temperatures. It is also observed that, for the same strain rate, the volume loss is more for the experiments performed with a low initial solid fraction. The distribution of volume fraction on a thixo-extruded sample is given in Fig.5.12. Thus, it can be concluded that the initial solid fraction is one of the important parameters responsible for volume loss and homogeneous deformation. Also it is observed that homogeneous deformation is obtained when the initial solid fraction is high.

5.4 Chapter Summary

An experimental and simulation studies have been performed on the thixo-extrusion of AA2017 aluminium alloy. The experiments were conducted at different temperature range from 570^0 C to 610^0 C, strain rates from 0.16 s^{-1} to 0.20 s^{-1} , approach angle of the die from 30^0 to 60^0 and percentage reduction in area from 35 to 75.

The following conclusions have been drawn.

1. The nature of effective strain has similar tendency as that of solid fraction. This shows that the amount of deformation is closely related to the densification of the solid phase.
2. Increasing approach angle of die and percentage reduction of area increases the effective strain and the deformation load. Approach angle and the percentage reduction in area at the exit portion of the die plays a vital role in the deformation behaviour of the alloy.
3. The simulation results and experimental results are close to each other.

CHAPTER 6

Fracture Criterion for Predicting Surface Cracking of AA2017 alloy in Semi-Solid Forming Process

6.1 Introduction

The aim of the present research work is to establish a fracture criterion for AA2017 alloy in the semi-solid state, capable of predicting the initiation of crack during the forming process and to optimize the processing parameters in such a way that the initiation of crack is delayed or avoided. For this purpose, a series of semi-solid compression tests were conducted over a wide range of process conditions in addition to finite element simulations. The procedure adopted and the critical damage factors found have been reported below.

6.2 Experimental Procedures

AA2017 alloy discs with 15 mm diameter and 15 mm height were used in this study. Its nominal chemical composition is 0.376 % Si, 0.345 % Fe, 3,33 % Cu, 0.66 % Mn, 0.65 % Mg, 0.180 % Zn, 0.034 % Cr, 0.076 % Ti , and 97.349 % Al (Wt %). Cylindrical specimens of 15 mm diameter and 15 mm in length were machined from a 16 mm diameter rod. Compression tests at temperatures of 570^0C, 590^0C and 610^0C and strain rates of 0.16 s^{-1}, 0.18 s^{-1}, and 0.2 s^{-1} have been performed on a 50 ton hydraulic press. Samples were held at

the test temperature for about 30 min and they were upset till the onset of crack. Compressed samples with their microstructures are shown in Fig 1.

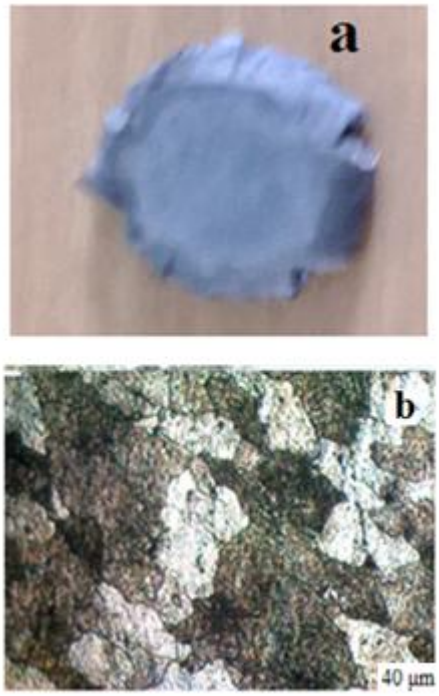

Fig.6.1 (a) Fracture samples and (b) Microstructures with internal cracks at temperatures at 570^0C

6.3 True stress-true strain curves

The true compressive stress-strain curves of AA2017 alloy are shown in Fig.2. The flow stress and the shape of the flow curve dependent largely on the temperature and strain rate. For all of the specimens, the stress of the specimens increased initially and then dropped due to recrystallization and softening mechanism. The softening mechanism was experienced for different strain rates and temperatures. These true stress-strain curves were used in DEFORM 2D for simulating the process. The simulations were performed on cylindrical discs of size 15 mm diameter and 15 mm height. The discs were compressed between two dies at different temperature namely 570^0C, 590^0C and 610^0C and at different strain rates such as 0.16 s^{-1},0.18 s^{-1} and 0.2. Axisymmetric analysis was performed as the shape of the specimen is axisymmtric. The solid fraction of the alloy in the initial stage of the experiment was assumed to be homogeneous.

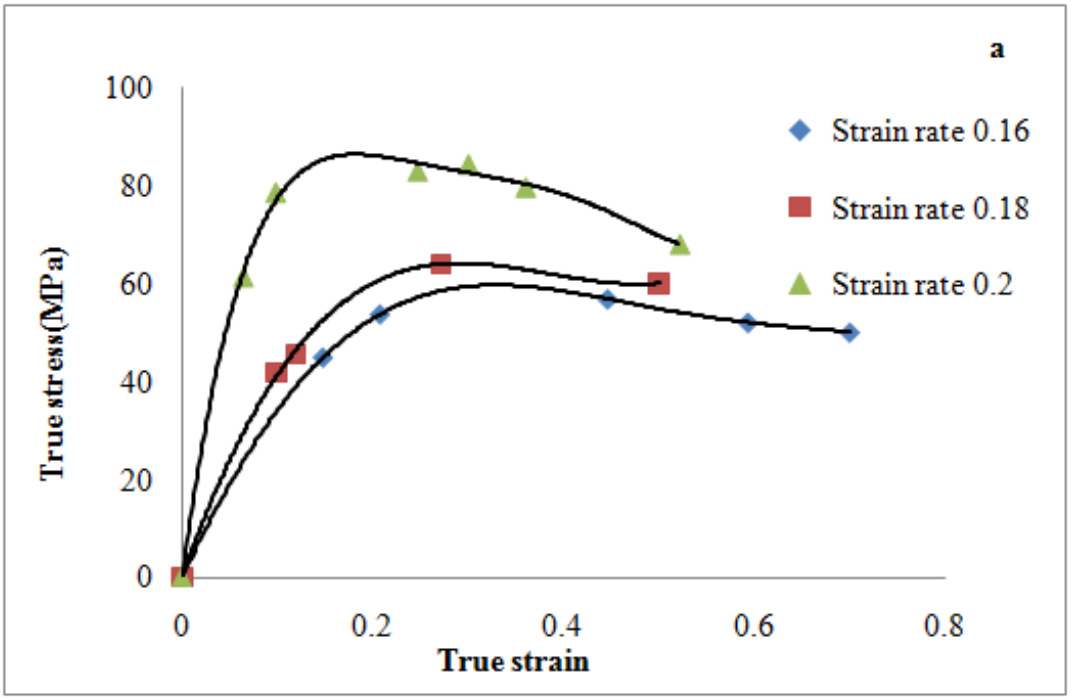

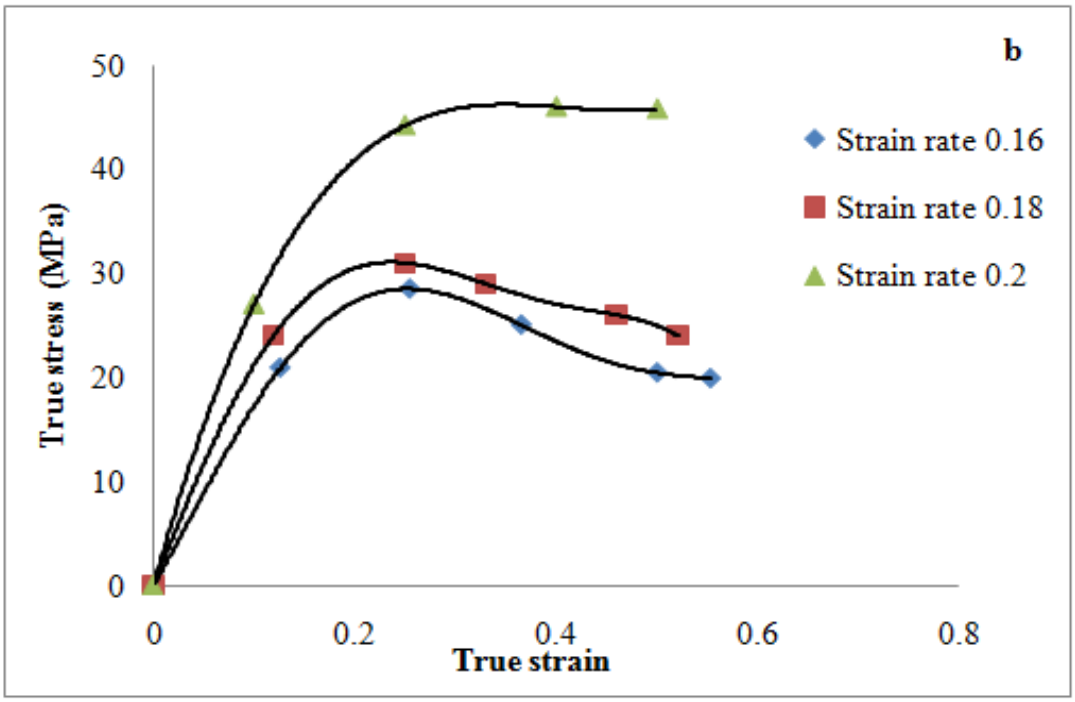

Fig.6.2 Compressive True stress-True strain curves at different temperatures of (a) 570^0C and (b) 610^0C

6.4 Critical damage factor of AA2017 alloy based on Cockcroft and Latham damage

6.4.1 Cockcroft and Latham damage

The simulation part of the present work has been performed on DEFORM 2D. DEFORM predicts the initiation of crack using a critical value of Cockcroft Latham based algorithm. The critical damage factor is the critical value of the stress that causes failure of the metal due to the accumulation of stress leading to fracture. Cockcroft and Latham developed a damage computation module based on cumulative damage theory that has been applied successfully to different loading conditions (Polmear I.J [1996] and Hatch J.E [1984]).Cockcroft and Latham expressed damage in plastic deformation as an amount of work that the ratio of maximum tensile stress σ_T to effective stress σ_{eff} carries out through the applied equivalent strain ε_f in metal working process. It is given mathematically as

$$\int_0^{\varepsilon f} \frac{\sigma_T}{\sigma_{eff}} d\varepsilon = C \qquad (6.1)$$

Where ε_f is the total equivalent strain at the end of forming process. The magnitude of C cannot exceed a maximum value of C max (critical damage factor) to failure. By comparison of C with C max, the danger of material to failure throughout the process is estimated

6.5 Results and discussion

6.5.1 Determination of critical damage factor for AA2017 alloy

The critical value of the damage factor depends on the mechanical and metallurgical state of the metal before and after the deformation process. As such, the factors such as the initial microstructure, alloy constituents, grain size, grain form, non-metallic inclusion content, hardness etc affect the critical damage factor and they are different for different initial and final conditions. In the present work, as the temperature, strain rate and solid and liquid contents change during the deformation process, these are the critical factors that affect the damage factor. In order to predict the incidence of surface fracture, the value of the Cockcroft-Latham equation expressed by means of Eq.(6.1) has been calculated for the different process condition chosen in the present investigation. Moreover, as the damage factor is calculated based on the cumulative

damage theory, the damage value of a preceding deformation step will be lesser than the current step and it will increase progressively till a critical value, beyond which the actual failure of the metal will happen. This progressive increase of damage factor has been assessed by calculating a incremental damage ratio (I_{DR}) given by the formula

$$I_{DR=}\ \Delta D/\ D_{accum.} \qquad (6.2)$$

Where $I_{DR=}\ \Delta D/\ D_{accu}$ is the ratio of the damage increment at a particular step (ΔD) to the immediately next step (accumulated value) (D_{accu}) (XIA Yu-feng et.al.[2010]).

The damage factor was retrieved from the simulation data up to the onset of failure. The simulation was performed by giving the true stress strain curve generated from the experiments as input in the constitutive relation. The incremental damage ratios have been calculated from the simulation till the onset of fracture and have been plotted in Fig 6.3-6.4. Fig.6.3 shows the damage distribution at last step (height reduction of 70%) at 570^0C and strain rate of $0.16s^{-1}$. From the simulation results, it is found that the maximum damage value is found in the edge of the disc sample and it is minimum in the middle of the disc. As the deformation starts from the middle and progresses towards the edge, the metal that was deformed a little while ago in the middle will be pushed away from the centre towards the periphery and fresh metal from the height side of the sample will be pushed towards the centre. Thus, with each step, fresh metal will be deformed and will be pushed towards the edge. Thus, a deformation gradient would have been formed from the centre to the edge. The metal at the edge would be the metal that has deformed more and thus would have undergone more workhardening. This is the reason for fracture to initiate at the edge first and also for its highest damage factor.

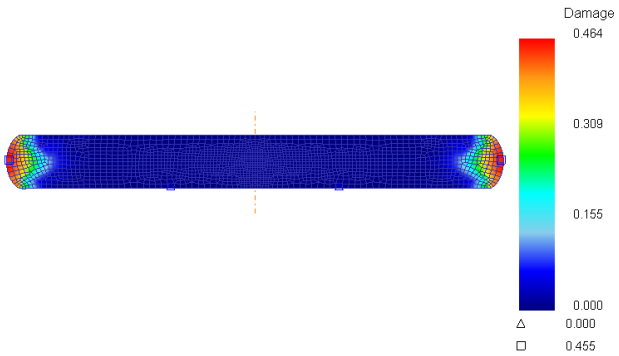

Fig.6. 3 Damage distribution at last step (height reduction of 70 %) at 570^0 C and strain rate of $0.16\ s^{-1}$

Figure 6.4 shows the variations in the incremental ratio during the compression process at different temperatures and strain rates. The inset shows the variation of the incremental ratio after 60 steps. It can be seen that the I_{DR} decreases to trough point rapidly, then it has a slight increase, soon after it decreases to zero gradually. To know the fracture time (step), the point arrays after step 60 were taken from each incremental ratio curve and fitted linearly as shown in Fig.6. 4.

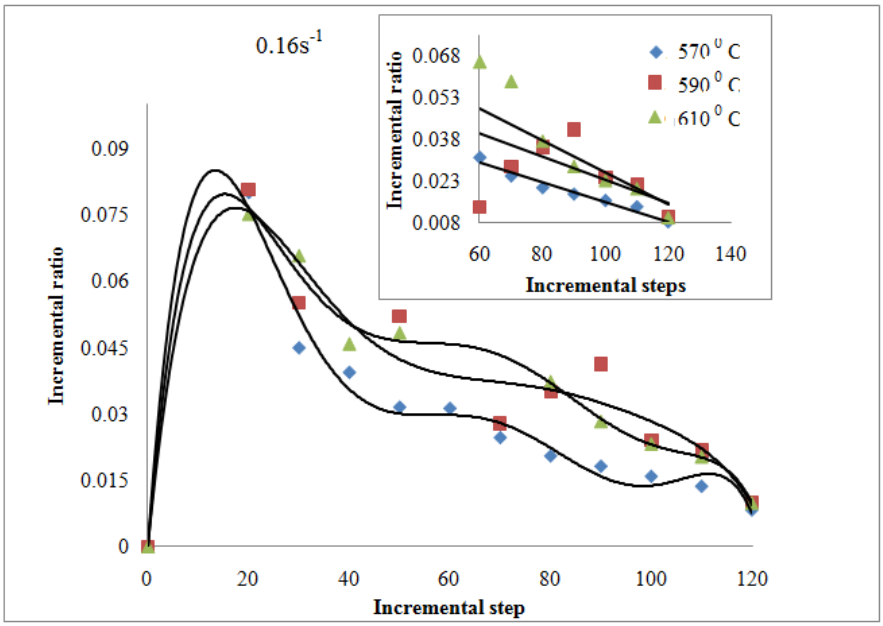

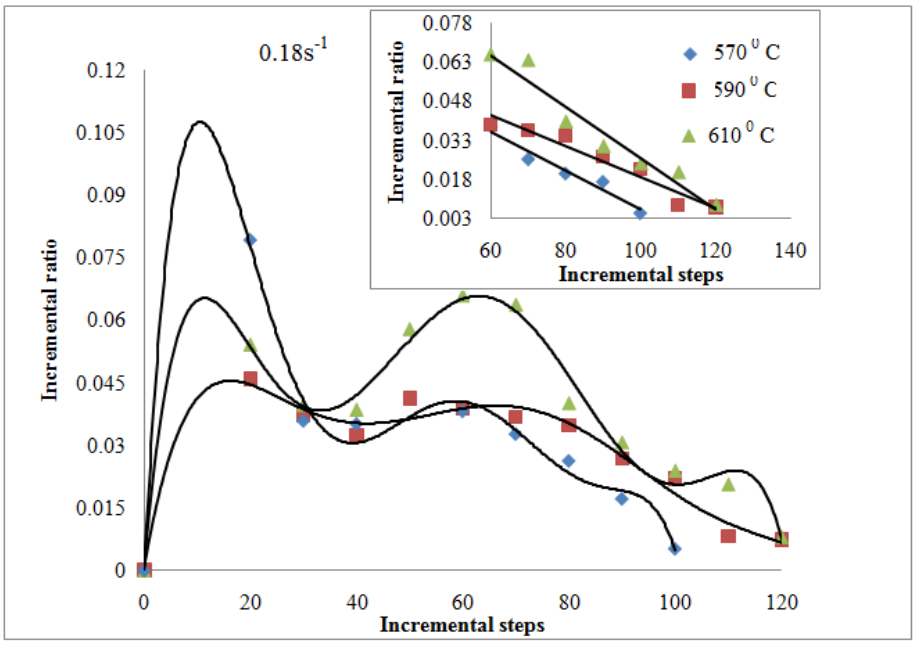

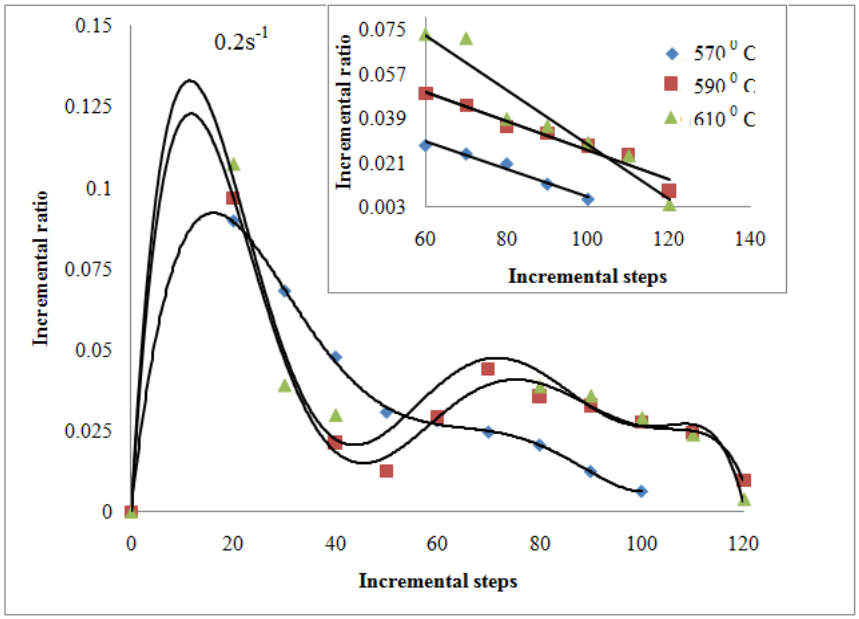

Fig.6. 4 Variation of Incremental ratio of Cockcroft-Latham damage during compression process at different temperatures and different strain rates.

The maximum cumulative damage value at last step or the critical damage factor is obtained. In this way, the critical damage factor of AA2017 alloy was computed.

6.5.2 Effect of Strain rate and temperature on damage values

The critical damage factor at 570^0C, 590^0C and 610^0C and at strain rates of 0.16 s^{-1}, 0.18 $s^{-1}$and 0.2 s^{-1} are given in Table 6.1. The critical damage factor varies from 0.471 to 0.264. Further, the critical damage value decreases significantly with increase in strain rate.

Table 6.1. Critical damage factor at different temperatures and strain rates.

Strain rate	570^0C	590^0C	610^0C
0.16 S^{-1}	0.471	0.349	0.379
0.18 S^{-1}	0.467	0.345	0.370
0.20 S^{-1}	0.455	0.337	0.264

Figure 6.5 shows the variation of damage factor value with the true strain. It can be seen that the damage increases non-linearly as the compressive true strain increases from 0 to 0.5, and

then it increases nearly linearly. Comparing the results with one another, it is found that for fixed true strain the maximum cumulated damage decreases with increase in temperature.

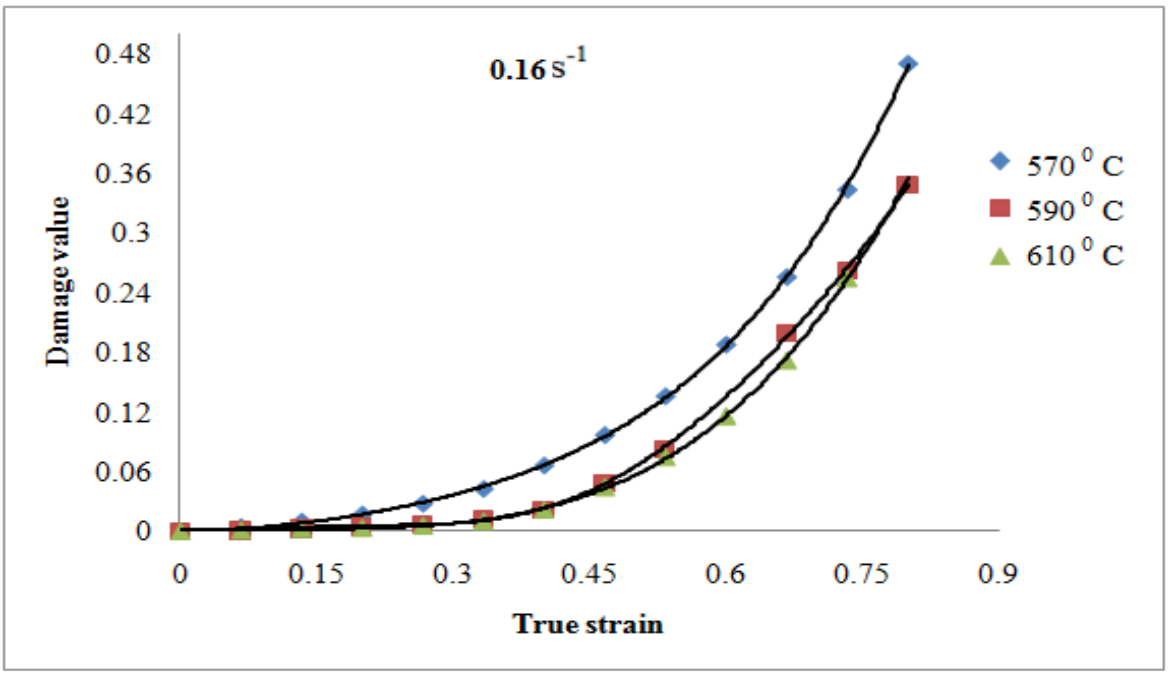

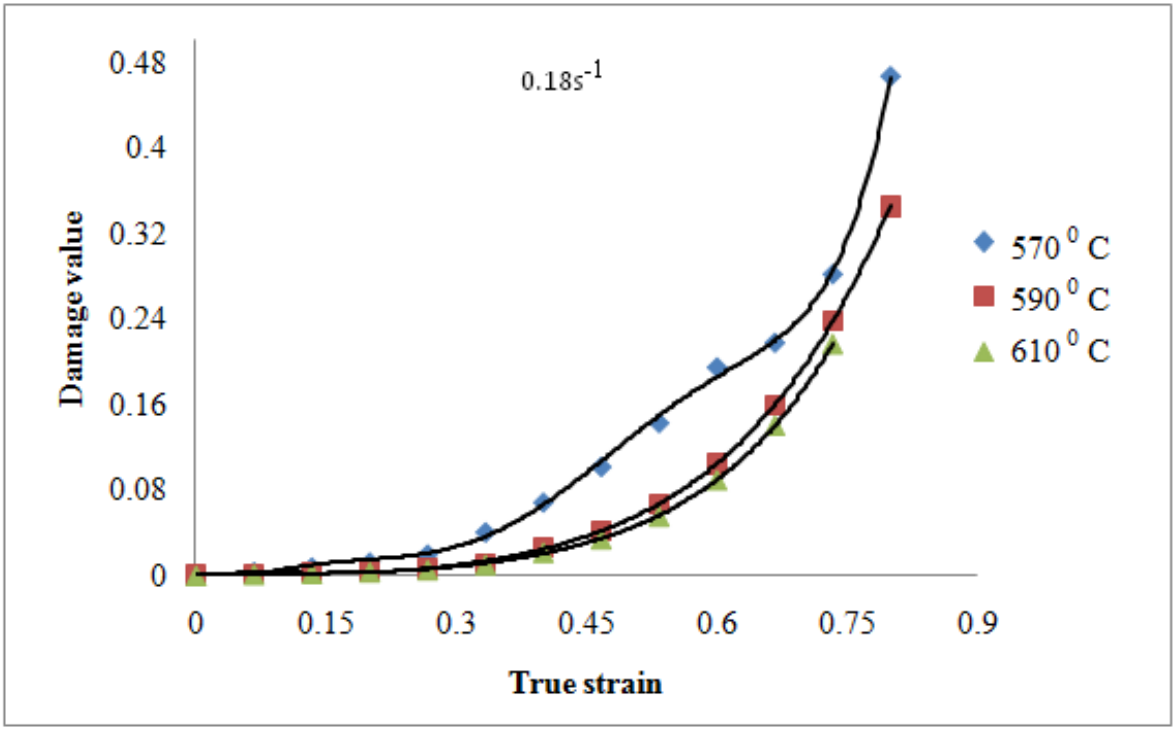

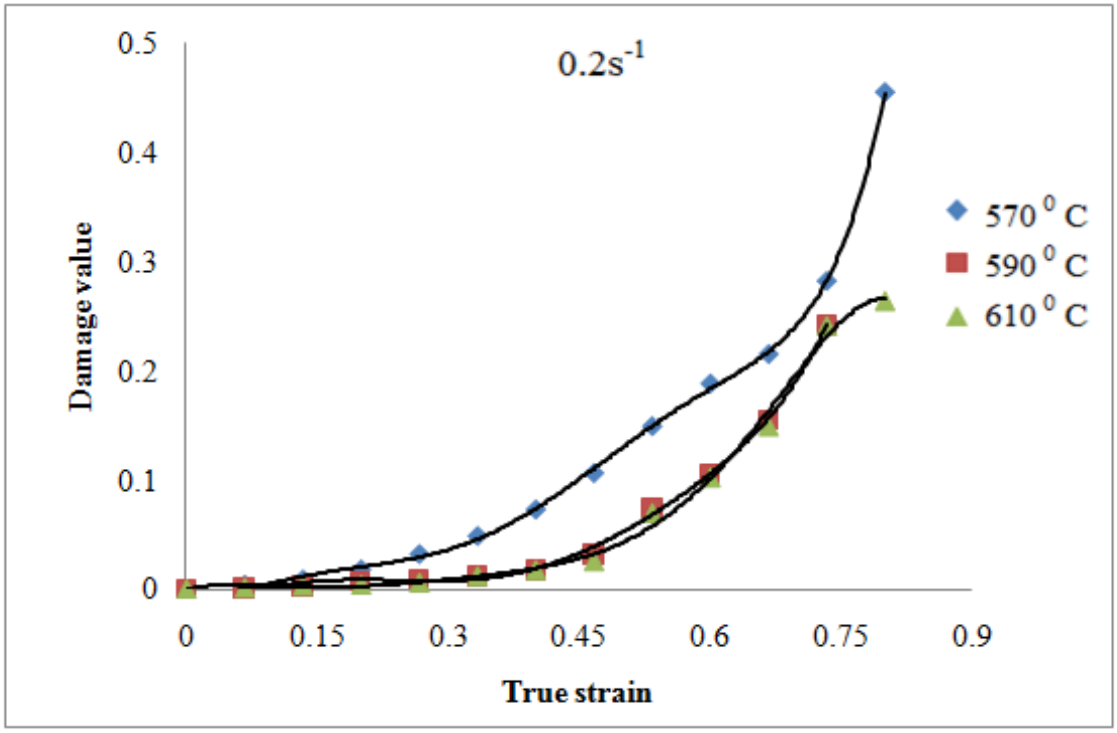

Fig.6. 5 Variation of damage value with true strain during compression process at different temperatures and strain rates.

6.5.3 Constitutive Model for Hot Forming

At high temperature, the deformation is controlled by a thermal activation method. (C.M. Sellars [1985]) stated that the steady-state flow stress of the thermal deformation depends on the deformation temperature and also on the strain rate, which might be expressed by the equation.

$$\dot{\varepsilon} \exp\left(\frac{Q}{RT}\right) = Z = A\,(\sinh\ (\alpha\sigma))^n \qquad (6.3)$$

where Z is the temperature compensating strain rate factor, i.e. the Zener-Hollomon parameter; $\dot{\varepsilon}$ is the strain rate, Q is the deformation activation energy, σ is the steady state flow stress, R is the gas constant,(8.31 J.mol $^{-1}$ K $^{-1}$) and T is the temperature. The material constants such as A, α, β, and n, where α the stress multiplier, n the stress exponent, A and β the material constants, have been evaluated by performing disc compression tests at temperatures of 570^{0}C, 590^{0}C, and 610^{0}C and strain rates of 0.16 s^{-1},0.18 s^{-1},and 0.2 s^{-1}. Figure 6.6 shows the relationship between critical fracture strain C_s and ln Z. A linear relationship was observed

between these two. This means that fracture is mainly controlled by ln Z rather than by temperature and strain rate separately. A regression equation containing the critical fracture strain has been computed and is given in Eq. (6.4).

$$C_s = 23.885\text{-}1.787 \ln Z \quad (6.4)$$

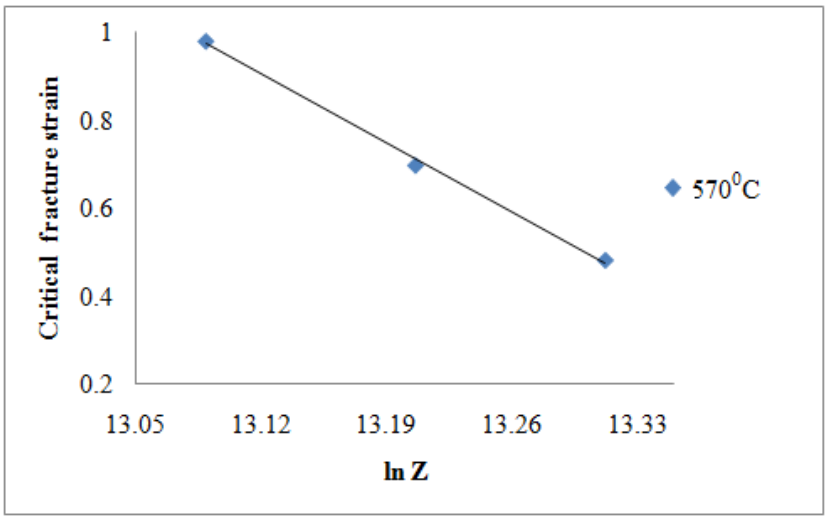

Fig. 6.6 Fracture strain as function of ln Z and temperature

6.5.4 Zener-Hollomon based fracture parameter for AA2017 alloy at Semi-solid forming

Figure 6.7 shows the relation between the critical fracture value C_f and ln Z. A linear relationship is seen between C_f and ln Z. Its regression equation is given by

$$C_f = 3.20 - 0.214 \ln Z \quad (6.5)$$

The correlation coefficient is 0.9072. The regression line is seen as a boundary separating the safe and the unsafe regions. If the damage value at any particular simulation step falls within the regression line, it is considered safe forming and the damage value that crosses the regression line implies that failure has actually taken place. Taking the above into consideration, the Cockcroft and Latham can be written in the form shown below

$$\int_0^{\varepsilon f} \frac{\sigma_T}{\sigma_{eff}} d\varepsilon > 3.20\text{-}0.214 \ln Z \quad (6.6)$$

Eq.6.6 is the fracture criterion of AA 2017 alloy in the semi-solid forming process. The left hand side is the damage that the material exhibits during the plastic deformation at any particular strain value and the right hand side is the critical fracture value. The equation of the above form involves the role of temperature compensated strain value for damage calculation, thus relating the forming temperature and strain rate in the damage parameter.

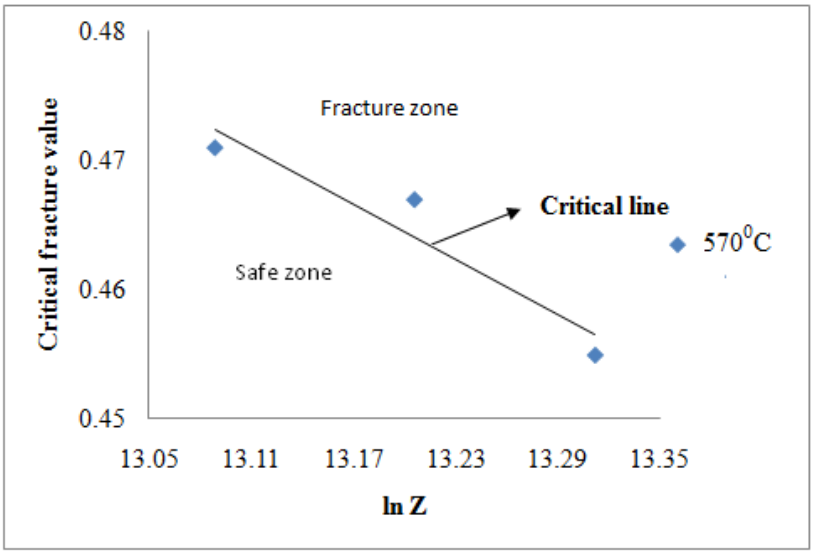

Fig.6.7 Relation between ln Z and critical fracture value, C_f

6.6 Chapter Summary

In the present work, the critical damage factor of AA 2017 alloy based on Cockcroft and Latham equations was found and it was observed that the critical damage value is not a constant but varying between 0.471 to 0.264. It decreases significantly with the strain rate and it increases with temperature. It can be seen that the damage increases non-linearly as the compressive true strain increases from 0 to 0.5, and then it increases nearly linearly. The progression of damage with deformation has been identified and the critical damage for different temperatures and strain rates has been calculated. These damage factors can be used by the users of semi solid forming process for setting the forming limits at simulation studies.

CHAPTER 7

Microstructure Studies on the Thixo-extruded bar of AA2017 alloy

7.1 Introduction

The main advantage of thixo extrusion process evolves from the presence of globular grains at the semi solid range compared to the presence of dendritic grains in conventional casting processes. Thus, it is essential to analyze the evolution of microstructural characteristics in a semi solid forming process at different process temperatures and strain rates. However, the process development for thixo forming of AA2017 is yet to be developed completely as far as the knowledge of the investigators goes and there is a challenging task for the scientific community to device the forming temperatures, the strain rate, the tooling temperature, cooling rate etc which favours globular microstructure. The present work was undertaken to study the microstructural changes of thixo extruded samples at different temperatures and strain rates, which on completion will help the investigators and the scientific community to design the process parameters for thixo-extruded products.

7.2 Macrograph of the sample edge

Figure 7.1 shows the surface quality of thixo-extruded samples at low and high liquid fractions. The surface shown in Fig.7.1 (a) is smooth and free from defects, whereas

Fig.7.1 (b) shows some defects such as cracks, scratches and pit holes. This may be due to excess liquid flowing out from the die and also due to the reaction of the extruding object with the environment. The liquid phase segregation and the subsequent accumulation at the end of forming cycle could also be one of the reasons for crack formation. As this happened only at higher forming temperatures, it is inferred that it is due to the excess liquid fraction.

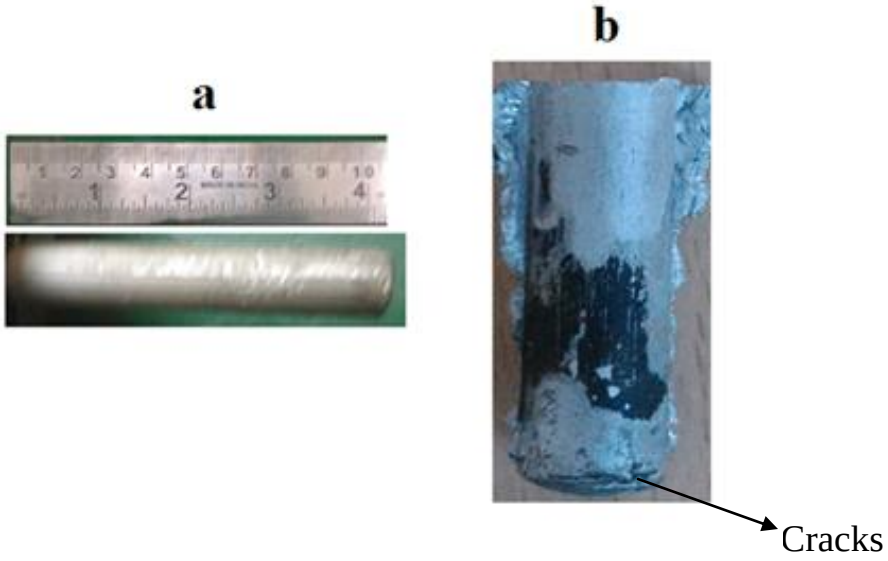

Fig.7.1 (a) Surface appearance of thixo-extruded sample at 570^0C
(b) Surface appearance of thixo-extruded sample at 610^0C

7.3 Microstructure

The initial as received microstructure of AA 2017 alloy is shown in Fig.3.2. The microstructures of thixo-extruded samples at temperatures of 570^0C, 590^0C and 610^0C for constant strain rates of 0.16 s^{-1} and 0.2 s^{-1} are shown in Figs. 7.2, 7.3 and 7.4 respectively. The primary grain boundary starts melting when the temperature of the samples is raised above the solidus temperature. Subsequently, the percentage of liquid fraction increases when the sample is heated further. At this state, the liquid particles will start surrounding the islands of solid particles and sometimes, liquid particles will also be trapped inside the solid, if subsequently, the solid layer surrounded by the liquid coalesces. In the previous case, the deformation will be caused by the gliding of the solid phase over the liquid pool. If the liquid is trapped inside a solid medium, the deformation will take place over the solid and not on the liquid medium. The entrapped liquid subsequently becomes solid during the deformation process and increase the solid fraction

(Favier,V [2009]).The microstructures of the specimens at 570^0 C and 610^0 C are shown in the Fig. 7.2 (a) and Fig. 7.2 (b) respectively.

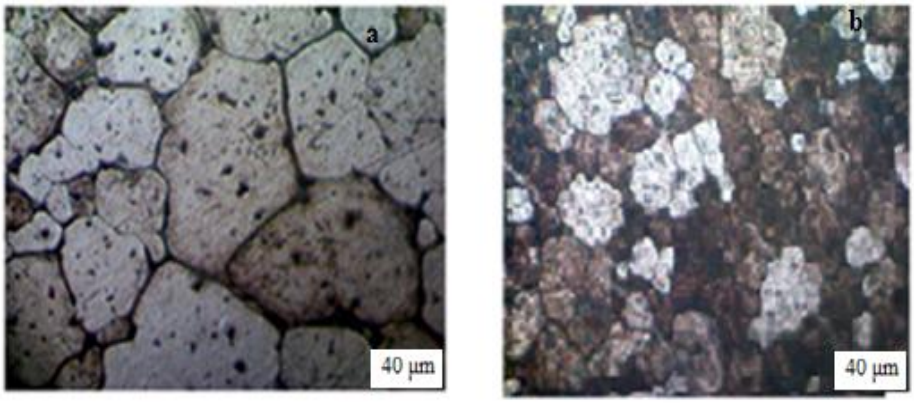

Fig. 7.2 Microstructures of thixo-extruded sample at (a) 570^0C 0.16 s^{-1} strain rate
(b) 610^0C 0.16 s^{-1} strain rate

From Fig.7.2 (a) and Fig.7.2 (b), it is observed that the liquid content is low at lower temperatures and is concentrated at the grain boundaries. However, at 610^0 C, the segregation of liquid and solids have taken place and islands of solids are found in a liquid matrix. The grains too have been refined and are globular in nature. It is also observed that the microstructure shows non uniform grains with discontinuous grain boundaries at lower temperatures. As the temperature is further increased, the grain boundaries disappear and uniform globular grains starts forming in a pool containing minimum solid particles.

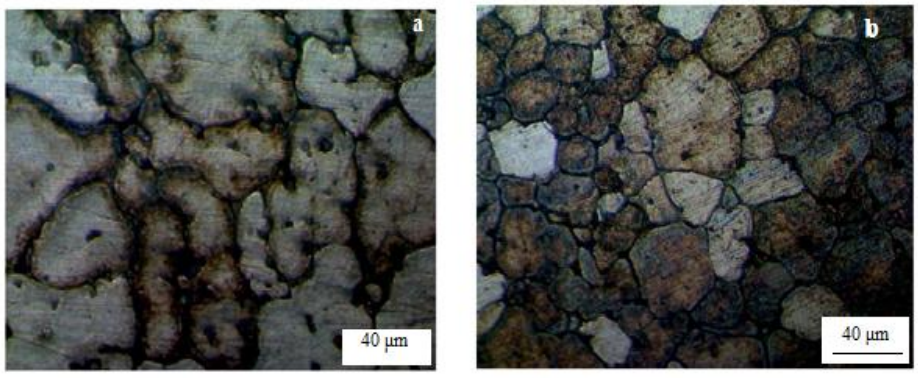

Fig 7.3 Microstructures of thixo-extruded sample at (a) 570^0C, 0.2 s^{-1} strain rate
and (b) 610^0C, 0.2 s^{-1}strain rate

The microstructures of the samples at 570^0C and 610^0C and at 0.2 s^{-1}strain rates are shown in Fig.7.3 (a) and Fig.7.3 (b) respectively. Strain rates determine the time available for the

sample to grow or refine. An optimum strain rate is required for the samples to attain the required liquid fraction and also the shape and size. Comparing Fig.7.2 (a-b) and 7.3 (a-b), it is inferred that a higher strain rate can refine the grains at 610^0C as it is evident from Fig.7.3 (b). However, at 570^0C, higher strain rate has increased the non uniformity of the samples further as it is seen from Fig. 7.3 (a). This consists globules of solid surrounded by liquid. As the heating temperature increases, equiaxed grains can be obtained. At higher temperatures and strain rates, the larger grains have been divided into smaller globular grains by the simultaneous grain boundary breakage and the liquid segregation. At the higher strain rate condition, then liquid particle during deformation has not obtained the necessary time to grow into bigger size as the deformed liquid would have lost the thermal energy required for grain growth during the deformation process resulting in fine, smaller and globular grains than a lower strain rate condition.

Moreover, another reason for the irregular shape of the sample at lower forming temperature is coalescence. At lower temperatures, due to low liquid fraction, the possibility of two grains meeting each other will be more than the sample at higher liquid fraction which will be surrounded by liquid particles. A solid particle in touch with another solid particle will merge together resulting in irregular shaped grains and also larger grains. From Fig.7.4 (a) and (b), it is observed that the grain boundaries between grains A and B disappears leading to increase in grain growth and irregular shaped grains.

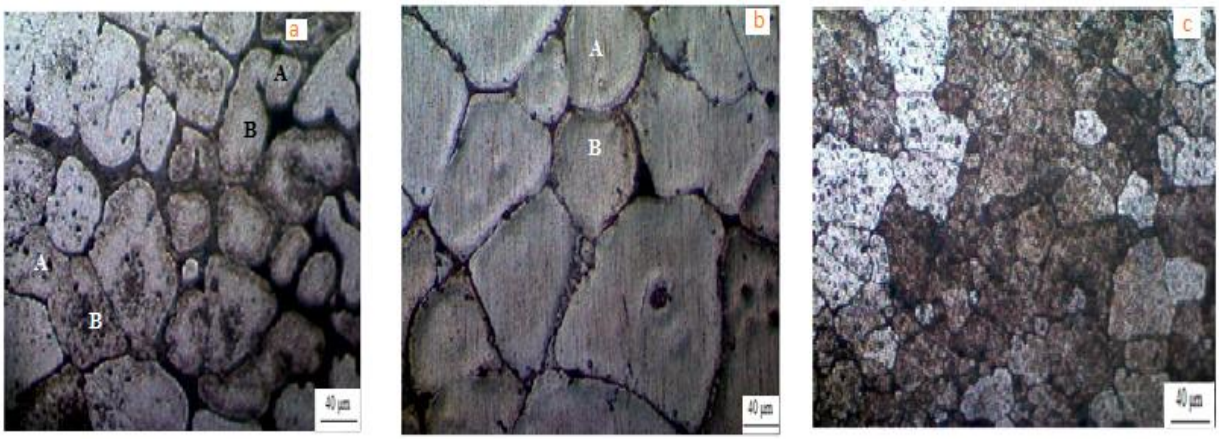

Fig. 7.4 Microstructures of thixo-extruded sample at (a) 570^0C, 0.16 s^{-1} strain rate (b) 590^0C, 0.16 s^{-1} strain rate and (c) 610^0C, 0.16 s^{-1} strain rate

The samples were tested for the presence of intermetallic particles and it was found that at 570^0C intermetallic compounds such as Al_2Cu and Al_2 (Fe, Mn, Cu, Si) were found as seen in

Fig.7.5. However, these intermetallics gradually decreased when the forming temperature was increased to 610^0C. The Scanning electron microscopy image (SEM) and EDS analysis is shown in Fig. 7.5 (a) and Fig. 7.5 (b).

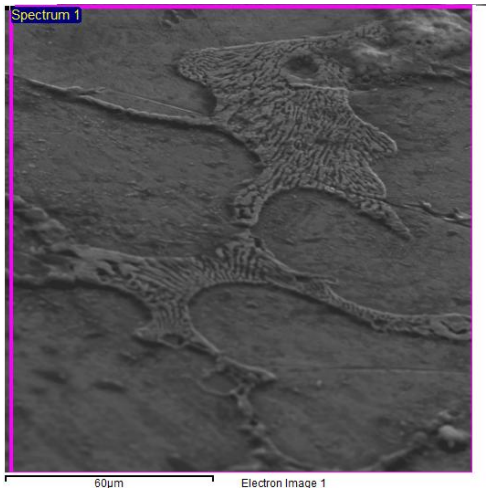

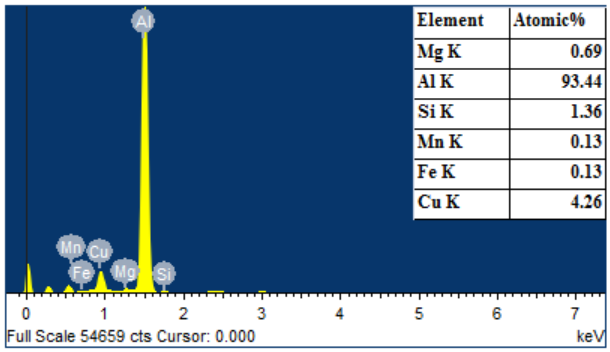

Element	Atomic%
Mg K	0.69
Al K	93.44
Si K	1.36
Mn K	0.13
Fe K	0.13
Cu K	4.26

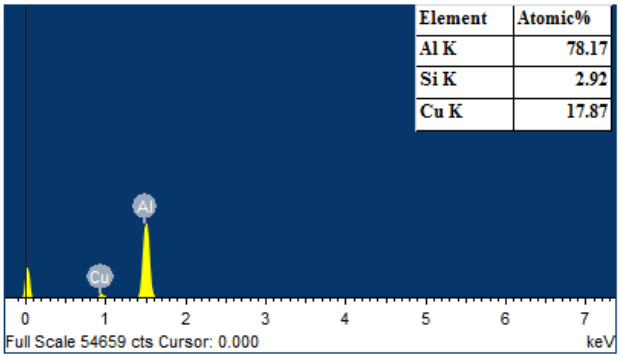

Element	Atomic%
Al K	78.17
Si K	2.92
Cu K	17.87

Fig. 7.5 (a) SEM Image of 2017 at 570 ^{0} C and (b) EDS spectra and analysis results

To understand the temperature profile that exists during the process of deformation, the extruded sample was divided into three regions. Figure 7.6 and Fig. 7.7 show the microstructures

of the AA2017 alloy bar at different positions in the direction of extrusion. The position 1 is the rear end of the thixo-extruded rod. As the metal at this end will be the last to be extruded and also as this end will be transferring some of the heat to the lower part of the die, a different temperature profile will be experienced by this portion of the sample. The time lag and the heat transfer will increase the solid fraction of the alloy. An equiaxed grain structure is observed at the rear end of the thixo-extruded rod which proves the above observations. The position 2 is the middle part of the thixo-extruded rod, where globular grains are observed. The position 3 is the leading edge of the thixo-extruded rod. As this portion will be rich in liquid phase and as this region would have been the first to be extruded in the semi solid range, a globular microstructure was observed. Also, the microstructure in Fig.7.6 (c) and Fig.7.7 (c) suggests the presence of more liquid fraction.

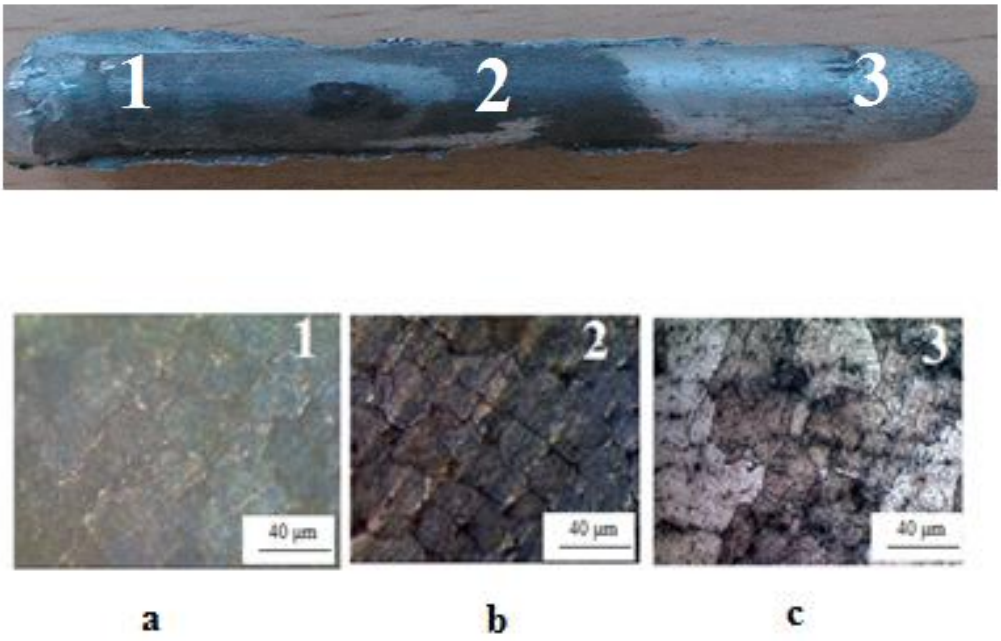

Fig.7.6 Microstructure of thixo-extruded rod at 590 ^{0} C and at (a) Rear (b) Middle and (c) Front ends of the sample.

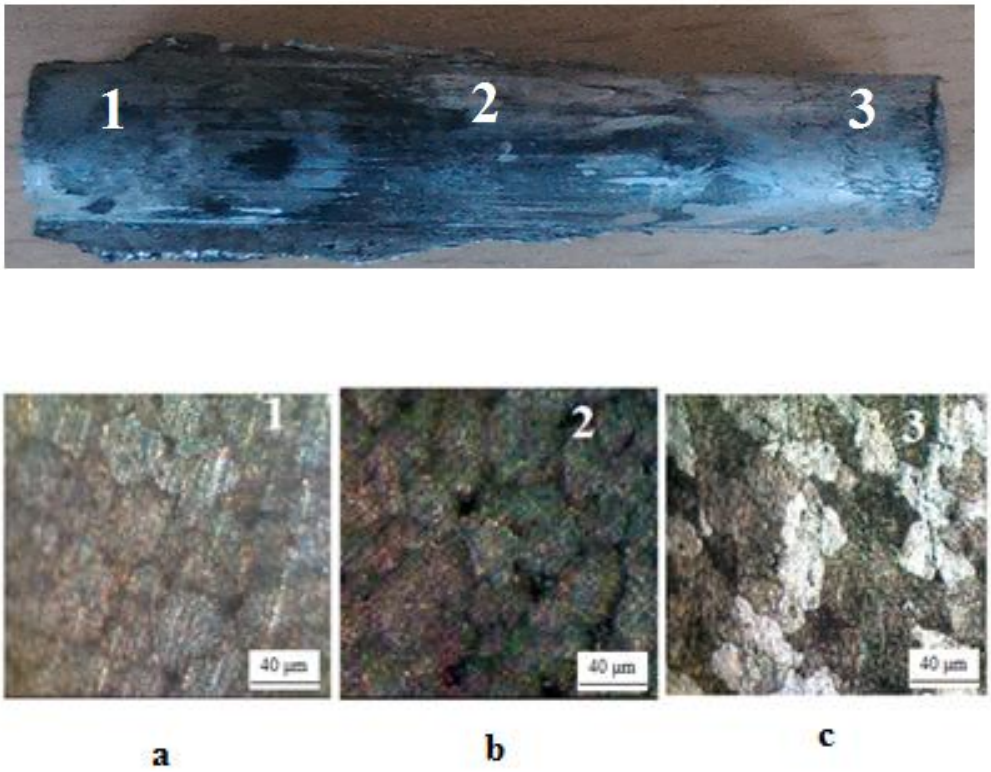

Fig.7.7 Microstructure of thixo-extruded rod at 610 ^{0} C and at (a) Rear (b) Middle and (c) Front ends of the sample

7.4 Mechanical properties

7.4.1 Tensile strength

The tensile stress –strain curves of thixo-extruded samples are shown in Fig.7.8. The average values of mechanical properties such as ultimate tensile strength, proof stress, percentage of elongation, percentage reduction in area and grain size are shown in Table 7.1. The ultimate tensile strength decreases with increasing temperature due to the presence of liquid phase in the grain boundaries and inside the globular grains with smaller ratio. This leads to the formation of shrinkage porosities after solidification. At higher deformation temperature, the accumulation of metallic contents in grain boundaries increases and the extruded sample strength decreases. The precipitated phase is dissolved in the liquid matrix at higher temperatures as shown in Fig.7.9. The variation in yield strength is due to the variation in the grain size. According to the Hall-Petch equation (Azushima A et.al. [2008] and Meyer Marc Andre, [1999]) the strength depends on the grain size. The average grain size of thixo extruded sample increases with increasing

deformation temperature resulting in decreased yield strength of specimens. From Fig.7.8, it can be seen that there is no significant difference between the stresses at 590^0C and 610^0C. This may be due to the liquid segregation.

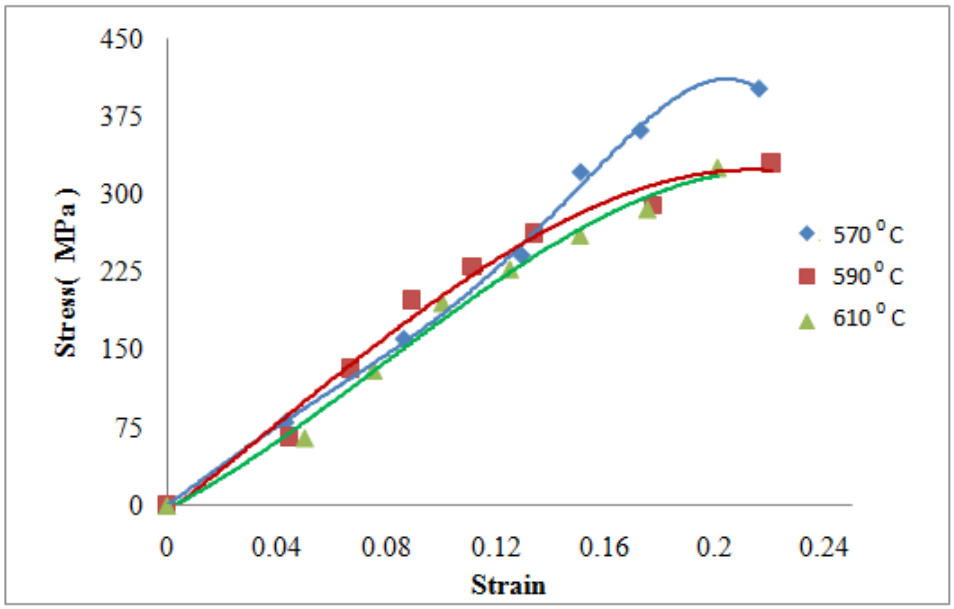

Fig.7.8 The tensile stress-strain curves of thixo-extruded samples at different temperatures

Table 7.1 the average values of tensile test and grain size at different temperatures

Temperature in ^{0} C	**Ultimate tensile strength (MPa)**	**Yield strength (MPa)**	**Percentage of Elongation**	**Percentage Reduction in area**	**Grain size (µm)**
570	378	285	15.41	16.58	42
590	347	238	15.48	18.46	47
610	243	251	14.74	15.4	49

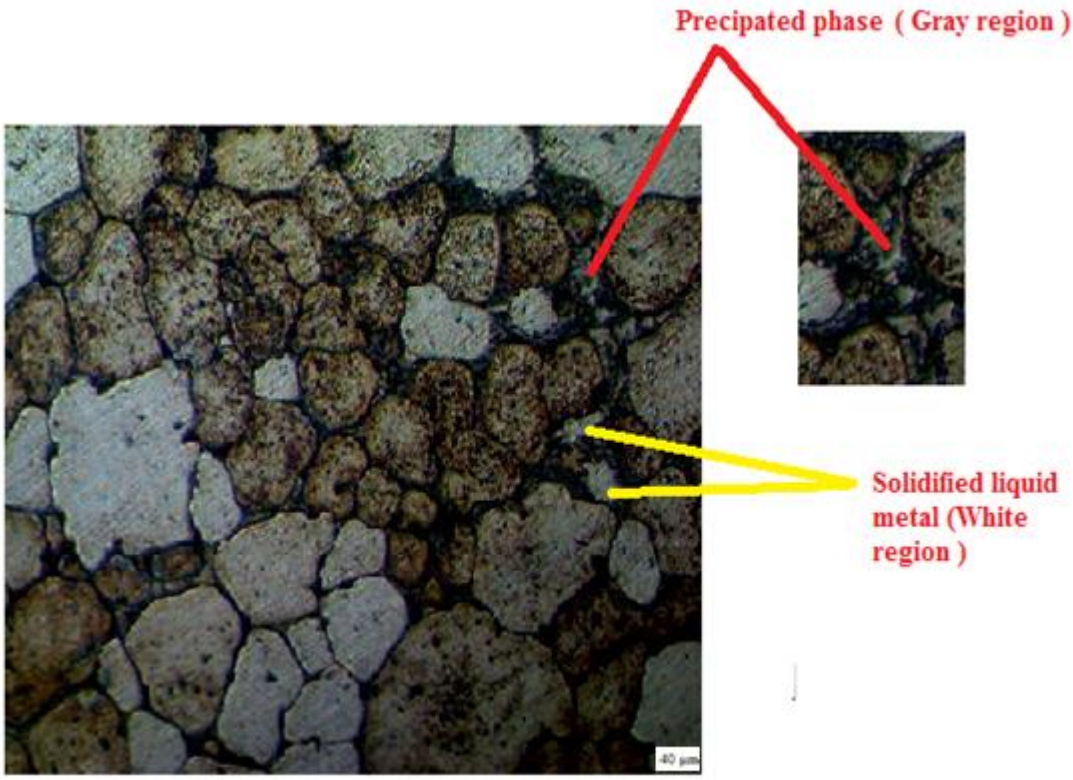

Fig.7.9 Microstructure of thixo-extruded sample at higher temperature

7.4.2 Hardness

In order to study the hardness characteristics, the thixo-extruded sample was cut in to half and then hardness was measured along the length in three different positions as shown in Fig.7.10. From Fig. 7.10, it is clear that there is a change in the hardness value from front to rear end along the length of the bar.Figure.7.6 and 7.7 show the changes in the microstructural features of the thixo-extruded bar in the marked regions. Hardness profile shows the forming mechanism involved in the different regions of the thixo-extruded bar. The front end of the rod is evidence for semi-solid extrusion but the rear end has failed to extrude in the semi-solid state due to the variation in temperature. As the thixo-extrusion process continues, the temperature decreases and the solid fraction increase. This causes sudden increase in the forming load during the end of the thixo-extrusion process.

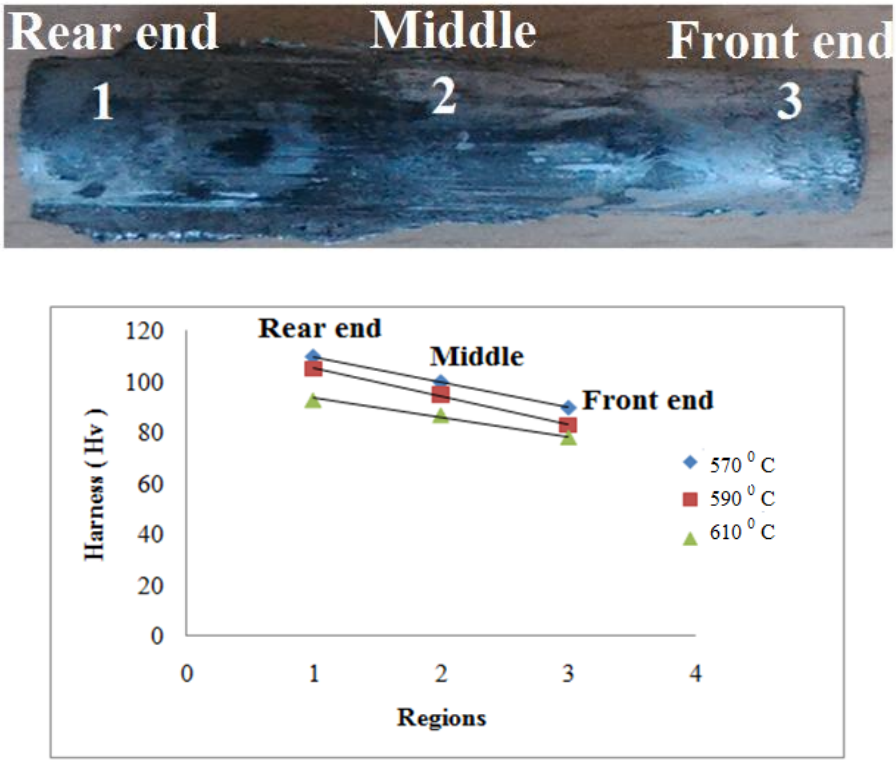

Fig. 7.10 Vickers hardness values along the length of thixo-extrusion rod of AA 2017 alloy

7.5 Chapter Summary

In the present research, the microstructures of thixo-extruded samples of AA2017 aluminium alloy have been studied and the following results are drawn.

1) Discontinuous grain boundaries with non uniform grains are observed from the samples extruded at lower isothermal temperatures. This is due to the liquid phase is not so much to soak in to the grain boundaries.
2) The microstructures of samples extruded at high temperature (610^0C) and at strain rates of 0.16 s^{-1} and 0.2 s^{-1} consist of globules of solids surrounded by liquid, confirming the presence of thixo extrusion conditions.
3) The samples at the rear ends lost thixo conditions due to heat loss, resulting in plastic deformation conditions, which are confirmed by the presence of equiaxed grain structure.
4) The average grain size of thixo extruded sample increases with increase in deformation temperature.

CHAPTER 8

Influence of Process Parameters on the Mechanical Properties of Semi-Solid Extruded AA2017 alloy Rods

8.1 INTRODUCTION

To get most optimum results in semi-solid process, the most important process parameters, that influence the product quality namely the temperature of billet, strain rate, approach angle and percentage reduction in area have to be optimized and thus they have been considered in this paper. Taguchi and ANOVA techniques were used to find the percentage contribution of each process parameter on the mechanical properties. Statistical analysis software MINITAB was used for the design and analysis of experiments and to perform ANOVA analysis.

8.2 Methodology

8.2.1 Taguchi method

Taguchi suggested a special design of orthogonal arrays, which are the shortest possible matrix of permutations and combinations of the controlling factors. This orthogonal array helps to know the influence of process parameters on the outcomes of thixo extrusion sample of AA2017 alloy with a small number of experiments only. The orthogonal array is chosen based on the number of degrees of freedom, which is determined from the number of

factors, number of selected interactions, and the number of levels of each factor. Once the acceptable orthogonal array has been selected, the main factors and interactions, if any, will be allotted to the various columns. After setting the test strategy the experimental results are then transformed in to signal to noise (S/N) ratio. Signal- to- noise ratio is used as a measure of quality characteristics changing from or nearing to the desired value. There are three different S/N ratios available depending up on the quality characteristics, such as lower the better (LTB), nominal the better (NTB) or higher the better (HTB). In the present work, higher the better quality characteristics have been used.

Lower the better: It is used where the lower value is desired.

$$\text{S/N ratio } (\eta) = -10 \log_{10} \frac{1}{n} \sum_{i=1}^{n} y_i^2 \quad (8.1)$$

Where y_i= observed response value and n= number of replications.

Higher the better: It is used where the larger value is desired

$$\text{S/N ratio } (\eta) = -10 \log_{10} \frac{1}{n} \sum_{i=1}^{n} y_i^2 \quad (8.2)$$

Where y_i= observed response value and n= number of replications.

8.2.2 Selection of process parameters

In the present investigation, the main aim is to identify the process parameters which would optimize the tensile strength and percentage of elongation of thixo extruded specimen. The control factors and their levels are shown in Table 8.1.

Table 8.1 Control factors and their levels

SI.No	Control factor	Label	Level 1	Level 2	Level 3
1	Temperature of billet in (^{0}C)	A	570	590	610
2	Strain rate(s^{-1})	B	0.16	0.18	0.20
3	Approach angle in (^{0})	C	30	45	60
4	Percentage reduction in area	D	35	55	75

According to Taguchi design of experiments, for 4 parameters and 3 levels, L9 orthogonal array has been selected and is shown in Table 8.2.

Table 8.2 the basic Taguchi L9 (34) orthogonal array with control factors and their levels

Experiment No	A	B	C	D
1	1	1	1	1
2	1	2	2	2
3	1	3	3	3
4	2	1	2	3
5	2	2	3	1
6	2	3	1	2
7	3	1	3	2
8	3	2	1	3
9	3	3	2	1

8.2.3 ANOVA

ANOVA is a statistical technique which is used to find degree of differences or similarity in two or more groups of data. It is based on the comparison of an average value of a common component. In this work, Pareto ANOVA (Venkateswarulu G et.al. [2010]) which measures the importance of each process parameter in thixo-extrusion experiments is used. Pareto ANOVA, which is a simplified ANOVA method, is based on Pareto principle. Pareto ANOVA is a quick and simple technique to analyze results of the parameter design. It does not need F-test. This method identifies the important process parameters and analyzes the percentage contribution of each parameter on different quality characteristics. The use of both Pareto ANOVA method and S/N ratio approach makes it less cumbersome to analyze the results and hence it takes less time to arrive at the conclusion (Roy RA [1990]). The S/N ratios were calculated for all responses and are given in Table 8.4 and 8.5. From the S/N ratios, the overall S/N ratio is expressed as

$$\overline{S/N} = \frac{1}{9}\sum_{i}^{9}(S/N)_i \tag{8.3}$$

Where $\overline{S/N}$ is the overall mean of S/N ratio and $(S/N)_i$ is the S/N ratio for i^{th} parameter

The sum of squares due to variation about over all mean is

$$SS = \sum_{i=1}^{9}((S/N)_i - \left(\overline{S/N}\right)^2 \tag{8.4}$$

Where SS is the sum of squares.

For i^{th} process parameter, the sum of squares due to variation about over all mean is

$$SS_i = \sum_{j=1}^{3}((S/N)_{ij} - \left(\overline{S/N}\right)^2 \tag{8.5}$$

Where SS_i is the sum of square for the ith parameter and $(S/N)_{ij}$ is the average S/N ratio of i^{th} parameter of j^{th} level

$$\% \text{ Contribution} = (SS_i / SS) * 100 \quad (8.6)$$

8.3 Results and discussion

The experimental results of tensile strength, percentage elongation and of each sample are shown in the Table 8.3. The results were transformed into S/N ratio using Eq. (8.2). The values of S/N ratios for tensile strength, and percentage elongation are given in Table 8.4 and 8.5 respectively. Table 8.4 and Fig.8.2 show the effect of control factors on tensile strength in terms of S/N ratio.

From Fig. 8.2, it can be observed that the tensile strength decrease with increase in forming temperature. Though, the ease with which the forming can be performed increases with increase in temperature, the porosity problem increases as the liquid fraction of the alloy increases. Moreover, at high solid fraction, the forming pressure densifies and strain hardens the alloy more compared to the alloy with more liquid fraction. This is the reason for the decrease in tensile strength of the alloy at 610^0C, where the liquid fraction will be more. This can also be verified with microstructural evidence. Figure 8.1 shows the microstructure of the alloy extruded at 610^0C.

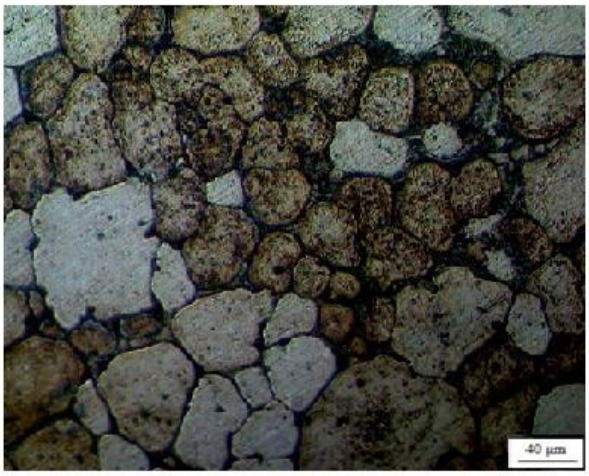

Fig.8.1 Microstructure of thixo-extruded bar at 610^0C

Strain rate is another important factor that influences the mechanical properties. In semi solid forming, at initial stage of forming, the perform should have more liquid phase and at the end of the forming stage, the perform should be having more solid phase. This transition can be effectively controlled by the strain rate. Thus, an optimum strain rate successfully controls the

solid and liquid phases of the alloy to give better mechanical properties. In the present work, from Fig.8.2, it is found that, at low strain rates the tensile strength is less and it increases with increase in strain rate. Moreover, it is found that very small variation is found between the levels 1 and 2 strain rates and the tensile strength increases drastically at level 3. At a higher strain rate, enough time was not available for the alloy to transit itself from liquid to solid phase within the forming stage, and thus has not attained the densification and strain hardening properties. This observation has been in consistence with that of the forming temperature and thus the solid and liquid fraction percentages discussed a little while earlier. Also, the strain rates create two types of phenomenon in the liquid during the forming cycle, liquid segregation and liquid splashing (V.Pouvafar et.al. [2010]). At low strain rates, the liquid phase will have enough time to surround the solid matrix and within the forming cycle, these segregated liquid phases becomes solids and thus contributing to the enhanced mechanical property. However, at higher strain rates, the liquid phase separates out from the solid phase uncontrollably due to the high speed of the ram and splashes away from the solid phase. This creates tearing and porosity problems in the alloy, thus decreasing their mechanical property. This is clearly evident from the results obtained in the present work. The approach angle and percentage reduction in area assists in the densification and work hardening phenomenon of the process. As the die with 30^0 approach angle and percentage reduction in area contributes more towards the above phenomenon, high tensile strength has been achieved at 30^0 approach angle and 55 % percentage reduction. Thus, the optimum process parameters on the tensile strength are obtained at the forming temperature kept at level 1 (570^0C), strain rate kept at level 3 (0.2 s^{-1}), approach angle at level 1(30^0) and percentage reduction in area at level 2 (55 %).

Table 8.3 Experimental results

Experiment No.	**UTS (N/Sq mm)**	**Percentage of elongation (%)**
1	362.350	19.25
2	400.824	12.6
3	372.240	14.4
4	318.39	17.46
5	329.556	15.06
6	395.270	13.4
7	359.58	14.66
8	325.109	13.44
9	347.195	16.13

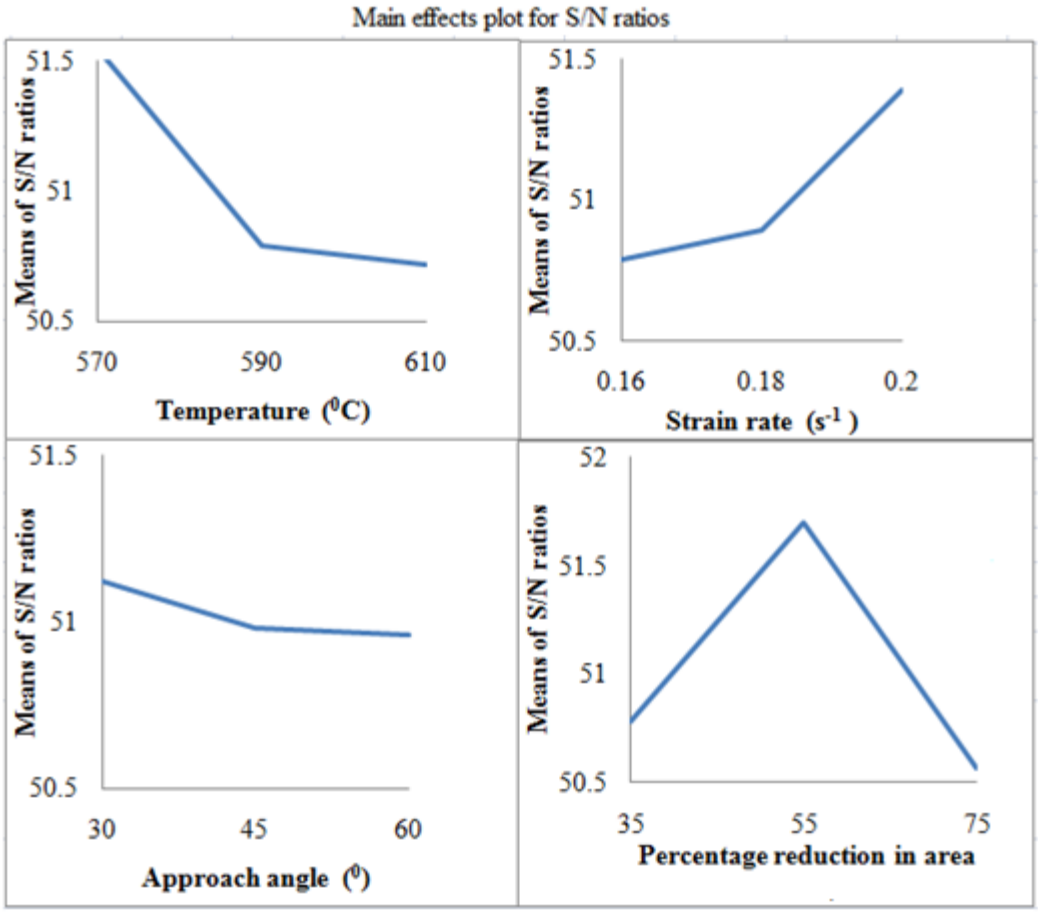

Fig. 8.2 Main effects plot for S/N ratio (tensile strength)

Table 8.4 Response table for S/N ratio for tensile strength

Level	Temperature (^{0}C)	Strain rate (s^{-1})	Approach angle (^{0})	Percentage reduction area
1	51.55	50.79	51.12	50.78
2	50.79	50.89	50.98	51.70
3	50.72	51.39	50.96	50.57
Delta	00.83	00.60	00.16	01.13
Rank	2	3	4	1

Table 8.5 and Fig.8.3 show the influence of process parameters on the percentage of elongation. The optimum process parameters are obtained at temperature kept at level 2 (590^{0}C), strain rate at level 2 (0.18 s^{-1}), approach angle at level 1(30^0) and percentage reduction in area at level 3 (75).

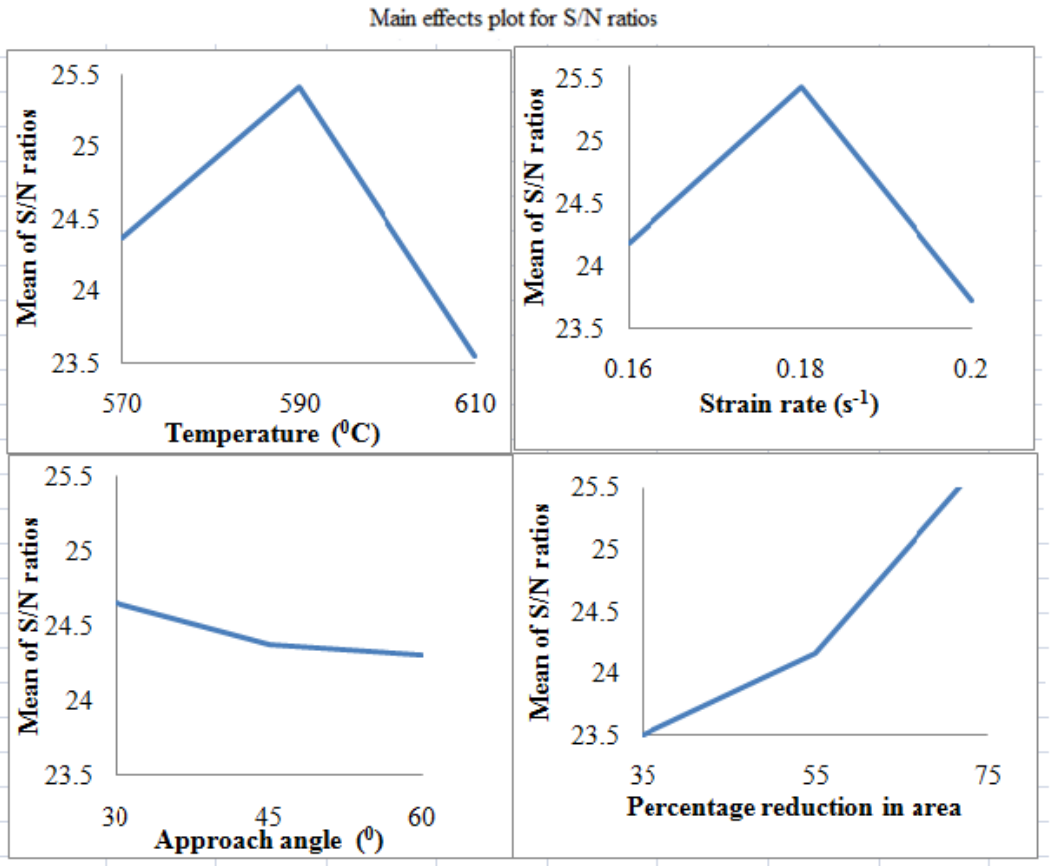

Fig. 8.3 Main effects plot for S/N ratio (percentage of elongation)

Table 8.5 Response table for S/N ratio for elongation

Level	Temperature,(^{0}C)	Strain rate (s^{-1})	Approach angle (^{0})	Percentage reduction in area
1	24.37	24.18	24.66	23.42
2	25.42	25.44	24.38	24.16
3	23.55	23.72	24.31	25.76
Delta	1.87	1.72	0.35	2.34
Rank	2	3	4	1

To identify the process parameters which contribute to enhanced mechanical properties of thixo-extruded sample, ANOVA test was conducted and the results are shown in Fig. 8.4 and 8.5 and also in Table 6 and 7 for tensile strength and percentage of elongation respectively. From Table 8.6, it is observed that percentage reduction in area (53.45 %) is the major factor influencing the tensile strength of thixo-extruded specimen, followed by temperature (30.67 %)

and strain rate (14.69 %). From Table 8.7, it is observed that percentage reduction in area (48.04 %) is the most significant factors affecting the percentage of elongation followed by temperature (26.11%), strain rate (24.71%) and approach angle (1.15%).

Table 8.6 Contribution of process parameter for tensile strength

Process parameter	**Sum of squares$(SS)_i$**	**Percentage Contribution**
Temperature	2149.71	30.67
Strain rate	1029.97	14.69
Approach angle	83.07	1.19
Percentage reduction in area	3746.32	53.45

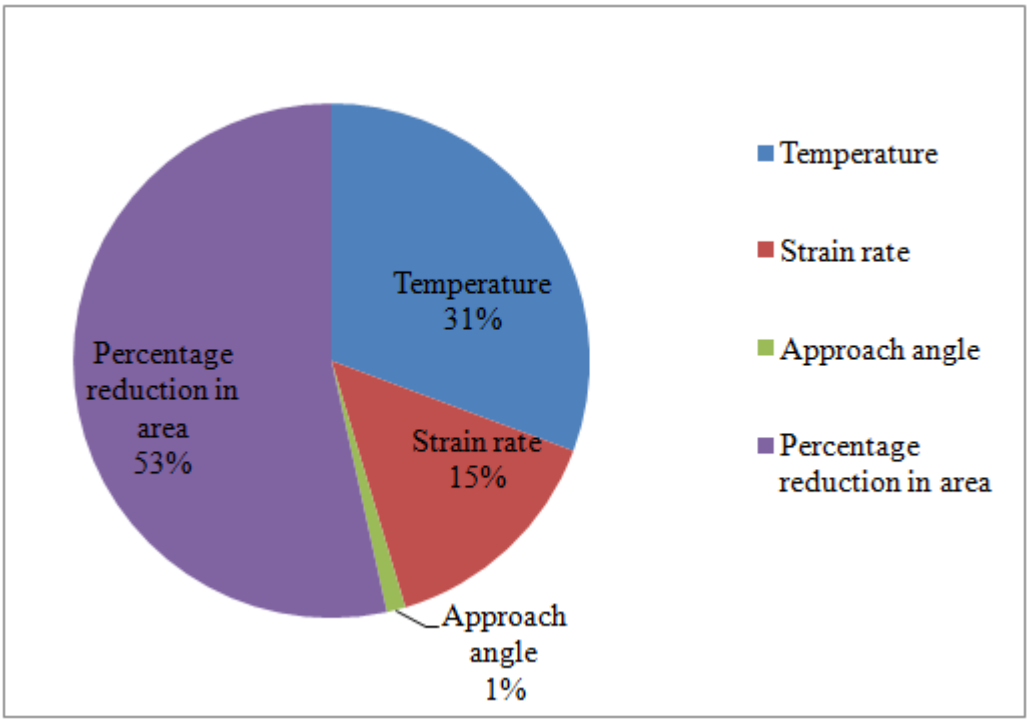

Fig. 8.4 Percentage contribution of process parameters for tensile strength

Table 8.7 Contribution of process parameter for % elongation

Process parameter	Sum of squares$(SS)_i$	Percentage Contribution
Temperature	17.14	26.11
Strain rate	16.22	24.71
Approach angle	0.76	1.15
Percentage reduction in area	31.54	48.04

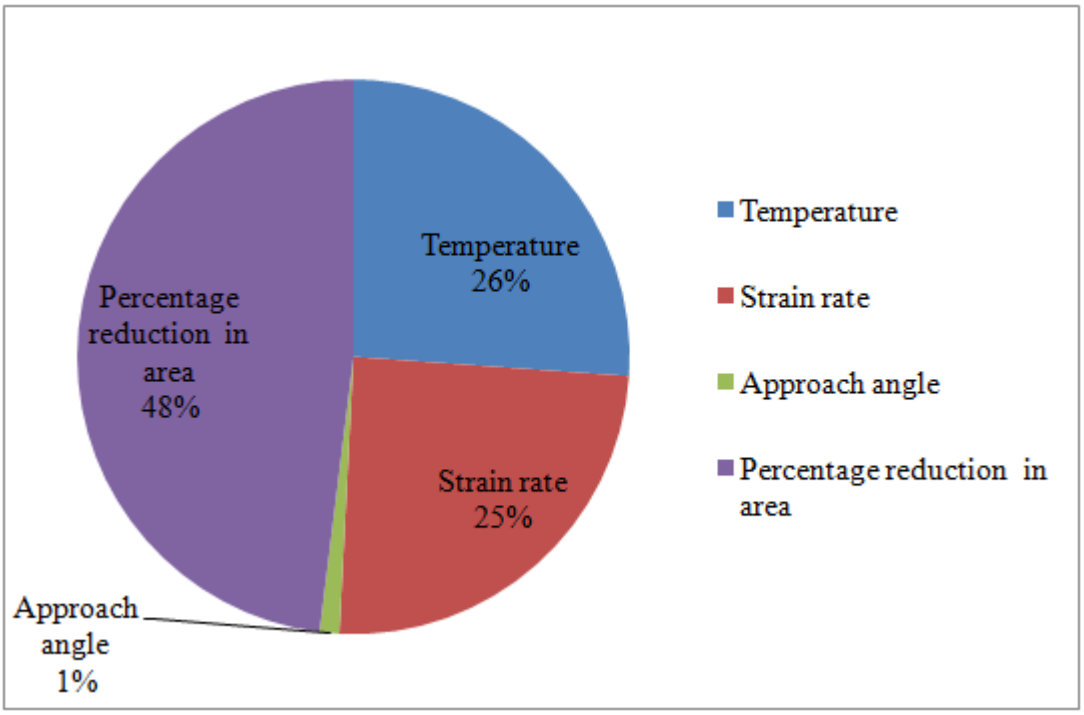

Fig. 8.5 Percentage contribution of process parameters for percentage of elongation

The model adequacy check has been performed after performing ANOVA analysis to verify the normality assumption of the residual. If the model is adequate, the points on the normal probability plots of the residuals should form a straight line. Figure 8.6 and 8.7 show the normal probability plots of the residual and these figures reveal that almost all the residual follow a straight line pattern.

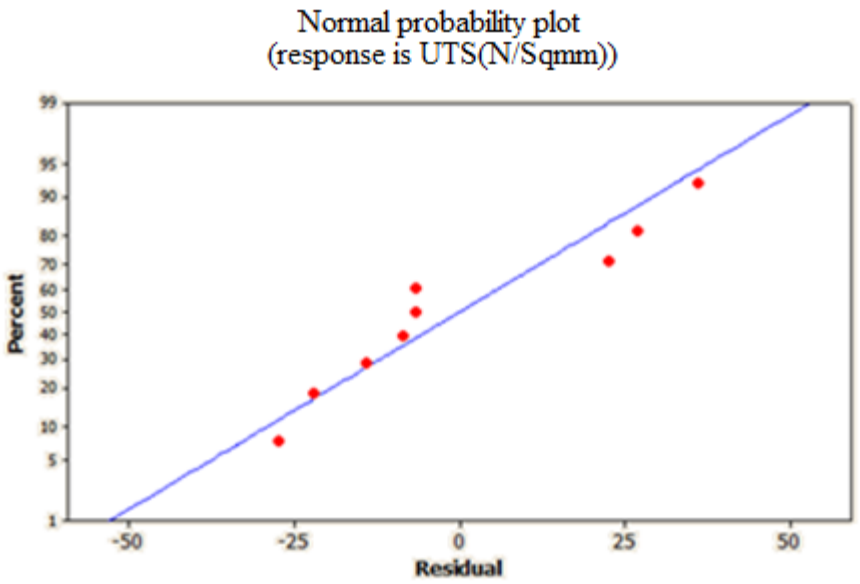

Fig. 8.6 Normal probability plot of residual for tensile strength

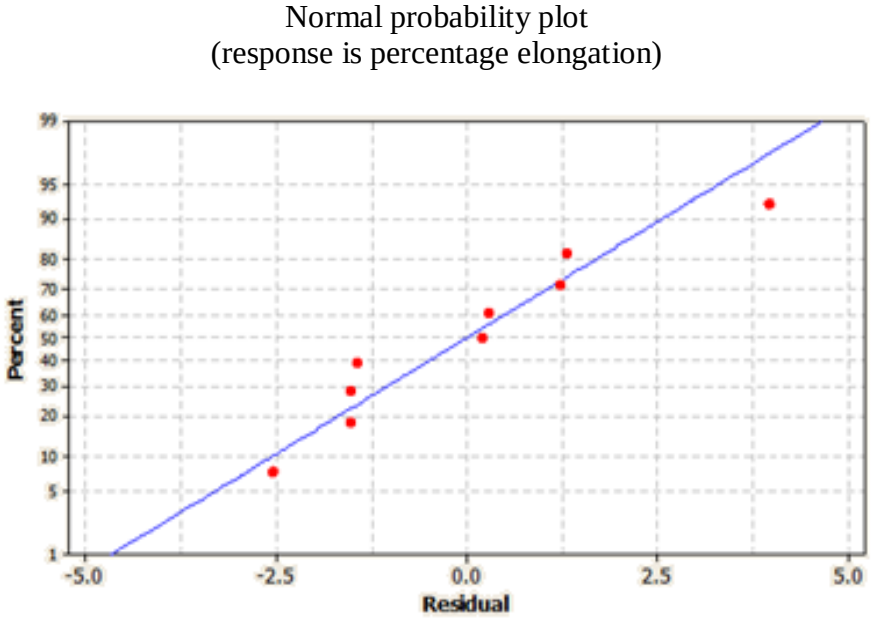

Fig. 8.7 Normal probability plot of residual for percentage elongation

8.4 Chapter Summary

This paper presents the findings of the test performed to optimize the thixo-extrusion process parameters namely temperature, strain rate, approach angle and percentage reduction in area. It reveals the effect of process parameters on the mechanical properties of thixo-extruded sample of AA 2017 alloy by using Taguchi and ANOVA tests. Conclusions drawn from the present investigations are as follows.

1) The optimum process parameters on the tensile strength are obtained at the forming temperature kept at level 1 (570^0C), strain rate at level 3 (0.2 s^{-1}), approach angle at level 1 (30^0) and percentage reduction in area at level 2 (55).

2) The optimum process parameters on the percentage of elongation are obtained at temperature kept at level 2 (590^0C), strain rate at level 2 (0.18 s^{-1}), approach angle at level1 (30^0) and percentage reduction in area at level3 (75).The ANOVA results reveal that percentage reduction in area and temperature are the most significant factors on mechanical properties.

CHAPTER 9

CONCLUSIONS AND SCOPE FOR FUTURE WORK

9.1 Conclusions

An experimental and simulation based investigations were performed on the thixo-extrusion of AA 2017 aluminium alloy. The following major observations are drawn.

Thixo forming combines the better properties of forging as well as casting as it is a hybrid process of the two. Thus, the final mechanical properties are better than the casting process and the process is easier than the forging process. Major contributions of the work can be listed as below.

(i) Developed the constitutive relation for thixoforming of AA2017 alloy in the thixo range

(ii) Found the material constants of AA 2017 alloy in hot and thixo conditions , which were used in simulation process to analyze the material flow path and its stresses and strains

(iii) Established the fracture criterion of AA 2017 alloy in the semi-solid state to predict the crack and optimized the process parameters to avoid or delay the crack propagation

(iv) Performed the microstructure analysis and found the mechanical properties of specimen after thixoforming.

Ensuring fast solicitation subsequent to forming and ensuring thixo forming conditions during forming are the most challenging tasks during any thixo forming process. Both have been successfully achieved in this work. Very few studies have been performed on the simulation studies of thixo forming. This work has resulted in the evaluation of thixo forming material parameters of AA2017 alloy and the constitutive equation relating the process conditions have been evaluated.

The mechanical properties have been correlated with the material flow paths during the simulation study.

The solid fraction of the alloy is an important process condition for obtaining good quality products. The experimental investigations revealed that it is preferable to have the workpiece with more liquid fraction in the initial stage of extrusion and more solid fraction in the final stage of extrusion cycle.

It was found that too much liquid fraction at the end of extrusion cycle results in cracking of the workpiece at the end.

The importance of approach angle during forming was realized at the end of the forming experiments. The variation in the approach die angle creates different frictional conditions on the interface of the wall and the metal. The effective strain is found to be less for the metal extruded with a die with 30^0 approach angles and it is more for the die with 60^0 approach angles. A low effective strain implies that the metal being pressed is stronger than the alloy which has undergone higher strain. This implies that a narrower die is required to produce a stronger alloy. Thus, along with higher solid fraction a narrower die produces alloy with higher strength.

A micro structural evaluation of the samples drawn at different temperatures and approach angles revealed that the in homogeneity of the samples increased as the approach angle is increased. The above fact was confirmed in the simulation studies performed. It is observed that, the distribution of strain is uniform at higher liquid fraction and within the temperature ranges; the strain distribution is uniform on the samples extruded with higher approach angle.

The percentage reduction area was another contributor to good quality products. The percentage reduction in area of the extrudate is proportional to the die diameter. The narrower the die, the stronger will be the alloy at the end of the extrusion stroke. It was observed that with increase in percentage reduction, the solid fraction increases. This shows that the amount of

deformation is closely related to the densification of the solid phase. The densifications attained by the samples were measured by noting down their densities after the forming cycle. The large force with which the semi solid alloy is squeezed through the die has made the alloy to densify in the narrow exit portion of the extrusion die. This is the reason why the solid fraction increases with increase in percentage reduction. the same has been confirmed in the simulation performed.

It is evident that the approach angle and the percentage reduction in area of the exit portion of the die plays a vital role in the deformation behaviour of the alloy. A narrow approach angle of die and increased percentage reduction in area increases the solid fraction and the deformation load. This shows that, at the exit portion of the die, due to the above factors, the solid fraction of the alloy increases and the alloy is extruded nicely.

The critical value of the damage factor depends on the mechanical and metallurgical state of the metal before and after the deformation process. As such, the factors such as the initial microstructure, alloy constituents, grain size, grain form, non-metallic inclusion content, hardness etc affect the critical damage factor and they are different for different initial and final conditions. As the temperature, strain rate and solid and liquid contents change during the deformation process, these are the critical factors that affect the damage factor. The critical damage factor of AA 2017 alloy based on Cockcroft and Latham equations was found and it was observed that the critical damage value is not a constant but varying in between 0.471 to 0.264. It decreases significantly with the strain rate and it increases with temperature.

The main advantage of thixo extrusion process evolves from the presence of globular grains at the semi solid range compared to the presence of dendritic grains in conventional casting processes. Thus, it is essential to analyze the evolution of microstructural characteristics in a semi solid forming process at different process temperatures and strain rates. The optimum process parameters on the tensile strength are obtained at the forming temperature kept at level 1 (570^0C), strain rate at level 3 (0.2 s^{-1}), approach angle at level 1 (30^0) and percentage reduction in area at level 2 (55). The optimum process parameters on the percentage of elongation are obtained at temperature kept at level 2 (590^0C), strain rate at level 2 (0.18 s^{-1}), approach angle at level1 (30^0) and percentage reduction in area at level3 (75).The ANOVA results reveal that

percentage reduction in area and temperature are the most significant factors on mechanical properties.

A microstructural evaluation conducted on the deformed samples revealed elongated grains for the samples with high solid fraction and spherical and evenly distributed grains for samples deformed with high liquid fraction. Discontinuous grain boundaries with non uniform grains are observed from the samples extruded at lower isothermal temperatures. This is due to the liquid phase is not so much to soak in to the grain boundaries. The microstructures of samples extruded at high temperature ($610\ ^{0}$ C) and at strain rates of 0.16 $s^{-1}$and 0.2 s^{-1} consists of globules of solids surrounded by liquid, confirming the presence of thixo extrusion conditions. The samples at the rear ends lost thixo conditions due to heat loss, resulting in plastic deformation conditions, which are confirmed by the presence of equiaxed grain structure. The average grain size of thixo extruded sample increases with increase in deformation temperature.

The constitutive equation that was developed in the semi solid range simulated the semi-solid forming condition closer to the experimental and the relation thus formed is given by $\sigma = 56.179 \ln\{(Z/A)^{1.628} + [(Z/A)^{3.257} + 1^{1/2}]\}$.

9.2 Scope for future work

1. The same work can be performed by different heating methods to obtain homogeneous microstructures.

2. The effect of post thixo-formed heat treatment can be studied to improve the mechanical properties after thixo-extrusion experiments

REFERENCES

REFERENCES

Abdelfattah, S., Robelet, M., Rassili, A and Bobadilla, M, 2000, Proceedings of the 6th International Conference on Semi-solid Processing of Alloys and Composites, pp. 283–288.

Arabshahi, H, 2009, Dynamic and static softening behaviours of AA2024 aluminium alloy under hot deformation applications , International Journal of Basic & Applied Sciences, Vol.9(9), pp.21−23.

Azushima A, Kopp R, Korhonen A, Yang D.Y, Micari F, Lahoti G.D, 2008, Sever plastic deformation (SPD) processes for metals, CIRP Annals Manuf. Technol., Vol. 57, pp.716–735.

BIROL Y. 2008, Thixoforging experiments with 6082 extrusion feedstock, Journal of Alloys and Compounds, 2008, Vol. 455(1/2), pp.178−185.

Birol, Y, Guven, E.A and Capan, L.J, 2011, Extrusion of EN AW-2014 alloy in semi-solid state, Materials and Technology, Vol., 27(12), pp.1851-1857.

Brozzo P, Deluka B, Rendirina R, 1972, A new method for the prediction of formability in metal sheets, Proceedings of the 7th Biennial Conference of the International Deep Drawing Research Group, C/3/72, Page 28.

Clift SE, Hartley P, Sturgess CEN, Rowe GW, 1990, Fracture prediction in plastic deformation processes, International Journal of Mechanical Sciences, Vol.32, pp. 1-17.

Cockcroft M.G, Latham D.J, 1968, Ductility and workability of metals. Journal of the Institute of Metals, Vol.96., pp. 36-39.

De Figueredo, A, (ed.), 2001, Science and Technology of Semi-solid Metal Processing, North American Die Casting Association, Rosemont, IL.

Fan,Z, 2002, Semisolid metal processing, International Materials Reviews,Vol.47(2), pp.49–85.

Favier,V, Cézard, P and Bigot, R, 2009, Transient and non-isothermal semi-solid behaviour 3D micromechanical modelling, Mater Sci. Eng. A, Vol. 517, pp.8–16.

Flemings, M.C, Riek,R.G and Young, K.P, 1976,Rheocasting,Materials Science and Engineering, Vol.25 , pp.103 – 117.

Flemings, M.C., 1991, Behaviour of metal alloys in the semisolid state, Metallurgical and MaterialsTransactions **A, Vol.** 22(5), pp. 957-981.

Freudenthal AM, 1950, The inelastic behaviour in solids, First Edition, Wiley, New York.

Gunasekara, J.S and Zhou,Z, June1992, Development of a Constitutive Model for Mushy (Semi-Solid) Materials, Proceedings of the Second International Conference on the Semi-Solid Processing of Alloys and Composites, Cambridge, MIT, pp. 211-222,

Hartley, C.S and Srinivasan,R, July 1983, Constitutive Equations for Large Plastic Deformation of Metals, Journal of Engineering Materials and Technology, Vol. 105(3), pp.162-167.

Hatch J.E, (ed.), 1984, Aluminium properties and physical metallurgy, ASM, Materials Park, OH, pp 242-350.

Hong-min, G ,Xiang-jie, Y and Meng.Z,2008, Microstructure characteristics and mechanical properties of re-formed wrought aluminium alloy 2024, Trans. Non-ferrous Met. Soc. China., Vol.18, pp.555– 561.

Hossein Mohammadi and Mostafa Ketabchi, July 2013, Backward extrusion of 7075 Al alloy in the semi-solid state, Int. J. chem. and Mater.sci. Vol. 1(7), pp, 182-188.

Joly, P.A, 1974, Rheological properties and structure of a semi-solid tin-lead alloy, PhD Thesis, Dept. Mater. Sci. Eng., Massachusetts Institute of Technology, Cambridge.

Jong-Hoon Yoon, Yong-Taek Im, and Nak-Soo Kim, 2001, Finite Element Modelling of the Deformation Behaviour of Semi-Solid Materials, J. Mater.Process.Technol.,Vol.113,pp.153–159.

Ju-fu JIANG, Ying WANG, Jun LIU, Jian-jun QUP, Zhi-ming DU, Shou-jing LUO. March, 2013, Microstructure and mechanical properties of AZ61 magnesium alloy parts achieved by thixo-extruding semisolid billets prepared by new SIMA, Trans. Nonferrous Met. Soc. China, Vol. 23(3), 576−585.

Kang, C.G Kang, B.S and Kim, J.I., August 1998, An investigation of mushy state forging process by the finite element methods, J. of. Material Processing Technology, Vol.(80-81), pp.444-449.

Kang, C.G, Jung, H. K and Jung, K.W, 2001, Thixoforming of an Aluminium Component with a Die Designed by Process Simulation, J. Mater. Process. Technol., Vol.111(1–3), pp. 37–41.

Kenny, M.P, Courtois, J.A, Evans, R.D, Farrior, G.M, Kyonka, C.P, Couch A.A and Young, K.P, 1988, Semi-Solid Metal Casting and Forming, in 'Metals Handbook', 9th Edition, ASM International, Metals Park, Ohio, USA, Vol.15, pp. 327-338.

Kim HS, Im YT, Geiger M, 1999, Prediction of ductile fracture in cold forging of aluminum alloy. ASME Journal of Manufacturing Science and Engineering,Vol. 121,pp.336-344.

Kiuchi, M, Sugiyana.S, and Arai.K, 1979, Extrusion of Alloy in Mushy-State, J. Jpn. Soc. Technol. Plast., Vol.20(223), pp. 762-769.

Kiuchi, M, Yanagimoto,J and Yokobayashi, H, 2001,Flow stress Yield criterion and constitutive equation of semi-solid alloys, CIRP Annals-Manufacturing Technol.,Vol.50(1), pp.157-160.

Kiuchi, M., Sugiyama, S and Arai, K. 1979, Study of metal forming in the mushy-state, 2nd Report, Extrusion of tube, bar and wire of alloys in mushy-state, Proceedings of the 20th International Machine Tool Design and Research Conference, pp. 79-86.

Kiuchi, M., Sugiyama, S and Aria, K, 1979, Study of Metal Forming in the Mushy State, 1st Report, Flow Stress and Deformation Behaviour of Alloys in Mushy State, Proceedings of the 20th International Machine Tool Design and Research Conference, pp. 71-78.

Kiuchi,M. and Sugiyama,S, June 1994,Mushy state Extrusion, Rolling and Forging, Proceedings of the 3rd International Conference on Semi-solid Processing of Alloys and Composites, Tokyo, Japan, pp. 245–257.

Ko, D.C, Min, G.S and Choi, J.C, 2000, Finite Element Analysis for the Semi-Solid State Forming of Aluminium Alloy Considering Induction Heating, J. Mater. Process. Technol., Vol. 100, pp. 95–104.

Kumar, P, Martin, C.L and Brown, S.B, 1994, Constitutive modelling and characterization of the flow behaviour of semi-solid metal alloy slurries, Acta Metall. Mater., Vol.42, pp.3595–3614.

Kumar, P, Martin, C.L and Brown, S.B. May 1993,Shear Rate Thickening Flow Behaviour of Semi-Solid Slurries, Metall. Trans., A, 24A, pp.1107–1116.

Kumar,P, Martin, C.L and Brown,S.B. 1994, Constitutive Modelling and Characterization of the Flow Behaviour of Semi-Solid Metal Alloy Slurries-1.The Flow Response, Acta Metall. Mater., Vol.42(11), pp. 3595–3602.

Laxmanan, V and Flemings, M.C, 1980, Deformation of Semi-Solid Sn–15Pct Pb Alloy, Metall. Trans., A, Vol. 11(12), pp. 1927-1937.

Lin, Y.C. Chen, M.S. and Zhong J, 2008, Constitutive Modeling for. Elevated Temperature Flow Behavior of 42CrMo Steel , Comput. Mater. Sci., Vol. 42(3) , pp. 470–77.

Lucas Bertolino Ragazzo, Davi Munhoz Benati, Rodolfo Lopez Nadal, and Eugênio José Zoqui, July 2015, Obtaining Martensitic Structures during Thixoforming of Hypoeutectic Gray Cast Iron, Advances in Materials Science and Engineering,Vol.2015,Article ID 170562.

Ludwik, P,1909, Elemente der Technologischen Mechanik, Springer-Verlag, Berlin Heidelberg GMBH

Mada, M and Ajersch, F, January 1996,Rheological Model of Semi-Solid A356 SiC Composite Alloys, Part 1, Dissociation of Agglomerate Structures during Shear, Mater. Sci. and Eng., A, Vol.212, pp. 157–170.

Mandal, S, Rakesh, V, Sivaprasad, P.V, et.al.2009,Constitutive Equations to Predict High Temperature Flow Stress in a Ti-modified Austenitic Stainless Steel, Mater. Sci., Eng. A, Vol. 500(1), pp. 114–21.

Marc Andre Meyer and Krishan Kumar Chawla, 1999,Mechanical behaviour of materials, Prentice-Hall, Inc., pp. 268–73.

Martin, C.L, Brown, S.B, Favier, D and Suery, M, 1995, Shear Deformation of High Solid Fraction (> 0.60) Semi-Solid Sn-Pb under Various Structures, Mater. Sci. Eng., A, Vol. 202, pp. 112–122.

Midson, S.P, 1996, Proceedings of the 4th S2P Conference, England.

Mirzadeh,H and Najafizadeh A, February 2010, Flow stress prediction at hot working conditions,Mater. Sci. Engg. A, Vol. 527(4-5), pp. 1160–64.

Miwa, K. and Kawamura, S., 2000,Semi-Solid extrusion forming process of Stainless steel, Proceedings of the 6th International Conference on Semi-solid Processing of Alloys and Composites, Turin, Italy, pp. 279–281.

Moller, 2004, Verfahrensentwicklung und Ermittlung des thermischen Prozessfensters beim Thixostrangpressen, Dissertation, RWTH Aachen.

Muammer, Koc,Vazquez,V, Witulski, T and Altan, T, 1996, Application of the Finite Element Method to Predict Material Flows and Defects in the Semi-Solid Forging of A356 Aluminium Alloys, J. Mater. Process. Te.chnol., Vol.59, pp.106–112.

Muammer, Koc,Vazquez,V, Witulski, T and Altan, T, 1996,Application of the Finite Element Method to Predict Material Flows and Defects in the Semi-Solid Forging of A356 Aluminium Alloys, J. Mater. Process. Technol., Vol. 59(1), pp.106–112.

Nguyen, T.G, Favier, D. and Suery, M., 1994,Theoretical and Experimental Study of the Isothermal Mechanical Behaviour of Alloys in the Semi-Solid State, Int. J. Plast., Vol. 10(6), pp. 663–693.

Oyane M., 1972, Criteria of ductile fracture strain". Bulletin of the JSME, Vol. 15, pp. 1507-1513.

Polmear I.J, 1996, Light alloys. Metallurgy of the light metals', [2], London, Halsted Press.ASM Metal Handbook. Vol .2

Pouvafar, V, Sadough, S.A, Hosseinj, F,Rahmani, M.R, 2010, Design of experiments for determination of influence of different parameters on mechanical properties of semi-solid extruded parts , Trans Nonferrous Met Soc. China.,Vol. 20, pp.794-797.

Qiang Chen,Baoguo Yuan,Jun Lin,Xiangsheng Xia, Zude Zhao and Dayu Shu. 2014, Comparisons of microstructure, thixo formability and mechanical properties of high performance wrought magnesium alloys reheated from the as-cast and extruded states, Journal of Alloys and Compounds, Vol.584, 63‑75.

Queen, M.C, H.J and Ryan,N.D,2002,Constitutive analysis in hot working, Mater. Sci. Eng., Vol. 322(1), pp.43-63.

Randhir Kumar and N. K. Singh. August 2012**,** Application of Taguchi Method for Process Parameters Optimization in Semi-solid Forging of A356 Al-Alloy**,** Engineering Science and Technology,Vol.2(4), pp.2250-3498.

Rao, K.P and Hawbolt, E.B,1992, J. Eng. Mater. Technol. Vol. 114, pp. 116–23.

Rao, K.P and Hawbolt, E.B, 1992, J. Mater. Process. Technol., Vol. 29, pp. 15–40.

Rouff, C, Bigot, R, Favier, V and Robelet, M, 2002, Proceedings of the 7th International Conference on Semi-solid Processing of Alloys and Composites, A63, pp.355–360.

Rovira M.M, Lancini, B.C and Robert. M.H, 1999,Thixo-forming of Al–Cu alloys, Mater Proc. Technol., Vol.(92), pp 42–49.

Roy K.R, 1990, A Primer on the Taguchi method , Van Nostrand Reinhol , New York ,NY

Salleh,M.S, Omar, Z , Syarif, J and Mohammed, M.N, 19 December 2012,An Overview of Semisolid Processing of Aluminium Alloys, ISRN Materials Science, Vol.2013,Article ID 679820.

Salvo, L. Loue, W.R. and Suery, M, 1995,Influence of Prior Solidification Conditions on the Structure and Rheological Behaviour of Partially Remelted Al–Si Alloys, ISIJ Int., Vol. 35(6), pp. 798–804.

Sellars,C and Tegart,W.M,1966,On the mechanism of hot deformation, Acta Mater,Vol.14(9), pp.1136-1138.

Sellars,C.M, 1985,Computer modelling of hot working process, Materials Science and Technology, Vol 1. Pp. 325-332.

Shujian Chenga, Hua Houa, Yuhong Zh aoa and Yuchun Jina, March 2016, Effect of Process Parameters on the Microstructure of Semi-solid ZL101 Aluminum Alloy, Materials Research, Vol.19(3), pp.555-561.

Shun-sheng Wang, March1994, Development of constitutive model for AL-2011 alloy in mushy state, PhD Thesis, The faculty of the College of Engineering and technology, Ohio University.

Simge Gencalp Irizalp and Nursen Saklakoglu, Aprilo 2014, Effect of Fe-rich intermetallics on the microstructure and mechanical properties of thixoformed A380 aluminum alloy, Engineering Science and Technology, an International Journal, Vol. 17 (2014) ,pp.58-62.

Spencer, D.B, Mehrabian, R.and Flemings, M.C., 1972," Rheological behaviour of Sn-15% pct Pb in the crystallization range", Metall. Trans., Vol. 3(7), pp.1925 -1932.

Spencer, D.B, Sc. D, 1971, Thesis, Rheology of liquid-- solid mixtures of lead-tin, Dept. Mater. Sci. Eng., Massachusetts Inst. Technol.

Suery, M and Flemings, M.C, 1982, "Effect of Strain Rate on Deformation Behaviour of Semi-Solid Dendritic Alloys", Metall. Trans. A, V0l. 13(10), pp.1809- 1819.

Toyoshima, S, June 13-15 1994,"A FEM simulation of densification in forming processes for semi-solid materials"[C], 3rd Int. Conf. on 'Semi-Solid Processing of Alloys and Composites', Tokyo, pp.47–62.

Venkateswarulu G, Davidson MJ, Tagore GRN, 2010, Influence of process parameters on the cup drawing of aluminium 7075 sheet , Int. J Eng Sci. Technol., Vol.2, 40–9.

Wakil, Sherif D. EI, 1984, A Model Study of Metal Forming in the Mushy State," Proceedings of the First International Conference of Technology of Plasticity, Vol.1,pp. 45-49.

Wifi AS, Abdel-Hamid A, El-Abbasi N, 1998, Computer-aided evaluation of workability in bulk forming processes, Journal of Materials Processing Technology, Vol. 77, pp.285-293.

XIA Yu-feng., QUAN Guo-zheng , ZHOU Jie,2010, Effects of temperature and strain rate on critical damage value of AZ80 magnesium alloy . Transactions of Nonferrous Metals Society of China, Vol.20, pp.580-583.

Yoon, H.J, Im, Y.T and Kim, N.S, 1999, Rigid Thermo viscoplastic Finite-Element Analysis of the Semisolid Forging of Al 2024, J. Mater. Process. Technol., Vol.(89–90), pp. 104–110.

Yoon, J.H, Im, Y. Tand Kim, N.S, 1999, Rigid-Thermo viscoplastic Finite-Element Analysis of the Semisolid Forging of Al 2024, J. Mater. Process. Technol., V0l. 89 (90), pp.104–110.

Yoshida, C, Moritaka, M, Shinya, S et.al.,1999, Semi-solid forging of Aluminium alloys,2nd int. Conf. on ‘Processing of Semi-Solid alloys and Composites,MIT,295.

Yoshida, C, Moritaka, M, Shinya, S, Yahata, S, Takebayashi, K and Nanba, A.1992, Semi-Solid Forging Aluminium Alloy, 2nd Int. Conf. on 'Processing of Semi-Solid Alloys and Composites', MIT, 95- 102.

Zhang, X Q, Peng Y H, Ruan X Y, 2000, Simulation and fracture prediction for sintered materials in upsetting by FEM .Journal of Materials Processing Technology,Vol.105(3), pp. 253−257.

Zhao, Z, Chen, Q, Chao, H, Huang, S, 2010, Microstructural evolution and tensile mechanical properties of thixo-forged ZK60- Y magnesium alloys produced by two different routes. Mater. Des. ,Vol.31, pp. 1906–1916.

Experimental data of disc compression tests at temperatures of 570^0C, 590^0C, and 610^0C and strain rates of $0.16s^{-1}$, $0.18s^{-1}$ and $0.2s^{-1}$

Table A 4.5 Experimental data measured at 570^0C and 0.16 s^{-1} strain rate

Disp. in mm	Load in KN	$H_F=H_0$-Disp	Engineering strain	H_0/H_F	Instantaneous Diameter in mm	Area in mm^2	Engineering stress in MPa	True strain	H_F/H_0	True stress in MPa
0.5	8.7	15.5	0.03	1.03	16.25	207.33	41.96	0.03	0.97	40.65
1.5	10.4	14.5	0.09	1.10	16.79	221.40	46.97	0.10	0.91	42.57
2.2	12.1	13.8	0.14	1.16	17.21	232.45	52.05	0.15	0.86	44.90
3	16.3	13	0.19	1.23	17.72	246.55	66.11	0.21	0.81	53.72
3.3	23.4	12.7	0.21	1.26	17.93	252.29	92.75	0.23	0.79	73.62
5.76	27.7	10.24	0.36	1.56	19.94	312.08	88.76	0.45	0.64	56.81
7.16	33.8	8.84	0.45	1.81	21.44	360.96	93.64	0.59	0.55	51.74
8.06	41.6	7.94	0.50	2.02	22.62	401.49	103.61	0.70	0.50	51.42
9.46	50.7	6.54	0.59	2.45	24.90	486.70	104.17	0.89	0.41	42.58
10.16	62.7	5.84	0.64	2.74	26.34	544.63	115.12	1.01	0.37	42.02
11.76	73.3	4.24	0.74	3.77	30.89	748.86	97.88	1.33	0.27	25.94

Table A 4.6 Experimental data measured at 570^0C and 0.18 s^{-1} strain rate

Disp. in mm	Load in KN	$H_F=H_0$-Disp	Engineering strain	H_0/H_F	Instantaneous Diameter in mm	Area in mm^2	Engineering stress in MPa	True strain	H_F/H_0	True stress in MPa
1.5	10.2	14.5	0.09	1.10	16.79	221.40	46.07	0.10	0.91	41.75
1.8	11.6	14.2	0.11	1.13	16.97	226.00	51.33	0.12	0.89	45.55
3	12.1	13	0.19	1.23	17.72	246.55	49.08	0.21	0.81	39.88
3.3	16.1	12.7	0.21	1.26	17.93	252.29	63.82	0.23	0.79	50.65
3.8	21.3	12.2	0.24	1.31	18.29	262.49	81.15	0.27	0.76	61.87
4.5	26.7	11.5	0.28	1.39	18.83	278.26	95.95	0.33	0.72	68.97
6.9	35.9	9.1	0.43	1.76	21.14	350.75	102.35	0.56	0.57	58.21
9.6	43.1	6.4	0.60	2.50	25.17	497.28	86.67	0.92	0.40	34.67
11.3	53.7	4.7	0.71	3.40	29.34	675.91	79.45	1.23	0.29	23.34
12.1	65.3	3.9	0.76	4.10	32.20	813.85	80.24	1.41	0.24	19.56

Table A 4.7 Experimental data measured at 570^0C and 0.2 s^{-1} strain rate

Disp. in mm	Load in KN	$H_F=H_0$-Disp	Engineering strain	H_0/H_F	Instantaneous Diameter in mm	Area in mm^2	Engineering stress in MPa	True strain	H_F/H_0	True stress in MPa
1	14	15	0.06	1.07	16.52	214	65.38	0.06	0.94	61.29
1.5	19.2	14.5	0.09	1.1	16.79	221	86.72	0.1	0.91	78.59
2.5	21.8	13.5	0.16	1.19	17.4	238	91.77	0.17	0.84	77.43
3.5	27.2	12.5	0.22	1.28	18.07	256	106.14	0.25	0.78	82.92
4	30	12	0.25	1.33	18.44	267	112.44	0.29	0.75	84.33
5.1	34.3	10.9	0.32	1.47	19.33	293	116.91	0.38	0.68	79.64
6.5	38	9.5	0.41	1.68	20.69	336	113.05	0.52	0.59	67.13
7.8	43.5	8.2	0.49	1.95	22.26	389	111.86	0.67	0.51	57.33
8.3	47	7.7	0.52	2.08	22.96	414	113.55	0.73	0.48	54.65
9.5	56	6.5	0.59	2.46	24.98	490	114.36	0.9	0.41	46.46
10.7	63	5.3	0.67	3.02	27.64	600	105.04	1.1	0.33	34.79

Table A 4.8 Experimental data measured at 590^0C and 0.16 s^{-1} strain rate

Disp. in mm	Load in KN	$H_F=H_0$-Disp	Engineering strain	H_0/H_F	Instantaneous Diameter in mm	Area in mm^2	Engineering stress in MPa	True strain	H_F/H_0	True stress in MPa
0.4	10.4	15.6	0.025	1.03	16.2	206	50.48	0.03	0.98	49.22
1	12	15	0.0625	1.07	16.52	214	56.04	0.06	0.94	52.54
1.4	13.2	14.6	0.0875	1.1	16.74	220	60.03	0.09	0.91	54.77
2	15.1	14	0.125	1.14	17.09	229	65.89	0.13	0.88	57.65
2.7	18.9	13.3	0.16875	1.2	17.52	241	78.4	0.18	0.83	65.17
3.5	22.3	12.5	0.21875	1.28	18.07	256	87.02	0.25	0.78	67.98
5.1	27.7	10.9	0.31875	1.47	19.33	293	94.41	0.38	0.68	64.32
6.5	35.2	9.5	0.40625	1.68	20.69	336	104.72	0.52	0.59	62.18

Table A 4.9 Experimental data measured at 590^0C and 0.18 s^{-1} strain rate

Disp. in mm	Load in KN	$H_F=H_0$-Disp	Engineering strain	H_0/H_F	Instantaneous Diameter in mm	Area in mm^2	Engineering stress in MPa	True strain	H_F/H_0	True stress in MPa
0.5	9.7	15.5	0.03	1.03	16.25	207.33	46.78	0.03	0.97	45.32
0.6	12.6	15.4	0.04	1.04	16.3	208.66	60.39	0.04	0.96	58.12
0.8	14.4	15.2	0.05	1.05	16.41	211.36	68.13	0.05	0.95	64.72
1.1	15.8	14.9	0.07	1.07	16.57	215.54	73.3	0.07	0.93	68.26
1.8	20.1	14.2	0.11	1.13	16.97	226	88.94	0.12	0.89	78.93
3.3	23.1	12.7	0.21	1.26	17.93	252.29	91.56	0.23	0.79	72.68
5.6	29.8	10.4	0.35	1.54	19.79	307.33	96.96	0.43	0.65	63.03
7.8	38.1	8.2	0.49	1.95	22.26	388.87	97.98	0.67	0.51	50.21

Table A 4.10 Experimental data measured at 590^0C and 0.2 s^{-1} strain rate

Disp. in mm	Load in KN	$H_F=H_0$-Disp	Engineering strain	H_0/H_F	Instantaneous Diameter in mm	Area in mm^2	Engineering stress in MPa	True strain	H_F/H_0	True stress in MPa
0.4	10.7	15.6	0.03	1.03	16.20	206.03	51.94	0.03	0.98	50.64
1.3	11.1	14.7	0.08	1.09	16.68	218.43	50.82	0.08	0.92	46.69
1.5	12.3	14.5	0.09	1.10	16.79	221.40	55.56	0.10	0.91	50.35
1.8	14.7	14.2	0.11	1.13	16.97	226.00	65.04	0.12	0.89	57.73
2.6	18.9	13.4	0.16	1.19	17.46	239.29	78.98	0.18	0.84	66.15
3.6	22.2	12.4	0.23	1.29	18.14	258.31	85.94	0.25	0.78	66.61
4.2	25.3	11.8	0.26	1.36	18.59	271.27	93.26	0.30	0.74	68.78
6	32	10	0.38	1.60	20.17	319.49	100.16	0.47	0.63	62.60

Table A 4.11 Experimental data measured at 610^0C and 0.16 s^{-1} strain rate

Disp. in mm	Load in KN	$H_F=H_0$-Disp	Engineering strain	H_0/H_F	Instantaneous Diameter in mm	Area in mm^2	Engineering stress in MPa	True strain	H_F/H_0	True stress in MPa
1.9	5.4	14.1	0.12	1.13	17.03	227.58	23.73	0.13	0.88	20.91
3.6	9.5	12.4	0.23	1.29	18.14	258.31	36.78	0.25	0.78	28.50
4.9	10.4	11.1	0.31	1.44	19.16	288.16	36.09	0.37	0.69	25.04
6.3	11.1	9.7	0.39	1.65	20.48	329.26	33.71	0.50	0.61	20.44
6.8	12	9.2	0.43	1.74	21.02	346.97	34.59	0.55	0.58	19.89
7.7	12.8	8.3	0.48	1.93	22.12	384.22	33.31	0.66	0.52	17.28
7.9	14.7	8.1	0.49	1.98	22.39	393.63	37.35	0.68	0.51	18.91
8.4	23	7.6	0.53	2.11	23.11	419.30	54.85	0.74	0.48	26.06
8.8	29.8	7.2	0.55	2.22	23.74	442.40	67.36	0.80	0.45	30.31
9.4	39.1	6.6	0.59	2.42	24.79	482.31	81.07	0.89	0.41	33.44

Table A 4.12 Experimental data measured at 610^0C and 0.18 s^{-1} strain rate

Disp. in mm	Load in KN	$H_F=H_0$-Disp	Engineering strain	H_0/H_F	Instantaneous Diameter in mm	Area in mm^2	Engineering stress in MPa	True strain	H_F/H_0	True stress in MPa
1.8	6	14.2	0.11	1.13	16.97	226.00	26.55	0.12	0.89	23.56
3.8	10.7	12.2	0.24	1.31	18.29	262.49	40.76	0.27	0.76	31.08
4.5	11	11.5	0.28	1.39	18.83	278.26	39.53	0.33	0.72	28.41
5.9	11.4	10.1	0.37	1.58	20.07	316.36	36.04	0.46	0.63	22.75
6.5	12	9.5	0.41	1.68	20.69	336.12	35.70	0.52	0.59	21.20
7.5	12.8	8.5	0.47	1.88	21.86	375.26	34.11	0.63	0.53	18.12
8.1	16	7.9	0.51	2.03	22.67	403.50	39.65	0.71	0.49	19.58

Table A 4.13 Experimental data measured at 610^0C and 0.2 s^{-1} strain rate

Disp. in mm	Load in KN	$H_F=H_0$-Disp	Engineering strain	H_0/H_F	Instantaneous Diameter in mm	Area in mm^2	Engineering stress in MPa	True strain	H_F/H_0	True stress in MPa
1.5	6.6	14.5	0.09	1.10	16.79	221.40	29.81	0.10	0.91	27.02
2	12.8	14	0.13	1.14	17.09	229.18	55.85	0.13	0.88	48.87
3.5	14.5	12.5	0.22	1.28	18.07	256.27	56.58	0.25	0.78	44.20
5.2	16.1	10.8	0.33	1.48	19.42	296.07	54.38	0.39	0.68	36.71
5.7	19.2	10.3	0.36	1.55	19.88	310.28	61.88	0.44	0.64	39.83
5.8	22.5	10.2	0.36	1.57	19.98	313.29	71.82	0.45	0.64	45.78
7.6	29.1	8.4	0.48	1.90	21.99	379.69	76.64	0.64	0.53	40.24
8.8	34.5	7.2	0.55	2.22	23.74	442.40	77.98	0.80	0.45	35.09

Stress –Strain Evaluation

The disc compression tests were conducted at different temperatures of 570^0C, 590^0C and 610^0C at different strain rates namely $0.16s^{-1}$, $0.18s^{-1}$ and $0.2s^{-1}$. The engineering stress (σ), engineering strain (ε), true stress (σ_t) and true strains (ε_t) were found by using the following equations. Tseng AA et al. [2001]

Stress (σ) = Load/ Area = $L / (\pi/4)*d_i^2$

Where di = Instantaneous diameter = $\sqrt{}$ $[(1-B_d)\ H_0/H_f + B_d] * D_o$

Where Bd = Degree of barrelling = $[(H_0/H_f) - (D_e / Do)^2] / [(Ho/H_f)-1]$

De = End section diameter, Do= Original diameter

H_0 = Initial height, H_f= Final height

Engineering strain (ε) = Displacement/Original length

True strain (εt) = ln (H_f/H_0)

True stress (σ_t) = $(L)\ (H_f\ ) / (\pi/4)*H_0*d_i^2$

Tseng AA , Horsky J, Raudensky M, et al .Deformation behaviour of steels in mushy state[J] .Materials and Design,2001, 22:83-92.

Incremental ratio of Cockcroft and Latham damage in plastic deformation

Table A 6.2 Damage factor measured at 570^0C and 0.16 s^{-1} strain rate

Step no	$D_{accumulate}$	Damage	Damage increment	Incremental ratio
10	15.60	0.0030		
20	16.04	0.0077	1.527869	0.09525
30	16.04	0.0145	0.880674	0.05489
40	16.22	0.0240	0.655172	0.04039
50	17.06	0.0371	0.545833	0.03200
60	17.79	0.0550	0.482480	0.02712
70	18.65	0.0795	0.445455	0.02388
80	19.75	0.1130	0.421384	0.02133
90	21.03	0.1590	0.407080	0.01936
100	22.75	0.2230	0.402516	0.01769
110	25.16	0.3070	0.376682	0.01497
120	28.42	0.4200	0.368078	0.01295

Table A 6.3 Damage factor measured at 570^0C and 0.18 s^{-1} strain rate

Step no	$D_{accumulate}$	Damage	Damage increment	Incremental ratio
10	15.22	0.0031		
20	15.60	0.0078	1.5273312	0.097906
30	16.04	0.0148	0.8829517	0.055036
40	16.89	0.0245	0.6554054	0.038787
50	17.19	0.0378	0.5428571	0.031575
60	17.97	0.0560	0.4814815	0.026783
70	18.79	0.0808	0.4428571	0.023563
80	19.75	0.1150	0.4232673	0.021426
90	21.10	0.1610	0.4121560	0.018952
100	23.22	0.2250	0.3975155	0.017120
110	26.00	0.3090	0.3733333	0.014359
120	30.00	0.4230	0.3689320	0.012298

Table A 6.4 Damage factor measured at 570^0C and 0.2 s^{-1} strain rate

Step no	$D_{accumulate}$	Damage	Damage increment	Incremental ratio
10	15.22	0.00333		
20	15.47	0.00843	1.531532	0.07658
30	15.93	0.01580	0.874259	0.02914
40	16.46	0.02610	0.651899	0.01630
50	16.94	0.04020	0.540230	0.01080
60	17.79	0.05930	0.475124	0.00792
70	18.65	0.08500	0.433390	0.00619
80	19.64	0.12200	0.411765	0.00515
90	20.96	0.16700	0.391667	0.00435
100	22.59	0.23200	0.389222	0.00389
110	23.22	0.31700	0.366379	0.00333
120	27.00	0.43300	0.365931	0.00305

Table A 6.5 Damage factor measured at 590^0C and 0.16 s^{-1} strain rate

Step no	$D_{accumulate}$	Damage	Damage increment	Incremental ratio
10	15.05	0.00097		
20	15.17	0.00265	1.7235355	0.08618
30	15.21	0.00533	1.0113208	0.03371
40	16.36	0.00952	0.7861163	0.01965
50	17.64	0.01600	0.6806723	0.01361
60	18.10	0.02590	0.6187500	0.01031
70	19.66	0.04130	0.5945946	0.00849
80	20.42	0.06510	0.5762712	0.00720
90	21.31	0.10200	0.5668203	0.00630
100	22.67	0.15600	0.5294118	0.00529
110	23.57	0.23400	0.5183100	0.00455
120	27.00	0.34100	0.4572650	0.00381

Table A 6.6 Damage factor measured at 590^0C and 0.18 s^{-1} strain rate

Step no	$D_{accumulate}$	Damage	Damage increment	Incremental ratio
10	15.11	0.00098		
20	15.14	0.00267	1.7217125	0.08609
30	15.63	0.00540	1.0224719	0.03408
40	16.76	0.00965	0.7870370	0.01968
50	17.67	0.01620	0.6787565	0.01358
60	18.18	0.02640	0.6296296	0.01049
70	19.68	0.04210	0.5946970	0.00850
80	20.31	0.06640	0.5771971	0.00721
90	21.36	0.10451	0.5662651	0.00629
100	22.49	0.15900	0.5288462	0.00529
110	23.23	0.23823	0.4968553	0.00452
120	24.78	0.34500	0.4495798	0.00375

Table A 6.7 Damage factor measured at 590^0C and 0.2 s^{-1} strain rate

Step no	$D_{accumulate}$	Damage	Damage increment	Incremental ratio
10	15.10	0.00103		
20	15.14	0.00282	1.7378641	0.08689
30	15.22	0.00575	1.0390071	0.03463
40	15.26	0.01040	0.8086957	0.02022
50	16.59	0.01751	0.6826923	0.01365
60	17.76	0.02860	0.6342857	0.01057
70	18.62	0.04562	0.5944056	0.00849
80	19.35	0.07163	0.5701754	0.00713
90	20.31	0.11121	0.5502793	0.00611
100	21.61	0.16810	0.5135135	0.00514
110	22.00	0.24865	0.4761905	0.00433
120	25.00	0.35810	0.4435484	0.00370

Table A 6.8 Damage factor measured at 610^0C and 0.16 s^{-1} strain rate

Step no	$D_{accumulate}$	Damage	Damage increment	Incremental ratio
10	15.10	0.00057		
20	15.14	0.00160	1.8169014	0.09085
30	15.20	0.00335	1.0937530	0.03646
40	15.78	0.00620	0.8507463	0.02127
50	16.63	0.01080	0.7419355	0.01484
60	17.32	0.01830	0.6944444	0.01157
70	17.89	0.03031	0.6557377	0.00937
80	18.46	0.04981	0.6435644	0.00804
90	19.46	0.08142	0.6345382	0.00705
100	20.79	0.13210	0.5970516	0.00597
110	23.74	0.20534	0.5769231	0.00524
120	24.62	0.31235	0.5219512	0.00435

Table A 6.9 Damage factor measured at 610^0C and 0.18 s^{-1} strain rate

Step no	$D_{accumulate}$	Damage	Damage increment	Incremental ratio
10	15.10	0.00067		
20	15.15	0.00189	1.8125420	0.09063
30	15.22	0.00394	1.0846561	0.03616
40	15.38	0.00727	0.8451777	0.02113
50	15.69	0.01260	0.7331499	0.01466
60	16.15	0.02120	0.6666667	0.01111
70	16.75	0.03430	0.6333333	0.00905
80	17.51	0.05550	0.6180758	0.00773
90	18.49	0.08920	0.6072072	0.00675
100	19.81	0.14631	0.5695067	0.00570
110	22.66	0.21650	0.5428571	0.00494
120	25.00	0.32601	0.5092593	0.00424

Table A 6.10 Damage factor measured at 610^0C and 0.2 s^{-1} strain rate

Step no	$D_{accumulate}$	Damage	Damage increment	Incremental ratio
10	15.10	0.00068		
20	15.14	0.00192	1.8193833	0.18194
30	15.23	0.00400	1.0833333	0.05417
40	15.40	0.00738	0.8457892	0.02817
50	15.68	0.01280	0.7344173	0.01836
60	16.12	0.02140	0.671875	0.01344
70	16.72	0.03480	0.6261682	0.01044
80	17.49	0.05620	0.6149425	0.00878
90	18.45	0.09010	0.6032028	0.00754
100	19.76	0.14120	0.5649279	0.00628
110	21.66	0.21831	0.5460993	0.00546
120	25.33	0.32843	0.5045872	0.00459

Table A 6.11 Variations of damage values with temperature and strain at 0.16 s^{-1} strain rate

Temperature	**570^0C**	**590^0C**	**610^0C**
strain rate (s^{-1})	**0.16**	**0.16**	**0.16**
True strain	**Damage**	**Damage**	**Damage**
0	0	0	0
0.07	0.00305	0.00097	0.00056
0.13	0.00771	0.00265	0.00160
0.20	0.01450	0.00533	0.00335
0.27	0.02400	0.00952	0.00620
0.33	0.03710	0.01600	0.01080
0.40	0.05500	0.02590	0.01830
0.47	0.07950	0.04130	0.03030
0.53	0.11300	0.06510	0.04980
0.60	0.15900	0.10200	0.08140
0.67	0.22300	0.15600	0.13201
0.73	0.30700	0.23400	0.20534
0.80	0.42000	0.34100	0.31201

Table A 6.12 Variations of damage values with temperature and strain at 0.18 s^{-1} strain rate

Temperature	570^0C	590^0C	610^0C
strain rate (s^{-1})	0.18	0.18	0.18
True strain	Damage	Damage	Damage
0	0	0	0
0.07	0.00311	0.00098	0.00067
0.13	0.00786	0.00267	0.00189
0.20	0.01480	0.00540	0.00394
0.27	0.02450	0.00965	0.00727
0.33	0.03780	0.01620	0.01260
0.40	0.05601	0.02640	0.02101
0.47	0.08080	0.04210	0.03430
0.53	0.11520	0.06640	0.05550
0.60	0.16102	0.10401	0.08920
0.67	0.22505	0.15920	0.14204
0.73	0.30900	0.23834	0.21603
0.80	0.42300	0.34500	0.32601

Table A 6.13 Variations of damage values with temperature and strain at 0.2 s^{-1} strain rate

Temperature	570^0C	590^0C	610^0C
strain rate (s^{-1})	0.2	0.2	0.2
True strain	Damage	Damage	Damage
0	0	0	0
0.07	0.00333	0.00103	0.00068
0.13	0.00843	0.00282	0.00192
0.20	0.01580	0.00575	0.00402
0.27	0.02610	0.01040	0.00738
0.33	0.04020	0.01750	0.01280
0.40	0.05930	0.02860	0.02140
0.47	0.08501	0.04560	0.03480
0.53	0.12420	0.07160	0.05620
0.60	0.16700	0.11120	0.09010
0.67	0.23205	0.16880	0.14105
0.73	0.31701	0.24867	0.21843
0.80	0.43346	0.35805	0.32808

Table A 6.14 Values of fracture strain and ln Z

Strain rate(s^{-1})	570^0C	Critical fracture strain	590^0C	Critical fracture strain	610^0C	Critical fracture strain
0.16	13.089	0.98	12.74	1.17	2.4086	0.63
0.18	13.206	0.699	12.855	0.678	12.52	0.586
0.2	13.312	0.484	12.96	0.582	12.631	0.533

LIST OF PUBLICATIONS IN JOURNALS

1. CH.Shashikanth. and M. J. Davidson:" Simulation studies on the deformation behaviour of AA 2017 alloy in the semi-solid state using FEA", **Journal of Materials at High Temperature**, 2014, VOL 31(3). (SCI Journal) Impact Factor: 0.7

2. CH.Shashikanth and M. J. Davidson: "Experimental and simulation studies on thixo-forming of AA 2017 alloy", **Journal of Materials at High Temperature, (Accepted)**

3. Shashikanth. and M. J. Davidson:":"Microstructure Studies on the Thixo-extruded bar of AA 2017 alloy",**Alexandria Engineering Journal(ELSEVIER),(Under review)**

4. Shashikanth. and M. J. Davidson:": "Determination of material constants and Zener-Hollomon parameter of AA 2017 aluminium alloy under hot compression test", **International Journal of Industrial and Manufacturing Engineering Vol:2, No:3, 2015**